UNSTEADY TOTAL PRESSURE MEASUREMENT FOR LAMINAR-TO-TURBULENT TRANSITION DETECTION

A Thesis presented to
The Faculty of California Polytechnic State University,
San Luis Obispo

In Partial Fulfillment of the Requirements for the Degree
Master of Science in Mechanical Engineering

by
Akane Sharon Karasawa
July 2011

COMMITTEE MEMBERSHIP

UNSTEADY TOTAL PRESSURE MEASUREMENT FOR LAMINAR-TO-TURBULENT TRANSITION DETECTION

TITLE:	Unsteady Total Pressure Measurement for Laminar-to-Turbulent Transition Detection
AUTHOR:	Akane Sharon Karasawa
DATE SUBMITTED:	July 2011
COMMITTEE CHAIR:	Russell V. Westphal, PhD, Mechanical Engineering
COMMITTEE MEMBER:	Patrick Lemieux, PhD, Mechanical Engineering
COMMITTEE MEMBER:	Kim Shollenberger, PhD, Mechanical Engineering

ABSTRACT

Unsteady Total Pressure Measurement for Laminar-to-Turbulent Transition Detection

Akane Sharon Karasawa

This thesis presents the use of an unsteady total pressure measurement to detect laminar-to-turbulent transition. A miniature dynamic pressure transducer, Kulite model XCS-062-5D, was utilized to measure the total pressure fluctuations, and was integrated with an autonomous boundary layer measurement device that can withstand flight test conditions. Various sensor-probe configurations of the Kulite pressure transducer were first examined in a wind tunnel with a 0.610 m (2.0 ft) square test section with a maximum operational velocity of 49.2 m/s (110 mph), corresponding dynamic pressure of 1.44 kPa (30 psf). The Kulite sensor was placed on an elliptical nose flat plate where the flow was known to be turbulent. The Kulite sensor was then evaluated to measure total pressure fluctuations in laminar, turbulent, and transition of boundary layers developed on the flat plate in the same wind tunnel. The root-mean-square value of total pressure fluctuations was less than 1 % of the local free-stream dynamic pressure in the laminar boundary layer, but was about 2 % in the turbulent boundary layer. The value increased to 4 % in transition, indicating that the total pressure fluctuation measurements can be used not only to distinguish the laminar boundary layer from the turbulent boundary layer, but also to identify the transition region. The unsteady total pressure measurement was also conducted in a with a 2.13 m (7.0 ft) by 3.05 m (10.0 ft) section with similar operational velocity range as the previous wind tunnel. The Kulite sensor was placed on a wing model under laminar and transition conditions. The testing yielded similar results, demonstrating the usefulness of total pressure measurement for identifying the laminar-to-turbulent transition.

Keywords: Unsteady total pressure, laminar-to-turbulent transition, turbulence, pressure fluctuation, boundary layer

ACKNOWLEDGMENTS

I would like to thank Dr. Russell Westphal for his endless support and guidance for the entirety of the project.

I would also like to thank Northrop Grumman Corporation for their continuous support and for allowing us to use their wind tunnel facilities.

Thank you to Drew Hutcheson, Rocky Ulk, Jonathan White, Will Harris, Eric Carpentier, Jonathan Grubb, William Neumeister, Bradley Schab, Andrew Olson, Kristen Heckman, and Spencer Lillywhite, for their support throughout the project.

Special thanks to Don Frame for constructing the Kulite signal conditioner and giving us technical support whenever it was needed.

TABLE OF CONTENTS

LIST OF TABLES

LIST OF FIGURES

NOMENCLATURE

C_f	=	Skin friction coefficient, $C_f \equiv \frac{\sigma_w}{q_e}$
d	=	Circular sensor or probe diameter
d^+	=	Viscous wall unit, $d^+ \equiv \frac{du_\sigma}{\nu}$
l	=	Probe length
p_s	=	Static pressure
p_t	=	Total pressure
q	=	Dynamic pressure, $q \equiv \frac{1}{2}\rho U^2$
U	=	Approaching flow velocity in a wind tunnel
u_σ	=	Shear velocity, $u_\sigma \equiv \sqrt{\frac{\sigma_w}{\rho}}$
u,v,w	=	Velocity components in x, y, z direction
x	=	Stream-wise distance measured from the leading edge of a flat plate
y	=	Distance measured normal to the surface of a flat plate
ϵ	=	dissipation rate per unit mass
ρ	=	Air density
δ	=	Boundary layer thickness
δ_l	=	Characteristic length scale for boundary layer thickness
θ	=	Momentum thickness
η	=	Kolmogorov microscale of length
τ	=	Kolmogorov microscale of time
σ_w	=	Wall shear stress

ν	=	Kinematic viscosity of a fluid
$\phi(\omega)$	=	Single point spectrum at a wavelength ω

SUBSCRIPTS

a	=	Acoustic noise, referring to pressure fluctuations due to acoustic and vibration noise
b	=	Electrical noise, referring to pressure fluctuations due to electrical noise
c	=	Connecting probe, referring to the diameter of connecting probe
e	=	Local, referring to local dynamic pressure or local velocity outside of boundary layer
k	=	Kulite, referring to pressure measured by a Kulite sensor
pin	=	Pin-hole transducer
raw	=	Raw, referring to raw data
ref	=	Reference, referring to backing pressure of a Kulite sensor
rms	=	Root-mean-square
w	=	Wall, referring to pressure measured at the surface of a flat plate
∞	=	Free-stream

1. INTRODUCTION

A turbulent fluid motion is defined as “an irregular condition of flow in which the various quantities show a random variation with time and space coordinates, so that statistically distinct average values can be discerned” [1]. Turbulent flow along a rigid body is categorized as boundary layer flow as the domain of the turbulence remains confined in a region where the effect of viscosity is significant. The behavior of this boundary layer flow over a rigid surface is a vital part of fluid mechanics. It is especially an important topic in aerodynamics because boundary layer behavior on the surface of a wing or a body determines the skin friction drag forces, thus affecting flight efficiency. The skin friction coefficient of a laminar flow is much lower than that of turbulent flow below transitional Reynolds number. Therefore, a considerable reduction in skin friction drag can be achieved by maintaining laminar flow over the lifting surface of an aircraft. For this reason, the detection of laminar to turbulent transition becomes crucial in the design of wings and bodies that maintain laminar flow for the lowest possible skin friction drag.

The state of flow over a surface and its corresponding skin friction can be predicted using computational analysis, but the result carries uncertainty. The computational analysis is carried out with many assumptions and approximations because there is no general solution for the turbulent flow model, despite the fact that the flow phenomena have been investigated for over a century. The solution has not been found because turbulent flow is highly non-linear, and no existing mathematical technique can

solve the problem. Another approach to evaluate the behavior of a boundary layer over an aircraft wing is through an experiment using a wing model in a wind tunnel. Simulating an actual flow condition in a wind tunnel can be challenging, however. The flow condition around the wing model in a wind tunnel may significantly differ because of flow disturbances present in the wind tunnel that doesn't exist in flight. Consequently, data obtained from a flight test is invaluable for the validation of the laminar flow wing design.

Northrop Grumman Corporation (NGC) is a leader in laminar flow design, and has sponsored the development of Preston Tube Data System (PTDS) and Boundary Layer Data System (BLDS) [2] [3]. These autonomous devices are capable of recording boundary layer properties on an aircraft or a model surface in flight [4]. The PTDS is used to measure time-averaged local skin friction and consists of a static pressure probe, a total pressure probe, and a Preston tube. The BLDS is a more elaborate device with a servo motor driven stage that traverses a total pressure probe or other pressure-based anemometer away from the surface. This enables the device to take boundary layer velocity profile data in addition to the skin friction data. The primary purpose for the development of these devices was to determine the laminar-to-turbulent transition location on an aircraft wing from the data obtained from the flight test. The location of the transition can be established by calculating skin friction values or the boundary layer velocity profile, or the combination of both. The successful identification of laminar-to-turbulent transition using these devices were reported through wind tunnel testing and flight tests [3] [4]. However, the time-averaged data obtained from the PTDS and the BLDS requires post-processing and analysis to determine the transition location. In this

thesis, a new technique that does not require post-processing or analysis was proposed to detect laminar-to-turbulent transition using pressure fluctuation measurements.

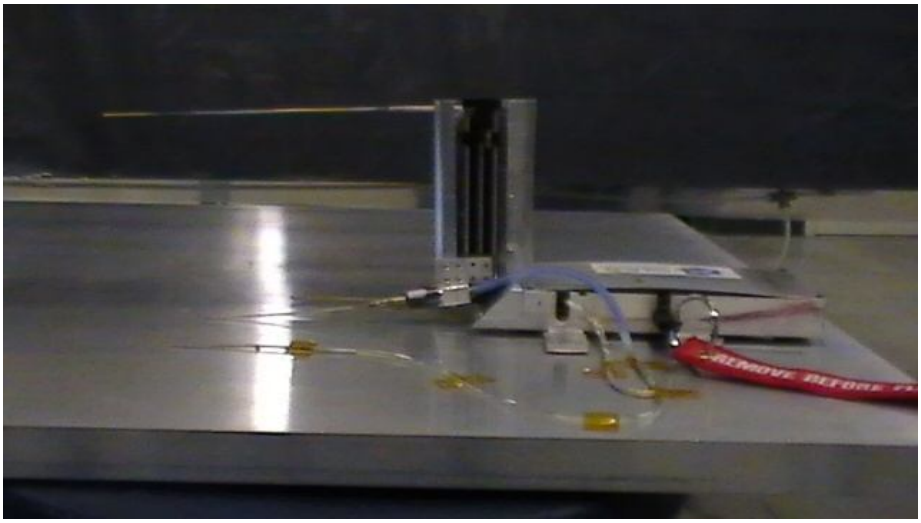

Figure 1.1 – The BLDS equipped with Kulite sensor on a flat plate.

In turbulence modeling, fluctuating parameters such as velocity components and their correlations are crucial in determining the flow characteristics. It is plausible to use velocity fluctuations in a turbulent boundary layer to determine the state of flow, but hot-wires that are used to measure the velocity fluctuation are fragile and therefore difficult to use in flight tests, especially with high Reynolds number flows [5]. Thus, the velocity correlations in turbulent boundary layer flow were further investigated. The fluctuating velocity components contribute to the pressure field in a turbulent flow, and this can be demonstrated as follows. For incompressible flow, the Poisson's equation below can be derived from the Navier-Stokes equation.

$$\frac{1}{\rho}\nabla^2 p_s = -\frac{\partial u_i}{\partial x_j}\frac{\partial u_j}{\partial x_i} \tag{1.1}$$

For turbulent flow, the Reynolds decomposition can be applied to the instantaneous value, and it is divided into mean and fluctuating components.

$$\frac{1}{\rho}\nabla^2(\overline{p_s} + p_s') = -\frac{\partial(\overline{u_\iota} + u_i')}{\partial x_j}\frac{\partial(\overline{u_j} + u_j')}{\partial x_i} \tag{1.2}$$

Averaging the entire Equation (1.2) results in the following.

$$\frac{1}{\rho}\nabla^2\overline{p_s} = -\frac{\partial\overline{u_\iota}}{\partial x_j}\frac{\partial\overline{u_J}}{\partial x_i} - \frac{\partial^2\overline{u_i'u_j'}}{\partial x_j\partial x_i} \tag{1.3}$$

Subtracting the Equation (1.3) from (1.2) yields the below equation that relates static pressure fluctuation and velocity fluctuation.

$$\frac{1}{\rho}\nabla^2 p_s' = -2\frac{\partial\overline{u_\iota}}{\partial x_j}\frac{\partial u_j'}{\partial x_i} - \frac{\partial^2}{\partial \mathrm{x_j}\,\partial \mathrm{x_j}}\left(u_i'u_j' - \overline{u_\iota'u_j'}\right) \tag{1.4}$$

The above relationship implies that static pressure fluctuation in a turbulent boundary layer at one point is produced by the summation of velocity fluctuations occurring elsewhere. More importantly, it shows that the pressure in a turbulent boundary layer fluctuates as a consequence of velocity fluctuations. Hence, the pressure fluctuations in turbulent boundary layer can be used as an indicator of turbulence.

Much research has been done over the past few decades to investigate the fluctuating static pressure at the wall beneath a turbulent boundary layer in order to improve our understanding of its structural and physical mechanism. The advancement of the research also owes to practical engineering problems such as aircraft cabin nose caused by the fluctuating static pressure at the wall. Willmarth [6] and Mull & Algranti [7] were among the first to experimentally measure fluctuating surface static pressures. Willmarth used transducers flush with the wall to measure pressure fluctuations beneath a

turbulent boundary layer in a wind tunnel while Mull & Algranti conducted in-flight experiments using condenser microphones. Willmarth reported that the ratio of root-mean-square of wall static pressure fluctuations to free-stream dynamic pressure was $\sqrt{\overline{p'^2_{s,w}}}/q_\infty = 0.0035$ over a wide range of Reynolds numbers based on the distance from the leading edge ($1.5 \times 10^6 < Re_x < 20 \times 10^6$). Mull & Algranti reported that the ratio decreased as the speed increased and reached constant value of $\sqrt{\overline{p'^2_{s,w}}}/q_\infty = 0.0013$ with flow speed above Mach 0.55.

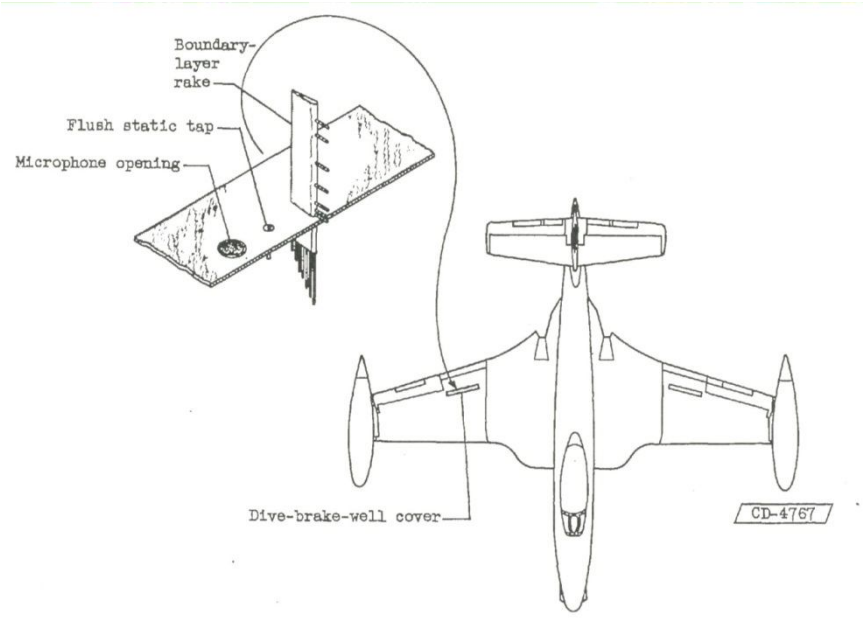

Figure 1.2 – Experimental setup used by Mull & Algranti to measure static pressure fluctuation on an airplane wing during flight [7].

Although the surface static pressure fluctuations research had progressed in the past few decades, the extent of our knowledge regarding the behavior of the surface static pressure fluctuations in turbulent boundary layer has not advanced as much as that of velocity fluctuations [8] [9]. This is due to the lack of an instrument that can accurately

measure the fluctuating quantity. Since a very wide range of eddies occur in a turbulent boundary layer, it is crucial for the pressure transducer to resolve both the largest and smallest eddies. A typical transducer can sense eddies that are larger than its size, but large-scale turbulence, corresponding to pressure fluctuation in the low frequency range, is often contaminated by facility-induced noise. Several solutions, including noise cancellation technique, have been suggested to eliminate this noise [10]. For small-scale eddies in the high frequency range, the spatial and temporal resolution of a transducer becomes an issue. When the transducer is larger than the smallest eddies in the flow, the fluctuations due to small eddies are integrated over its spatial extent and its energy content is included in its average value. As a result, the fluctuation value falls short of a true value. This error caused by the finite size of transducer was recognized in early experiments [6] [11], and considerable efforts to correct this error have been documented since then. The first attempt was made by Corcos [12], who introduced correction methods to the power spectra density of the wall static pressure fluctuations. Blake [13] used a very small condenser microphone behind a pinhole to alleviate the situation, but was not able to eliminate the resonance caused by the cavity of the pinhole-microphone system. Schewe [14] conducted a detailed study of the effect of spatial averaging on the wall pressure fluctuations measured at low Reynolds number, and measured $\sqrt{\overline{p'_{s,w}{}^2}}/q_\infty = 0.0098$ with the smallest sell-type transducer (d+ = 19). Schewe also stated that Corcos's correction became negligible when the smallest transducer was used. An increase in the intensity of the pressure fluctuation in figure 1.3 [14] suggests that the small-scale fluctuations are included when transducer size was reduced.

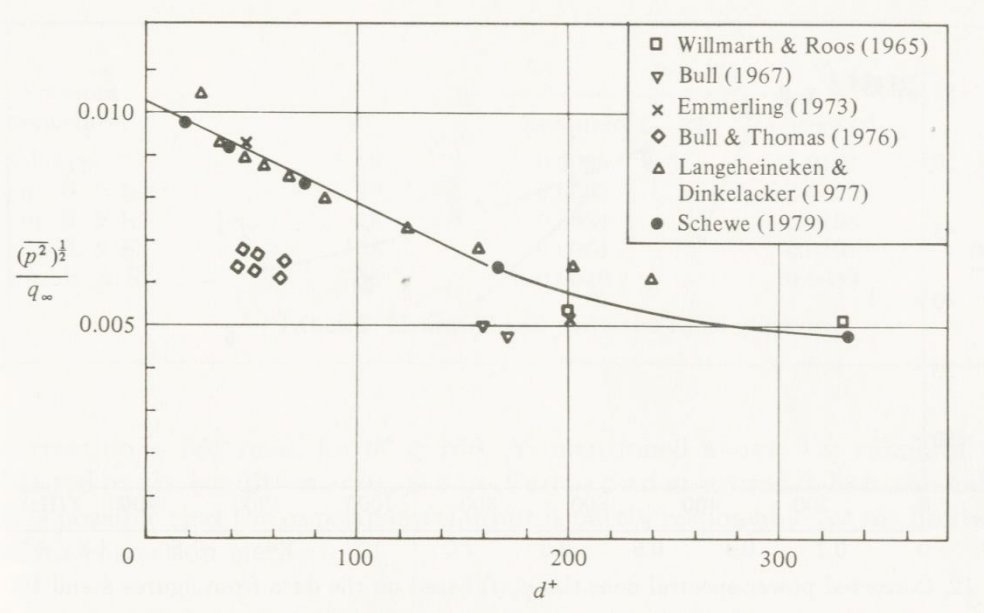

Figure 1.3 – Dependence of normalized static pressure fluctuation at the wall of turbulent boundary layer as a function of normalized transducer diameter [14].

The inaccuracy caused by the pressure attenuation may potentially be resolved with the development of Micro Electro Mechanical Systems (MEMS). MEMS are a collection of technology which produces mechanical devices that operate with integrated circuits (ICs), and has been evolving since the first discovery of piezoresistive effect of silicon and germanium in the early 1950s by Bell laboratories [15]. The MEMS sensors today are typically at least one order of magnitude smaller than traditional sensors and have characteristic length of less than 1mm. Since the smaller transducer can resolve smaller eddies, they can be utilized to measure unsteady flow quantities at high Reynolds number turbulent flows. Recent progress in turbulent boundary layer research has been made by the application of very small sensors. Tsuji and his colleagues [9] utilized a piezoresistive transducer and a condenser microphone to record surface static pressure fluctuations in high-Reynolds-number turbulent boundary layers. Their result showed the

ratio of root mean square of the fluctuating surface static pressure to the dynamic pressure of $\sqrt{\overline{p'_{s,w}{}^2}}/q_\infty$ = 0.008. Berns and Obermeier [16] developed AeroMEMS pressure sensor arrays and succeeded in high frequency laminar to turbulent transition measurement. The report showed that the piezoresistive pressure sensor with diaphragm length of 800 μm was able to accurately measure surface static pressure fluctuations up to at least 19 kHz. They succeed to obtain power spectrum proving the clear difference in energy content of the surface pressure fluctuations in transitional and turbulent flows. The table 1.1 below summarizes the surface pressure fluctuation measurements from various sources.

Table 1.1 – Comparison of the surface pressure fluctuation measurements from various sources.

Reference	Author(s)	Transducer Type	Measurement Type	$\sqrt{\overline{p'_{s,w}{}^2}}/q_\infty$
[6] [11]	Willmarth, W.	Flush mounted pressure transducer	Wind tunnel	0.0035
[7]	Mull, H.R., Algranti, J.S.	Microphone	Flight test	0.0013
[14]	Schewe, G.	Sell-type condenser microphone	Wind tunnel	0.0098
[9]	Tsuji, Y., Fransson, J.H.M., Alfredsson, P.H., Johansson, A.V.	Pin-hole static pressure probe	Wind tunnel	0.0080

In this thesis, a commercially available miniature dynamic pressure transducer, Kulite model XCS-062-5D, was evaluated for its possible application as a turbulence detector. Although somewhat larger in size, the Kulite sensor is constructed with the

same principle as MEMS piezoresistive pressure sensors. It utilizes a silicon diaphragm with four piezoresistors arranged in a Wheatstone bridge to detect the deflection of the diaphragm. For its similarity, the Kulite pressure sensor is often used as a reference sensor for the MEMS sensor development research [17] [18]. The Kulite sensor is often employed as a fast response pressure sensor with a total pressure probe to measure the unsteady flow downstream of rotating blades in turbo-machinery applications [19] [20] [21]. An example of the application of the Kulite pressure transducer in turbulent boundary layer measurements is by Rizzi et al [22]. They utilized the Kulite model XCS-062-15D in eleven instrumented window blanks along the fuselage in flight test to measure surface static pressure fluctuations and evaluated cabin noise.

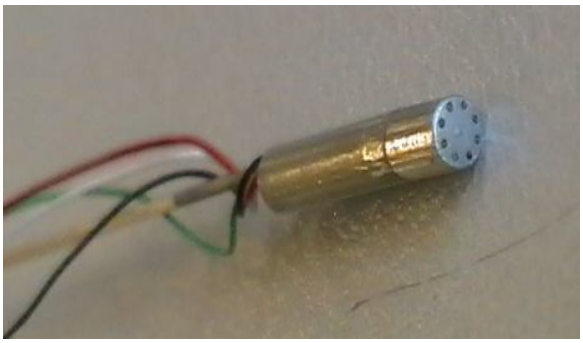

Figure 1.4 – The sensor head of the Kulite pressure sensor model XCS-062-5D.

For the purpose of developing a turbulent flow detecting device, the Kulite sensor was used to measure total pressure fluctuations rather than static pressure fluctuations at the wall. Measuring the total pressure fluctuations is advantageous because its energy content is greater than static pressure fluctuations, which will aid in distinguishing the laminar and the turbulent boundary layers. Goldstein's hypothesis [23] states that the total pressure is the sum of the static pressure and the dynamic pressure.

$$p_t = p_s + \frac{1}{2}\rho|\vec{V}|^2 \tag{1.1}$$

where

$$\vec{V} = u\hat{\imath} + v\hat{\jmath} + w\hat{z} \tag{1.2}$$

By applying Reynolds decomposition and rearranging, the square of the total pressure fluctuation can be derived. The detailed derivation can be found in Appendix B.

$$\overline{{p_t}'^2} = \overline{{p_s}'^2} + 2\rho\bar{u}\overline{p_s'u'} + \rho^2\bar{u}^2\overline{u'^2} \tag{1.3}$$

$$\frac{\overline{{p_t}'^2}}{\left(\frac{1}{2}\rho\bar{u}^2\right)^2} = \frac{\overline{{p_s}'^2}}{\left(\frac{1}{2}\rho\bar{u}^2\right)^2} + 4\frac{\overline{u'^2}}{\bar{u}^2} + \frac{8\overline{p_s'u'}}{\rho\bar{u}^3} \tag{1.4}$$

Equation (1.4) is a non-dimensional form of Equation (1.3). Notice that the total pressure fluctuation differs from the static pressure fluctuation by two terms. The second term $\overline{u'^2}/\bar{u}^2$ on the right hand side of the Equation (1.4) is well documented from measurements in boundary layers [1] [5] [24], and $0.01 \leq \sqrt{\overline{u'^2}}/\bar{u} \leq 0.12$ was reported for a turbulent boundary layer flow over a flat plate. The last term $\overline{p_s'u'}/\rho\bar{u}^3$ is predicted to be negative from Bernoulli's relationship, but if $\overline{p_s'}$ is of order $\overline{u'^2}$, it is at least one order-of-magnitude smaller than the previous term. Accordingly, the product of the static pressure fluctuation and the velocity fluctuation is likely to be negligible compared to the previous term. This suggests that the root-mean-square of total pressure fluctuations near the surface of a turbulent boundary layer is approximately three times larger than the static pressure. Since the pressure fluctuation in a turbulent boundary layer is a small fraction of the dynamic pressure, any increase in magnitude will aid the turbulence detection. The total pressure measurement is also beneficial because the probes can be affixed to the surface of an airplane or model surface without requiring any modifications

of the surface, whereas static pressure measurements usually require holes to be drilled in the surface.

The objective of this thesis is to develop a device that can discern laminar-to-turbulent transition on an aircraft or model surface during flight. The total pressure fluctuations in a turbulent boundary layer was chosen as an eligible identifier of turbulent flow, and the Kulite miniature dynamic pressure transducer model XCS-062-5D was used to measure the parameter. The device was developed with an intention that it will be used in a future flight test. This is the first attempt, as far as we know, to obtain information regarding the total pressure fluctuations in a turbulent boundary layer. The successful development of this approach will provide turbulent flow detection on an aerodynamic model or aircraft surface in fight and will significantly benefit the future research and design of the laminar flow wing.

2. INSTRUMENT DESIGN AND DEVELOPMENT

Achieving an accurate measurement of any property in a turbulent boundary layer is difficult because of its intricate structure. Review of the literature has revealed that the design of a device that can accurately measure pressure fluctuations in a turbulent boundary layer requires numerous considerations. An enormous amount of effort has been poured into research to assess the most effective form of the pressure transducer configuration for measurement of the static pressure fluctuations. All early experiments conducted before 1972 measured pressure fluctuation with transducers mounted flush to the wall or with holes in the wall communicating with microphones underneath. It was later discovered that the large discontinuities at the wall interfered with the turbulent field and skewed surface static pressure measurement [11]. Pinhole microphones were then introduced to compensate the pressure attenuation experienced by transducers with relatively large diameters. However, the effectiveness of the pinhole transducers is inconclusive, as they yield mixed results [8]. The recent development is mostly focused on MEMS transducers because small-sized transducers can minimize the attenuation of pressure fluctuations.

The size and frequency of the small-scale eddies in a turbulent flow can be estimated by using the Kolmogorov microscales of length η and time τ [25], which are defined as follows.

$$\eta \equiv \left(\frac{\nu^3}{\epsilon}\right)^{1/4} \tag{2.1}$$

$$\tau \equiv \left(\frac{\nu}{\epsilon}\right)^{1/2} \tag{2.2}$$

where ϵ $[m^2 \cdot s^{-3}]$ is the dissipation rate per unit mass and the ν $[m^2 \cdot s^{-1}]$ is the kinematic viscosity of the fluid. The Reynolds number of this form equals to one, ($\eta v/\nu = 1$) demonstrating that the small-scale motion is fairly viscous. The dissipation rate of the small-scale eddies can be estimated from the characteristic velocity fluctuation of order u, and the characteristic boundary layer thickness δ_l.

$$\epsilon \approx \frac{u^3}{\delta_l} \tag{2.3}$$

The variables u and δ_l are associated with large-scale eddies, and defined as "outer" variables. The correlation above represents the nonlinear mechanism of the turbulent flow; the energy transfer rate from the large-scale eddies to the small-scale eddies is proportional to the reciprocal of the time scale of the large-scale turbulence. By combining equation (2.1) and (2.2) with equation (2.3) respectively, the inner scale length η and time scale τ, and the outer variable δ_l can be related to Reynolds number.

$$\frac{\eta}{\delta_l} \approx \left(\frac{u\delta_l}{\nu}\right)^{-3/4} = Re^{-3/4} \tag{2.4}$$

$$\frac{\tau u}{\delta_l} \approx \left(\frac{u\delta_l}{\nu}\right)^{-1/2} = Re^{-1/2} \tag{2.5}$$

The above relationships are significant in several ways. They demonstrate that the magnitude of the small-scale eddies are much smaller than those of large-scale eddies. They also suggest that the ratio of the two widens as Reynolds number increases, provided that the flow maintains the same large scale dynamics. In other words, the small-scale structure of a flow with relatively low Reynolds number would appear sparse compared to the flow with high Reynolds number. Finally, the estimate of the size and

frequency of the smallest eddies can be made knowing the boundary layer thickness δ_l and velocity u. This is useful because a transducer with a characteristic active measuring length of the same order of the Kolmogorov scale is typically recommended for the accurate measurement of fluctuating parameters in a turbulent flow [25]. Löhdahl and Gad-el-Hak [8] suggested that a piezoresistive pressure sensor with a very thin diaphragm with its diameter on the order of 100-300μm is necessary for turbulent flow with Re_θ = 4000. The viscous wall unit, d^+, has also been a accepted to estimate the transducer size d for boundary layer pressure measurement.

$$d^+ = \frac{du_\sigma}{\nu} \tag{2.6}$$

where

$$u_\sigma = \sqrt{\frac{\sigma_w}{\rho}} \tag{2.7}$$

Schewe [14] reported that a transducer diameter that is 20 viscous wall units in diameter can capture small-scale pressure fluctuations while Keith et al [26] suggested that 10 viscous wall units or less is essential. A pinhole diameter with less than 20 viscous wall units was recommended for wall-pressure measurements conducted using pinhole microphones [9] [27]. As for the temporal resolution of a transducer, the kinetic energy spectra analyses have revealed that the energy content above 10 kHz is almost negligible [8].

The Kulite dynamic pressure transducer model XCS-062-5D was selected to measure total pressure fluctuations. The Kulite sensor operates in differential mode, meaning that the pressure fluctuations are measured from the reference pressure up to 5 psi. The Kulite transducer is very small with its head diameter of 0.066 inch OD and its

face surface is perforated with a circle of sensor holes. The pressure reference tube attached to the sensor head is 0.016 inch OD and 1.0 inch long. It can withstand future flight test conditions at temperature -50 ºF with operating temperature range of -65 to +250 ºF. The schematic of the Kulite sensor is shown in below figure 2.1, and the copy of the specification of the Kulite sensor is attached in Appendix A.

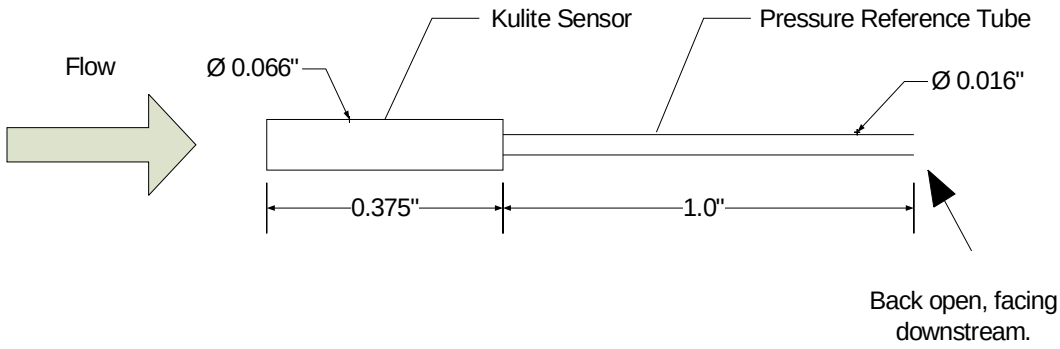

Figure 2.1 – Schematic of the Kulite dynamic pressure transducer model XCS-062-5D.

The specifications of the Kulite sensor were compared to the transducer requirements for surface static pressure measurements gathered from the existing literatures in table 2.1. The Kulite sensor satisfies all requirements except for its size. However, the sensor recommendations are based on efforts to resolve the smallest eddies in turbulent flow. It is not our desire to precisely measure the smallest eddies of the flow, but rather to distinguish between laminar and turbulent flow states. The extent to which the spatial resolution comes into play in turbulence detection using total pressure fluctuations is not known. Moreover, the above proposals are based on surface static pressure measurements and statistics, and not necessarily applicable for the total pressure measurements. Thus, it was necessary to reassess the transducer requirements specific to the purpose of detecting the laminar-turbulent transition by conducting experiments.

Table 2.1 – Transducer criteria for surface static pressure fluctuation measurements.

Criteria		Recommended	Kulite
Spatial resolution	η	100 ~300 μm	–
	d^+	10 ~20	126 ~222*
Temporal resolution		10 ~10,000 Hz	10 ~20,000 Hz
Sensitivity		±10 Pa	±35 Pa

*Based on Kulite sensor diameter with $1370 \sim Re_\theta \sim 3900$

In order to take pressure measurements, the Kulite sensor was integrated with the PTDS or the BLDS through a custom-made amplifier and operated through a "satellite" input. The detailed specifications of these mechatronic devices are explained in [3] [2] [4]. They are battery operated devices that consist of a master circuit board with two single-sided differential pressure sensors and one absolute pressure sensor. The BLDS additionally encompasses motor controls and limit switches for a stage used for probe positioning. The single-sided pressure sensors are plumbed to either a free-stream total pressure or a Preston tube on one end, but both are connected to a surface static pressure probe [28] on the other end. Therefore, the output is the differential of the total pressure and the static pressure, or dynamic pressure. The surface static probe is also connected to the absolute pressure sensor and records surface static pressures. The configurations of the Preston tube can be altered according to the purpose of a test. The Preston probe can be mounted flush on a wing surface with PTDS for skin friction measurement, or it can be used as a total pressure probe and positioned using a stage with BLDS for boundary layer velocity profile measurement. The inside of the BLDS unit is shown in below figure 2.2. Hidden underneath the TFX controller are another single-sided pressure sensor for the total pressure probe and the absolute pressure sensor for the surface static probe.

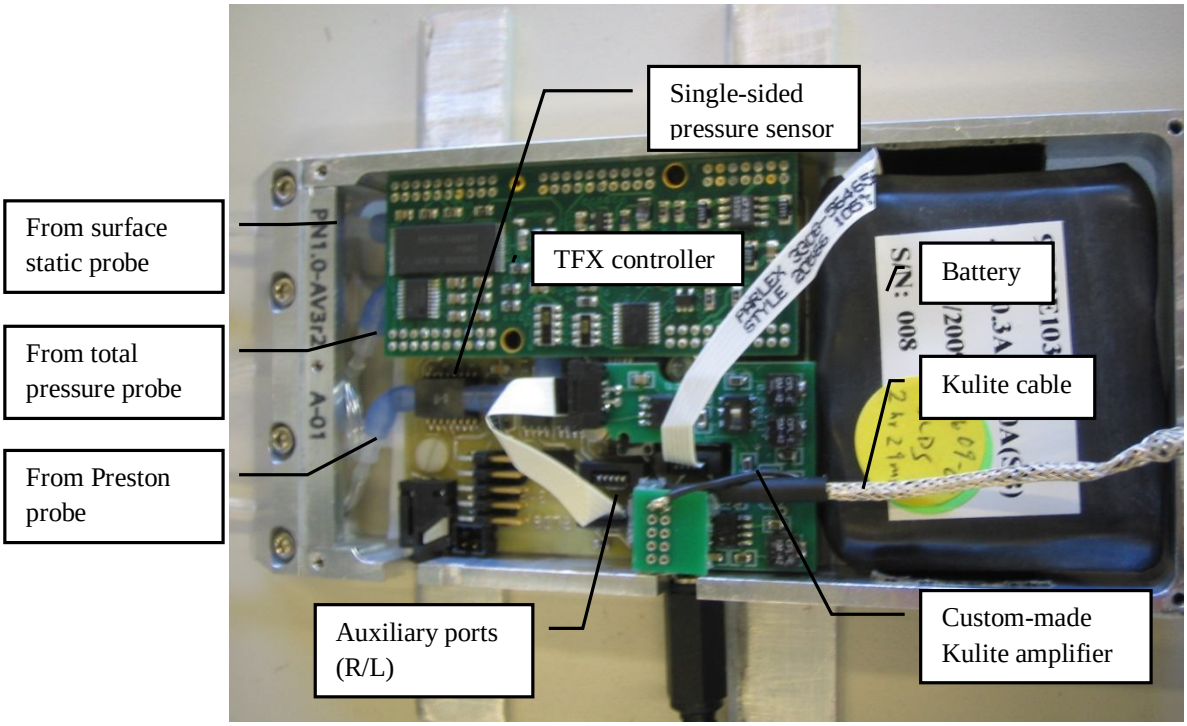

Figure 2.2 – The configuration of the BLDS board.

The existing data collection program was modified so that the average total pressure and the root-mean-square of the total pressure fluctuation values were stored. The Kulite model XCS-062-5D is a dynamic differential sensor, thus, the measured parameter is the actual difference between the total pressure $p_{t,k}$ and the reference pressure p_{ref}. The instantaneous total pressure can be decomposed into average and fluctuating components.

$$p_{t,k} = \bar{p}_{t,k} + p'_{t,k} \tag{2.8}$$

The sequence of operations to find the root-mean-square of the total fluctuation pressure is as follows. The software is first prompted to take the average of the difference between the total pressure and the reference pressure, which simply results in the following. Note that, because the Kulite reference port is connected to a capillary tube of only 0.016 inch ID and 1 inch length, it was assumed that p_{ref} was not fluctuating $(p_{ref} \cong \bar{p}_{ref})$.

$$\bar{p}_{t,k} = \overline{\left(\bar{p}_{t,k} + p'_{t,k}\right) - \bar{p}_{ref}} = \bar{p}_{t,k} - \bar{p}_{ref} \tag{2.9}$$

We denote this value as an average pressure, and it is stored in the memory. Next, the differential pressure is squared and averaged.

$$\overline{\left(\bar{p}_{t,k} + p'_{t,k} - \bar{p}_{ref}\right)^2} = \bar{p}_{t,k}^2 + \overline{p'^2_{t,k}} + \bar{p}_{ref}^2 - 2\bar{p}_{t,k}\bar{p}_{ref} \tag{2.10}$$

The square of the average pressure is now subtracted from equation (2.9). The final form is achieved by taking the square root of the resulting value.

$$\sqrt{\bar{p}_{t,k}^2 + \overline{p'^2_{t,k}} + \bar{p}_{ref}^2 - 2\bar{p}_{t,k}\bar{p}_{ref} - \left(\bar{p}_{t,k} - \bar{p}_{ref}\right)^2} = \sqrt{\overline{p'^2_{t,k}}} \tag{2.11}$$

The dynamic pressure of the free-stream was also obtained from the PTDS or the BLDS using the total pressure probe located just outside of the boundary layer.

$$q_e = \frac{1}{2}\rho U_e^2 = p_{t,e} - p_s \tag{2.12}$$

We denote this value as a local dynamic pressure q_e and distinguish it from the approaching free-stream dynamic pressure q_∞ because there is a discrepancy between the two when there's a pressure gradient present in the free-stream.

The Kulite sensor was operated with a nominal 5 VDC excitation and its output was amplified through a custom-designed BLDS interface. The sensitivity of the unamplified Kulite sensor is nominally 308 mV/BAR (about 21 mV/psi) for 10 VDC excitation with a zero pressure output within 5 mV of 0.000 VDC. With the lower excitation voltage, the sensitivity of about 10.5 mV/psi was expected. Since neither the amplifier gain nor the zero offset were known exactly, the calibration of the entire sensor/amplifier assembly was deemed necessary. Sensitivity of the sensor and amplifier was determined through direct calibration using a Fluke model 718-1G pressure calibrator with a 1 psi range and 0.05% full-scale accuracy. As expected, the calibration

showed a linear response; a slope of 0.301 psi/V fits the results and gives a sensitivity of 3.322 V/psi implying a nominal gain of 316 in good agreement with the amplifier design gain value. A substantial zero offset resulted from the amplification of the sensor zero output, which was about 1.5V/316 = 4.7 mV.

After the initial calibration, a zero trim and a gain switch features were added to the amplifier board. The gain switch was added because a higher amplifier gain was possible without saturating the voltage output as the result of the zero trim. After the modifications were made to the amplifier board, the same calibration was carried out to reassess the amplifier gains. As shown in figure 2.3, the calibration again showed a linear response with fitted slopes of 0.295 psi/V and 0.060 psi/V for position one and two, respectively. The corresponding sensitivities of 3.386V/psi and 16.67V/psi indicate signal gains of 322 and 1587. A significant reduction in zero offset to about 0.2V/316=0.4 mV was also observed.

Table 2.2 – Amplified Kulite sensor calibration results.

Calibration	Sensitivity [V/psi]	Nominal gain [-]	Zero offset [mV]
Initial	3.322	316	4.7
Position 1	3.386	322	0.4
Position 2	16.67	1587	0.1

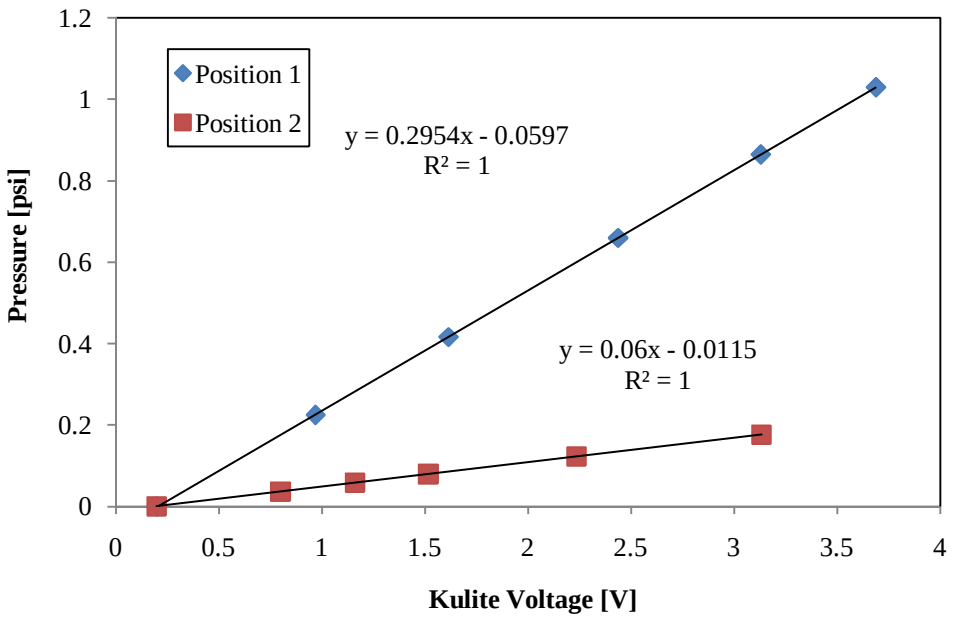

Figure 2.3 – Amplified Kulite sensor calibration results for two ranges at average temperature of 22 ˚C.

The span and the offset of a piezoresistive sensor are susceptible to temperature because the resistive impedance value of the piezoresistive elements depends not only on the strain they experience, but also on their temperature [20]. Thermal zero shift and thermal sensitivity of the Kulite sensor are both rated at 1 % per 100 ºF. In order to verify the level of thermal zero shift and sensitivity, the calibrations of the PTDS interfaced Kulite sensor were conducted at three different temperatures; 10.61˚C, 19.72 ˚C, and 29.80 ˚C. The lowest temperature was obtained by cooling the unit in a small fridge for about an hour. The average temperature of 19.72 ˚C represents a typical room temperature where the experiments were conducted. The highest temperature was achieved by leaving the unit outside on a sunny hot day for an hour. The average temperature during the calibration was recorded by two temperature sensors in the PTDS

unit [4], and the temperature of the Kulite sensor was assumed to be the same. The amplifier switch was positioned so that the highest gain was achieved (nominal 1587). The results from the calibrations were summarized in Table 2.1. The zero offset voltage of the Kulite sensor recorded a significant increase from 0.0721 V at 29.80˚C to 0.5689 V at 10.61 ˚C. The amplification of zero-shift resulted in large errors. The figure 2.4 also suggests that the thermal zero-shift is more substantial at lower temperature. It is expected that the amplification of thermal zero-shift becomes an issue when a large temperature change is expected during a test at lower temperature. Fortunately, the temperatures were relatively stable in the wind tunnel facility (±1 ˚C), and no calibration was necessary. For the future flight test, however, the calibration function to compensate the thermal zero shift should be calculated, but requires more data points in lower temperature settings. The change in sensitivity of the Kulite sensor was relatively small as expected with variation of 2.82% for the three calibration temperatures.

Table 2.3 – Calibration results for amplified Kulite sensor, nominal range = 0.2 psi.

Temperature [˚C]	Zero offset [V]	Slope [psi/V]	Sensitivity [V/psi]
10.61	0.5689	0.0602	16.605
19.72	0.2252	0.0594	16.822
29.80	0.0721	0.0611	16.333

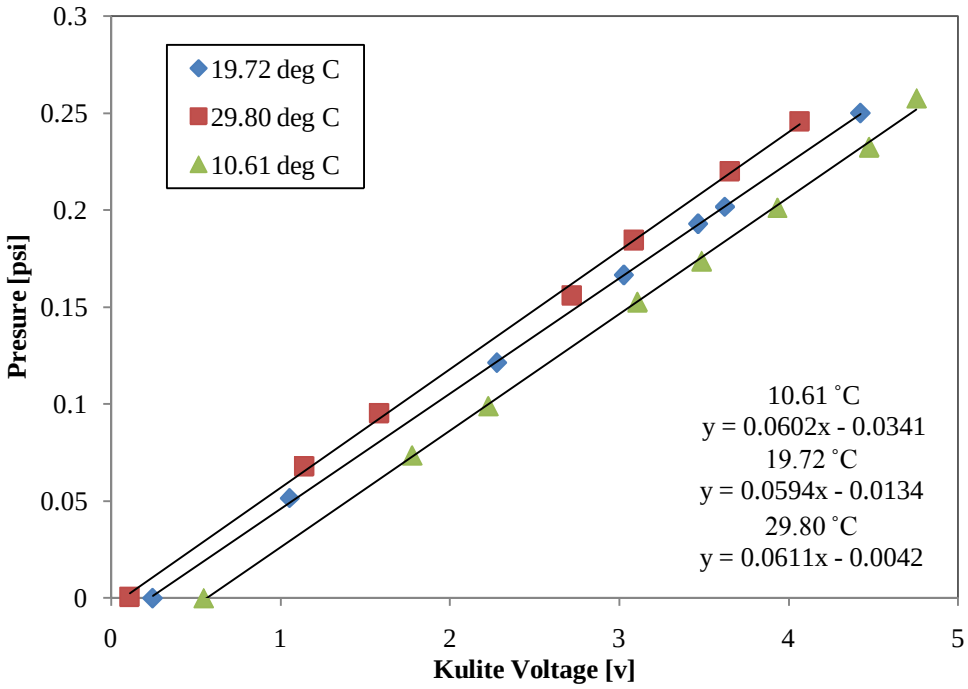

Figure 2.4 – The amplified Kulite sensor calibration at different temperatures.

The total pressure fluctuations measured by the Kulite is contaminated by noise, and needs to be corrected. The fluctuating pressure signal measured by the Kulite was modeled as being composed of desired flow-induced fluctuations p_t', and two noise sources; acoustic and vibration noise p_a', and electrical noise p_b'.

$$p_{t,k}' = p_t' + p_a' + p_b' \tag{2.13}$$

The facility-induced noise such as acoustic and vibration noise can affect the pressure signal, especially at lower frequencies. The frequency contents of the acoustic and vibration noise are generally below 50-100 Hz, and are known to disrupt the pressure signals at low Reynolds numbers [9] [29]. On the other hand, the effect of noise contamination may be negligible at high Reynolds numbers because the pressure fluctuations overwhelm the low-frequency disturbances [9]. The following procedure was

presented by Tsuji et al [9] to estimate the level of acoustic contamination in a wind tunnel. The parameter $p_w^{'}$ denotes pressure fluctuation measured at the wall and $p_y^{'}$ denotes total pressure fluctuation measured at $y \sim 2\delta$, and they were used to analyze the noise level. The fluctuating pressures sensed by a transducer can be described as the sum of noise due to acoustics and vibrations p'_a and the true pressure fluctuation p'_{true}.

$$p'_w = p'_{true,w} + p'_{a,w}, \quad p'_y = p'_{true,y} + p'_{a,y} \tag{2.14}$$

Since $p'_{a,w}$ and $p'_{a,y}$ are independent of turbulent statistics, the correlation function is calculated as follows.

$$\overline{p'_w p'_y} = \overline{p'_{true,w} p'_{true,y}} + \overline{p'_{a,w} p'_{a,y}} \tag{2.15}$$

Notice that $\overline{p'_{true,w} p'_{true,y}} \approx 0$ is expected since $p'_{true,y} = 0$ in the free-stream. Hence, the root-mean-square of the background noise is estimated from the root-mean-square of the product of the fluctuating pressures at the wall and at the free-stream.

$$p'_{a_{rms}} \equiv \sqrt{\overline{p'_{a,w} p'_{a,y}}} \cong \sqrt{\overline{p'_w p'_y}} \tag{2.16}$$

Tsuji et al [9] reported that the noise level decreased with increasing Reynolds number and reached a constant value of about 1×10^{-3} of the free-stream dynamic pressure. The equation (2.16) indicates that acoustic noise may be estimated from the root-mean-square of pressure fluctuations in free-stream, if the noise at the wall is approximately the same as at free-stream. The root-mean-square of total pressure fluctuations in the free-stream measured with a bare Kulite sensor in the Northrop Grumman Research Wind Tunnel (RWT) was relatively constant at 0.25-0.3 psf, corresponding to 4×10^{-3} of the free-stream dynamic pressure at 70 psf (refer to Appendix C). Similar results were obtained from the Cal Poly 2×2 wind tunnel where the total pressure fluctuations were at around

0.1 psf, or 6×10^{-3} of the free stream dynamic pressure at the maximum flow speed of 110 mph.

The electrical noise level may be estimated from pressure fluctuations measured at wind-off zero condition. The correction can be made by subtracting mean-square of the noise level measured wind-off from the mean square of the data measured by the Kulite, and taking the square root of it.

$$\sqrt{\overline{p_t'^2}} = \sqrt{\overline{p_{t,k}'^2} - \overline{p_b'^2}} \tag{2.17}$$

The electrical noise level p_b' was estimated from the of the root-mean-square pressure readings at wind-off zero condition $\overline{p_b'^2} \approx \overline{p_{t,k}'^2}|_{U=0}$. The electrical noise measured at the wind-off condition by the Kulite was lower than free-stream noise, as expected, indicating that the acoustic and vibration noise was added to the electrical noise once the wind tunnel was operating. For the purpose of detecting laminar-to-turbulent transition, the acoustic and vibration noise was not corrected because it requires additional pressure measurement in free-stream, and because the noise level should remain relatively the same regardless of the flow states. Therefore, the wind-off zero electrical noise was used to correct the raw data using the above equation (2.17). The table below is a summary of noise levels observed at three testing locations.

Table 2.4 – Comparison of the root-mean-square of total pressure fluctuations at three testing locations.

Location	Sensitivity [V/psi]	Wind-off zero [mV]	Wind-off zero [psf]	Free-stream at 30 psf [mV]	Free-stream at 30 psf [psf]	Free-stream at 70 psf [mV]	Free-stream at 70 psf [psf]
RWT	3.31	3.34	0.145	6.96	0.303	6.32	0.275
2 ft x 2 ft WT	16.6	11.1	0.096	22.3	0.193	-	-
7 ft x 10 ft WT	23.3	7.00	0.044	-	-	-	-

Once the turbulent total pressure fluctuation data was obtained and corrected, the data was scaled so that the results were consistent. In turbulent boundary layers, velocity fluctuations in all parts of the flow contribute to the wall pressure fluctuations. The structure of the wall pressure field is very complex because turbulent velocity fluctuations at various distances from the wall are convected at different velocities as a result of the mean velocity distribution in the boundary layer. Consequently, no effective single scaling has been found to collapse the experimental data even when the additional complications of transducer spatial resolution effects are taken into account [30]. Since Corcos [12] presented the first scaling technique, numerous scaling methods were introduced using the power spectra analysis. The power spectral density represents the Fourier-transformed space-time correlation of the wall pressure. The resulting spectrum at a given wavelength or frequency ω is called single-point spectrum $\phi(\omega)$ and it represents the mean energy contained in that wave [30]. The power spectral density analysis is useful because the spectra can be divided into regions where a scaling factor that is specific to a given frequency range can be applied to minimize error. The spectra are generally subdivided into the low frequency, mid frequency, universal, and high

frequency ranges for this reason [30]. The low frequency range was identified by Farabee and Casarella [29] who found that free-stream dynamic pressure $q_\infty \left(= \frac{1}{2}\rho {U_\infty}^2 \right)$ was the appropriate pressure scaling for the region. Additional correction may be applied because the facility related noise contaminates the pressure data in this range. Keith [26] reported that the pressure scale q_∞ is acceptable for the mid frequency range, while others found that scaling with σ_w gave better results. The inner variable σ_w is commonly used in high frequency range, but the pressure attenuation due to finite transducer size is prominent and requires further correction. Since the mean-square pressure is an integral of all frequencies, and no single scaling is satisfactory, it is subject to a significant error.

$$\overline{{p_s'}^2} = \int_{-\infty}^{\infty} \phi(\omega)\, d\omega \tag{2.18}$$

The root-mean-square static pressure fluctuations have traditionally been scaled with shear stress at the wall, σ_w, as it is the mutual scaling factor from the mid to high frequency ranges. In recent publications, however, the scaling factor q_∞ was more commonly used [30].

Other factors should also be taken into consideration when designing a sensor-probe configuration of the Kulite pressure transducer. According to Shaw [31], the non-dimensional error for the wall pressure measurement is a function of the viscous wall unit d^+, the pinhole diameter d_{pin}, the hole depth h, and the diameter of the connection to the sensor d_c, and characteristic length scale of the facility L_f.

$$\frac{\Delta p_w}{\tau_w} \approx f\left(d^+, \frac{d_{pin}}{L_f}, \frac{h}{d_{pin}}, \frac{d_c}{d_{pin}}\right) \tag{2.19}$$

For our instrumental design, d^+ and d_c/d_{pin} were chosen to be analyzed. Since a total pressure probe was used instead of a static pressure probe, probe diameter d was used in place of d_{pin}. Although the aspect ratio h/d is irrelevant for the total pressure probe design, the corresponding ratio L/d, where L is the distance from the tip of the total pressure probe to the Kulite sensor face, was measured and included in the analysis.

The dimensional analysis of the dynamic pressure measured by a total pressure probe of a particular geometry can be expressed in terms of the following variables,

$$C_p = f\left(\breve{\emptyset}, Re_d, M, \frac{\overline{u'^2}}{U_\infty^2}, \alpha, \frac{y}{d}\right), \tag{2.20}$$

where $\breve{\emptyset}$ is incoming flow angle relative to the probe, Re_d is the local probe Reynolds number, M is the Mach number, $\overline{u'^2}/U_\infty^2$ is turbulent intensity, α is a parameter that relates to the viscosity of a fluid, and y/d is proximity to surface [32]. The most relevant are incoming flow angle $\breve{\emptyset}$ and proximity parameter y/d, while others are expected to stay relatively constant throughout the experiments. To avoid error due to angle $\breve{\emptyset}$, the probes were carefully placed on the surface in-line with the mean flow while the effect of proximity was investigated as a part of initial testing at the Northrop Grumman Research Wind Tunnel (RWT). The objective of the initial testing was to evaluate the Kulite sensor's ability to measure total pressure fluctuations with free-stream dynamic pressure up to 70 psf (see Appendix C for the details). The result in figure 2.5 shows the difference in total pressure measured by the Preston tube and the average pressure measured by a bare Kulite, both placed on the surface of the RWT test section. The higher pressure readings by the Kulite sensor indicate that the proximity of the Kulite sensor to the surface increases the average pressure readings.

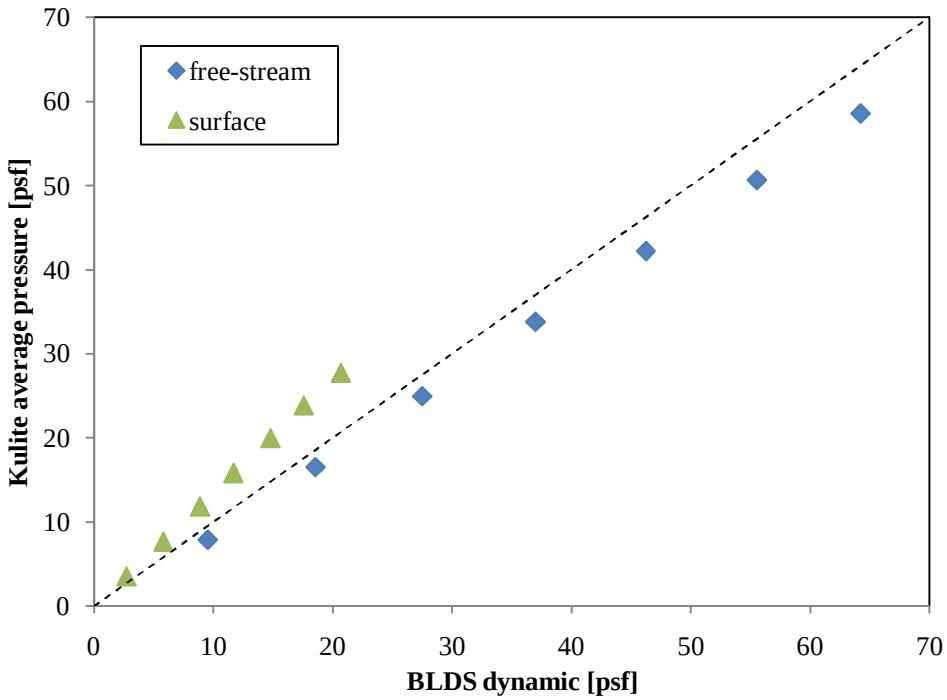

Figure 2.5 – Bare Kulite sensor average pressures plotted against BLDS dynamic pressures in RWT test section.

The sensor geometry was also of concern because the finite size of the pressure transducer influences the flow patterns in the region of stagnation point. Disturbances to the flow are the most prominent at the edge, which is where the sensor holes are located as the photographs of the Kulite sensor face reveal in figure 2.6.

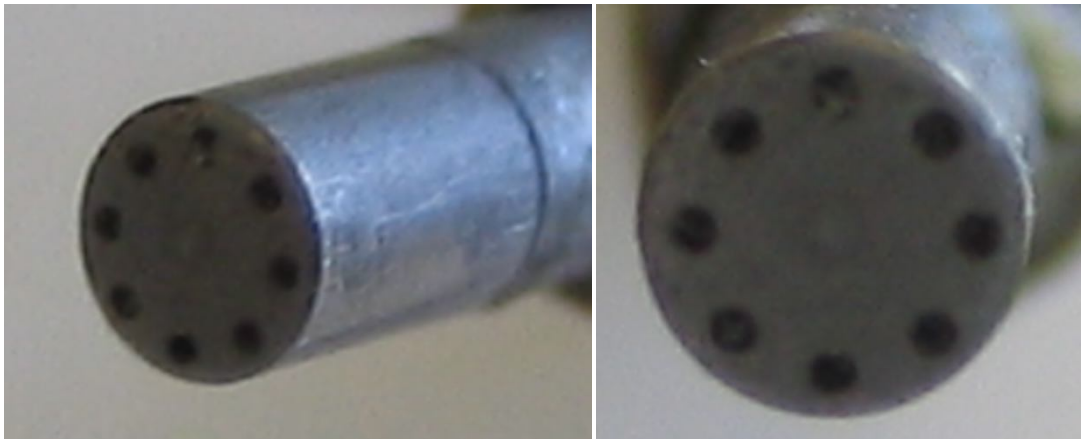

Figure 2.6 – Kulite sensor face's geometry.

The small ratio of inner to outer probe diameter d/D can generally be sought to alleviate the error, but $d/D = 0.6$ is generally accepted for square-ended total pressure probe [32]. It is evident that the centers of the sensor holes are located, where the inner to outer probe diameter d/D is greater than 0.6 ($d/D \approx 0.8$). Therefore, the effect of the bare Kulite sensor's geometry was estimated by comparing the average pressure measured by a bare Kulite sensor to the dynamic pressure measured by a total pressure probe of the BLDS at the initial testing at the RWT. A bare Kulite sensor was interfaced with the BLDS and placed in free-stream to eliminate the error related to the proximity of the sensor to the wall. The result in figure 2.5 above displayed that the average pressure from the bare Kulite sensor was consistently lower than dynamic pressure in free-stream by about 10% suggesting that the Kulite sensor's geometry had some affect. It is also possible, however, that the lower pressure experienced by the Kulite may be explained by the reference pressure of the Kulite being slightly higher than the static pressure. To further investigate the issue, the application of a shroud was used to test the former, and the latter was tested by connecting the backing port to the static pressure. The tested parameters of the Kulite sensor-probe configurations are summarized in table 2.5.

Table 2.5 – Summary of parameters tested. Refer to Kulite configurations in table 3.4.

Tested parameters	Dimensionless form	Configuration used	Description
Sensor geometry	*d/D*	#3	Bare Kulite measurements compared to Shroud with no extension (l=0)
Probe length, l	*l/d*	#2, #3, #4, #5	Probe or shroud length varied.
Total length, L	*L/d*	#2, #3, #4, #5	Probe or shroud length varied.
Plumbing diameter, d_c	d_c/d	#2, #3, #4, #5	Used plumbing with different diameters.
Probe diameter, d	d^+	#1, #2, #5	Viscous wall unit calculated for each configuration and compared.

The experiments were performed in the wind tunnel with 2 ft square test section located at the Cal Poly Mechanical Engineering Fluids Lab in San Luis Obispo. The wind tunnel is capable of attaining flow velocities up to 110 mph, corresponding to a nominal maximum free-stream dynamic pressure of 30 psf. All testing was carried out in the 2' test section with a 48 in elliptical nose flat plate mounted in the middle of the test section. The elliptical leading edge provides for laminar attachment and initial development of the boundary layer over the central span of the plate. The Kulite sensor was interfaced with the PTDS or the BLDS unit and was placed on the surface of the flat plate in various configurations. The distance, x, was measured from the leading edge of the flat plate to the tip of a probe. The schematic of the Cal Poly wind tunnel is shown below.

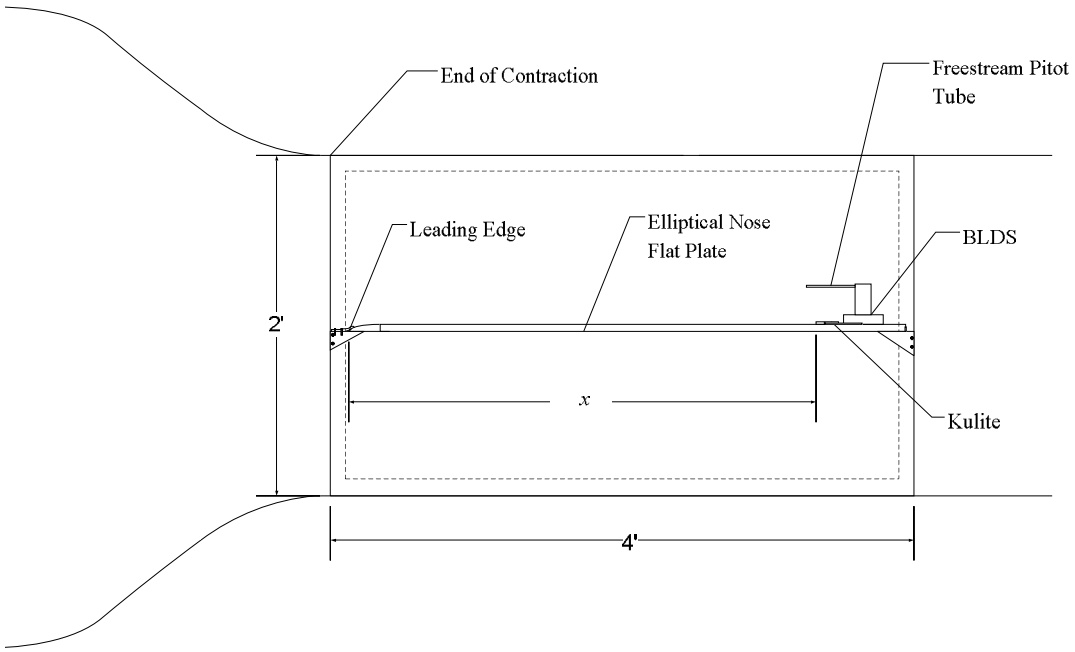

Figure 2.7 – Cal Poly 2x2 wind tunnel testing configuration.

Figure 2.8 – 2 ft x 2 ft wind tunnel with an elliptical nose flat plate installed in the test section.

To ensure that the flow was turbulent, the BLDS unit was placed 35.5 inches aft of the leading edge of the flat plate. The distance was measured from the leading edge of the flat plate to the tip of a total pressure probe. Boundary layer velocity profiles at the test section were measured using the BLDS with traversing the total pressure probe away from the surface. The profiles below confirmed that the boundary layer were turbulent for all cases except for the lowest speed of 20ft/s. The flow characteristics for each condition are summarized in table 2.6.

Figure 2.9 – BLDS unit placed x = 35.5 in AFT leading edge of the flat plate.

Table 2.6 – Boundary layer characteristics of flow over flat plate in the Cal Poly 2 ft x 2 ft wind tunnel at x = 35.5 in.

Dynamic Pressure, q_e [psf]		State	U_e [ft/s]	U_e [mph]	δ [inch]	θ [inch]	Re_θ	C_f
Nominal	Actual							
2	1.78	Laminar	19.07	1.2	0.17			-
7.5	7.44	Turbulent	80.0	54.5	0.29	0.0389	1370	0.00311
17	17.13	Turbulent	121.3	82.7	0.40	0.0393	2830	0.00265
30	30.44	Turbulent	162.5	110.8	0.42	0.0398	3900	0.00247

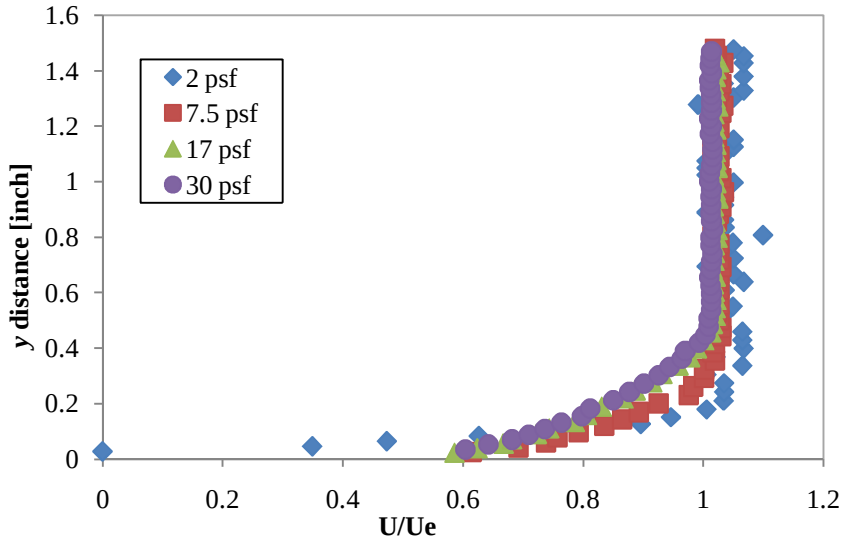

Figure 2.10 – Boundary layer profiles for flows with free-stream dynamic pressures of 2, 7.5, 17, 30 psf in the Cal Poly 2 ft x 2 ft wind tunnel, *x* = 35.5 in.

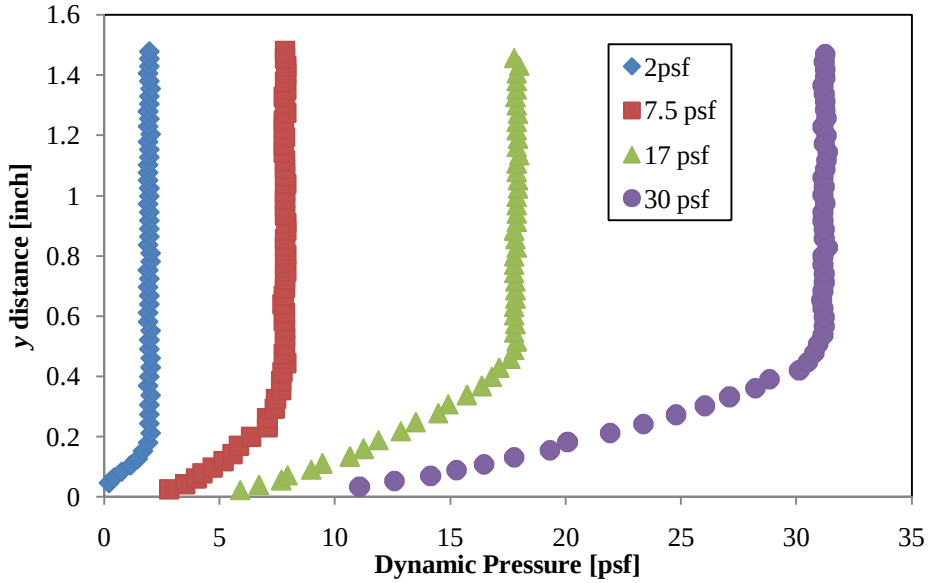

Figure 2.11 – Dynamic pressures in the boundary layer for flows with free-stream dynamic pressures of 2, 7.5, 17, and 30 psf in the Cal Poly 2 ft x 2 ft wind tunnel, *x* = 35.5 in.

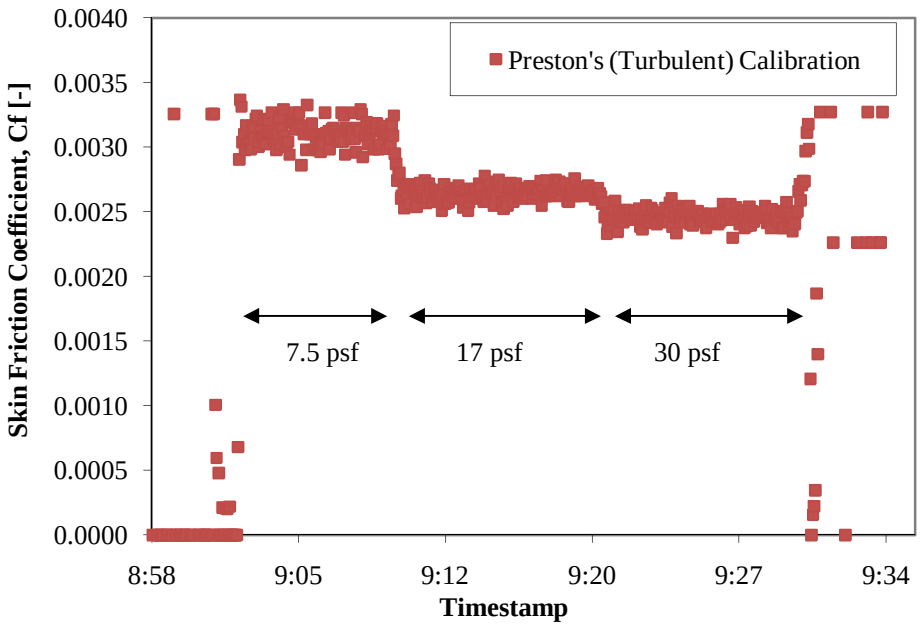

Figure 2.12 – Skin Friction in the Cal Poly 2 ft x 2 ft wind tunnel, x = 35.5 in. Preston's calibration was used to determine skin friction coefficient, C_f.

The Reynolds numbers based on the momentum thicknesses were calculated to evaluate the unsteady wall pressure. The following relationship was used to approximate the momentum thickness of a turbulent boundary layer on a flat plate [24].

$$\frac{\theta}{\delta} \approx \frac{7}{72} \tag{2.21}$$

The momentum thickness Reynolds numbers for the test conditions ranged from $1370 \leq Re_\theta \leq 3900$, which is in the same range as the previous experiments where the transducer requirements were set [8] [26]. Hence, it was assumed that the same transducer requirements apply for our sensor selection. The Preston's calibration method was used to calculate skin friction σ_w, and the skin friction coefficient was then found from the definition:

$$C_f = \frac{\sigma_w}{q_e} \tag{2.22}$$

The skin friction coefficient at nominal 30 psf free-stream dynamic pressure was about 0.0025, which agreed with values obtained from previous experiments.

After it was confirmed that the flow at the location was turbulent, five different probe configurations of the Kulite sensor were tested. The variations in parameters included probe length *l*, length *L* measured from the tip of a probe to the Kulite sensor face, and probe or shroud diameter *d* based on ID. In addition, the reference pressure was fixed for the configurations #4 and #5. The schematics of the sensor-probe configurations are summarized in table 2.7. All testing was done in the Cal Poly 2x2 wind tunnel with the Kulite probe as a satellite port of the BLDS at x = 35.5 in up to the maximum free-stream dynamic pressure of 30 psf, equivalent speed of approximately 110 mph. The tip of the total pressure probe was aligned with the tip of the Preston tube, and the side holes of the static probe whenever it was applicable. In our analysis, the root-mean-square of the total pressure fluctuation was scaled with local dynamic pressure. The detailed results of all configurations can be found in Appendix D; key results will be presented next.

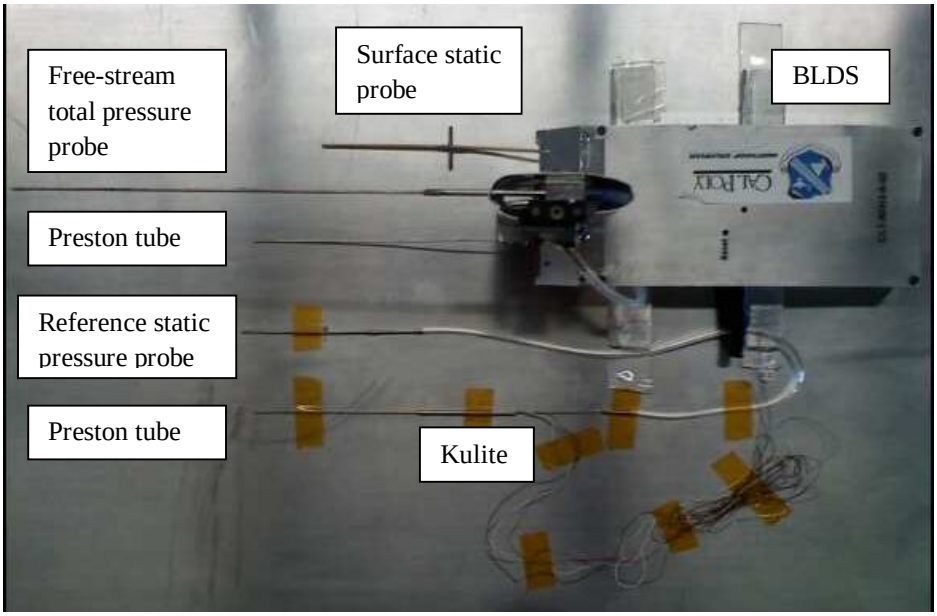

Figure 2.13 – A testing configuration on the flat plate in Cal Poly 2 ft x 2 ft wind tunnel. The Kulite probe was aligned with the static probe at x =35.5 in.

Table 2.7 – Summary of configurations and test variables.

Test Name	Kulite Configuration	Variables		Shroud	P_{ref} Location	d	d/δ	d^+
1. Bare Kulite	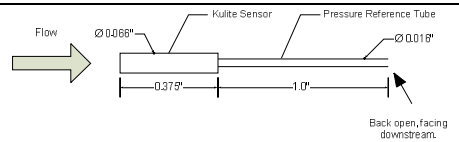	-		None	Vary	0.022"*	0.160	76
2. Probe via plastic tube	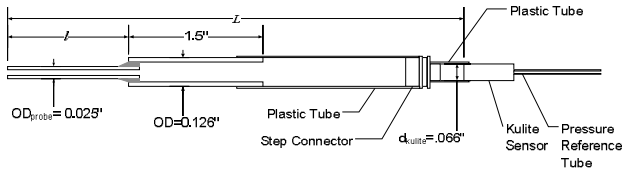	0.75" < l < 2.5" 44 < l/d < 147 338 < L/d < 441		None	Vary	0.017"	0.040	57
3. Shrouded	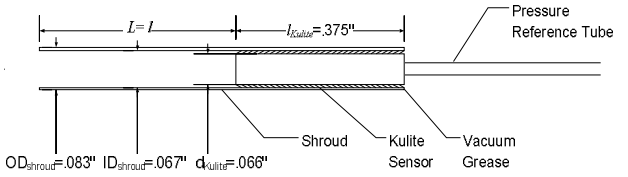	0" < l < 5.0" 0 < l/d < 75 0 < L/d < 75		Vary	Vary	0.067"	0.160	226
4. Shrouded with fixed P_{ref}	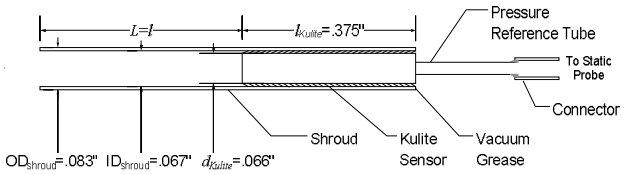	2" < l < 5.0" 30 < l/d < 75 30 < L/d < 75		Vary	Fixed	0.067"	0.160	232
5. Probe via shroud with fixed P_{ref}	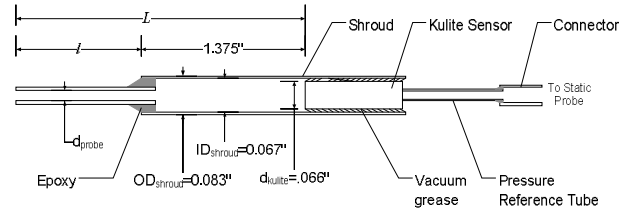	(1)	1.25" < l < 3" 63 < l/d < 150 131< L/d<219	Fixed	Fixed	0.048	0.048	69
		(2)	1.25" < l < 3" 104 < l/d < 250 218<L/d< 365			0.029	0.029	41

*effective diameter based on the eight sensing holes

After testing five different sensor-probe configurations, all test parameters were evaluated for their effect on the total pressure fluctuations. The effect of the sensor geometry was first examined by comparing the bare sensor result to the one with a shroud. The shroud was applied to the Kulite sensor with the edge of the shroud aligned to the sensor face with no extension. They were both placed flush on the flat plate with the reference pressure not fixed. The result in figure 2.14 shows that the root-mean-square pressures slightly increased when the shroud was applied to the sensor. After the root-mean-square pressure was scaled with the local free-stream dynamic pressure, however, the difference became small especially at high free-stream dynamic pressures. The application of the shroud gave an approximate inner to outer probe diameter ratio of about $d/D \approx 0.7$, close to the recommended range of $d/D \approx 0.6$ for a total pressure probe. A thicker walled shroud may increase the resolution, but errors associated with other geometry concerns such as flow disturbance might increase due to the larger size of the probe.

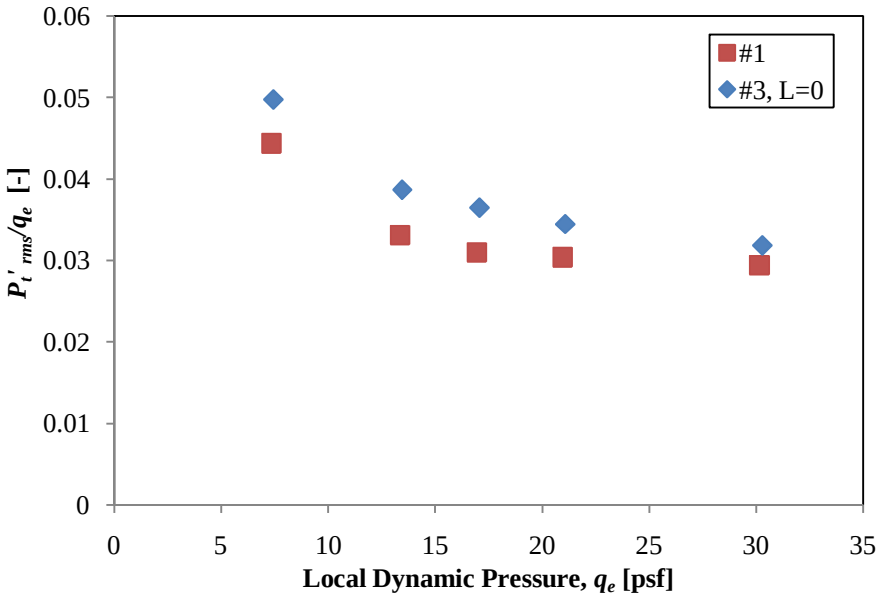

Figure 2.14 – The effect of the shroud with no extension on the total pressure fluctuations.

The following analysis were conducted with data obtained with a nominal free-stream dynamic pressure of 30 psf, corresponding to a free-stream speed of approximately 50 m/s or 110 mph. Below figure 2.15 shows the normalized probe lengths *l/d* and their corresponding total pressure fluctuation values. The data were scattered, so no general correlation was possible concerning the influence of probe length on the total pressure fluctuations. When analyzed for each configuration, the total pressure fluctuations decreased with increasing probe length *l*, except for the shrouded probe (configurations #3 and #4).

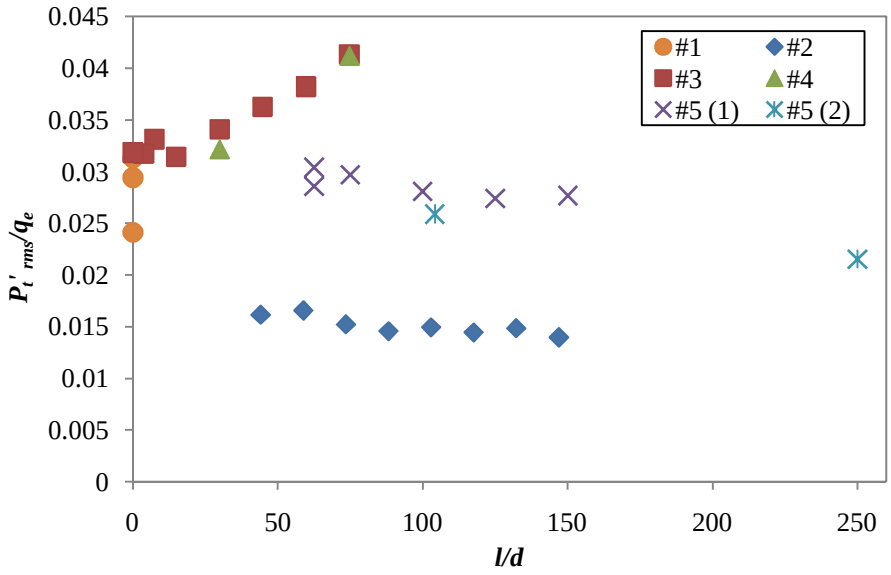

Figure 2.15 – The effect of probe length on root-mean-square of total pressure fluctuations.

The behavior exhibited by the shrouded probe where root-mean-square of the total pressure fluctuations increased with increasing probe length may be explained by resonance formation inside of the shroud. The resonance of a closed cylinder is defined as following [33],

$$f = \frac{nc}{2(l + 0.6d)} \tag{2.23}$$

where c is the speed of sound. For the range of shroud length l that was tested, the resonance frequency of the shroud for the first three harmonics were found within the range of 164 $Hz < f <$ 9,000 Hz, which might have affected the total pressure readings because the resonances are in the same frequency range as the turbulent pressure fluctuations. Although the exact reason for the increasing total fluctuations with the increasing shroud length was not resolved, it was concluded that the application of shroud to the sensor causes erroneous results. However, such error was not observed when a probe was attached to the shroud (configurations #5).

Next, the effect of total length *L*, which includes not only the probe length *l* but also the connecting shroud or tubing length, was examined. The total length was normalized by diameter *d* for the analysis. More data points are needed for a definitive conclusion, but results roughly suggest that the total pressure fluctuation measured by the sensor decreases linearly with increasing *L/d*.

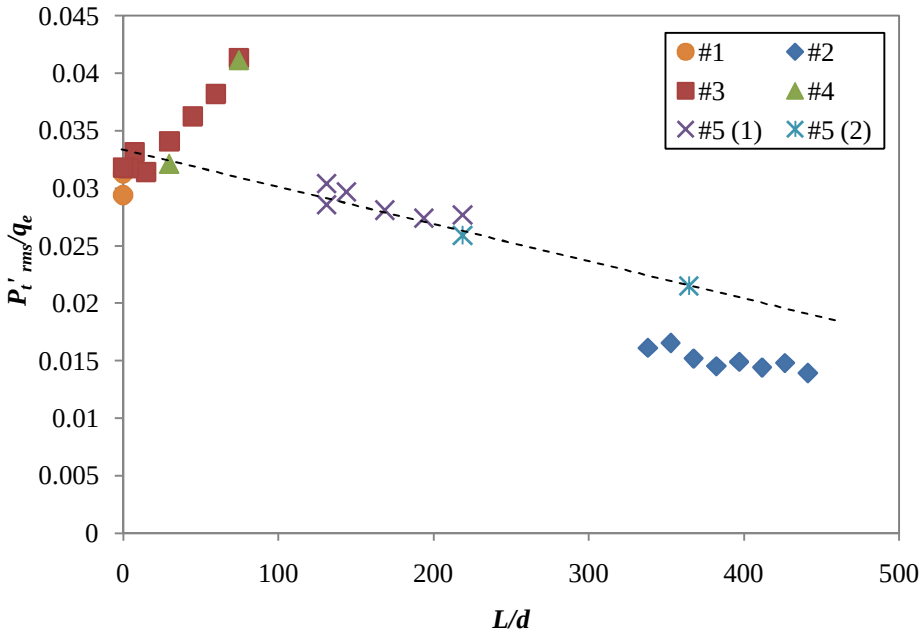

Figure 2.16 – The effect of total length from the tip of the probe to the sensor face.

The data obtained from the test #2 didn't fit to the curve in figure 2.16, however, and the cause of the error was investigated. All points on the trend line, including the *L/d* = 0 data of the test #3, utilized rigid plumbing between the sensor and the probe. The configuration of the test #2, on the other hand, was plumbed with flexible silicon tubing. It is likely that the elasticity associated with the silicon tubing damped the pressure fluctuation, resulting in lower values. The photograph of the sensor-probe configuration with the silicon tubing is shown in figure 2.17.

Figure 2.17 – Sensor-probe configuration for testing #2.

The diameter of connecting tube, d_c, was then analyzed. A decreasing trend of the pressure fluctuation was observed with the increasing dimensionless diameter of the connection probe d_c/d. The data points from the configuration #2 were again out of range, implying the significance of the error caused by the connecting silicon tube.

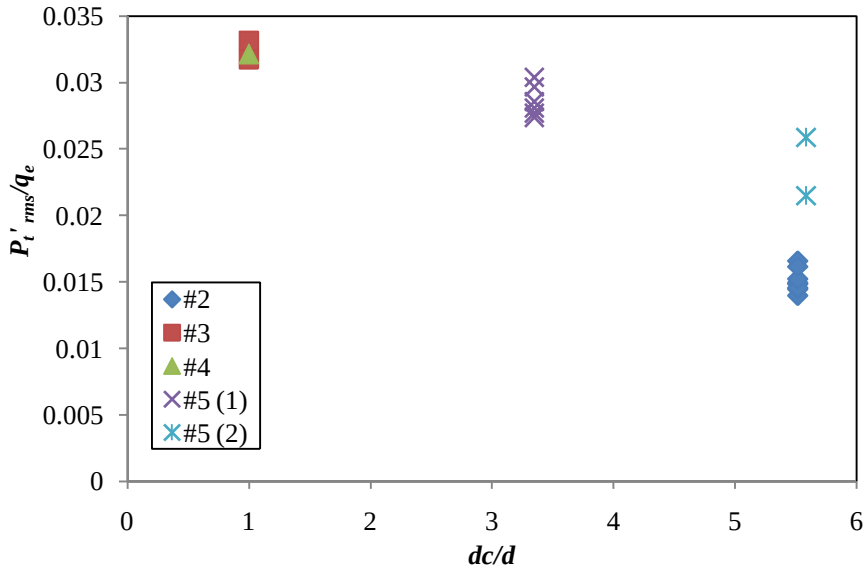

Figure 2.18 – The effect of plumbing diameter on the pressure fluctuation.

Finally, the normalized probe size was evaluated. The test results from configuration #3 were removed from the analysis because of the unresolved error. The rest of the results were superimposed on the figure prepared by Schewe [14]. The original

figure was scaled up three times based on the prediction that the total pressure fluctuation is expected to be three times larger than the static pressure fluctuation as discussed in chapter one. Although data were obtained from different sensor-probe configurations and no data was collected for $d^+ > 100$, the numbers somewhat fitted to the trend established by Schewe. The results in figure 2.19 suggest that the Kulite sensor adequately resolved small eddies in the flow when used bare or configured with probes with diameter less than $d^+ \approx 80$. It also shows that the Kulite results agreed with what was expected from the literatures, and the root-mean-square of total pressure fluctuations is approximately three times larger than static pressure fluctuations as calculated. It should be noted that the effective diameter of the bare Kulite sensor was calculated from the ratio of the total area of the eight sensing holes to the Kulite sensor face area.

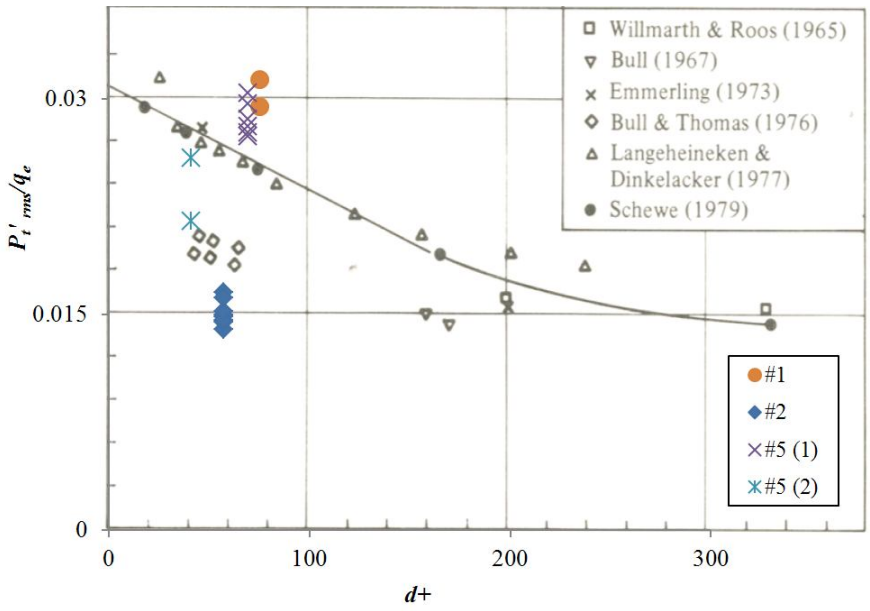

Figure 2.19 – The effect of the normalized probe size on the total pressure fluctuation. The data obtained were superimposed on the figure presented by Schewe [14].

In summary, the results from the testing demonstrated that the sensor-probe configuration should use the shortest possible plumbing, if necessary. The diameter of the connecting tube or shroud should also be small to prevent errors. The use of a shroud as a total pressure probe should be avoided because resonance may be formed inside of the shroud, but attaching a smaller diameter probe might relieve the error. Above all, the measurement of the root-mean-square of total pressure fluctuation was proven to be advantageous because even the least value recorded, $p'_{t_{rms}}/q_e \approx 0.015$, is greater than the surface static pressure fluctuation measured with the smallest transducer.

3. WIND TUNNEL TEST RESULTS

After the effects of sensor-probe configurations of the Kulite were established, wind tunnel testing was conducted to demonstrate the ability of the device to distinguish a laminar boundary layer from a turbulent boundary layer. The testing in the 2 ft x 2 ft wind tunnel consisted of three measurements. First, the Kulite sensor was tested inside of a boundary layer in both laminar and turbulent conditions in the 2 ft x 2 ft wind tunnel. Next, the Kulite sensor was tested in the proximity of laminar-to-turbulent transition to determine the state of the boundary layer that developed on the surface of an elliptical nose plate in the wind tunnel. Finally, the total pressure fluctuation of tripped flow was compared to the non-tripped turbulent flow. In addition, unsteady pressure measurements were conducted in cooperation with Northrop Grumman Corporation in their 7 ft x 10 ft wind tunnel located in Hawthorne, CA.

Table 3.1 – Test matrix for 2 ft x 2 ft wind tunnel evaluations.

Test	Configurations used	Location	Reynolds Number, Re_x	Mach Number
Laminar/turbulent profile	Kulite & BLDS	x = 6.25 in (laminar) x =35.5 in (turbulent)	1.72e6-3.40e6	0.14
Transition	Kulite & PTDS	4 in < x < 24 in	3.83e5-2.30e6	0.14
Tripped flow	Kulite & PTDS	x = 5 in	4.78e5	0.14

For the initial test, the Kulite sensor was operated as a satellite sensor of the BLDS unit to take total pressure fluctuation measurements in laminar and turbulent boundary layers. The Kulite sensor was plumbed to 0.032 in diameter probe via silicon tubing to allow vertical movement of the probe. The probe was traversed vertically away from the surface of the flat plate while recording total pressure fluctuations. The distance from the

surface of the flat plate to the center of the probe tip was denoted as *y*, and it is shown in the figure 3.1. The BLDS unit was placed at a location *x* = 35.5 in on an elliptical nose flat plate for the turbulent measurement while the laminar boundary layer measurement was carried out at *x* = 6.25 in. Two profiles were taken at each free-stream velocity to ensure that the data obtained were reliable and repeatable. Previous experiments have shown that connecting the Kulite sensor with a plastic tubing caused damping, resulting in lower pressure fluctuation values. Thus, we expect the normalized turbulent fluctuation pressure to be on the order of $p'_{rms}/q_e \approx 0.015$ at the wall for the nominal free-stream dynamic pressure of 30 psf.

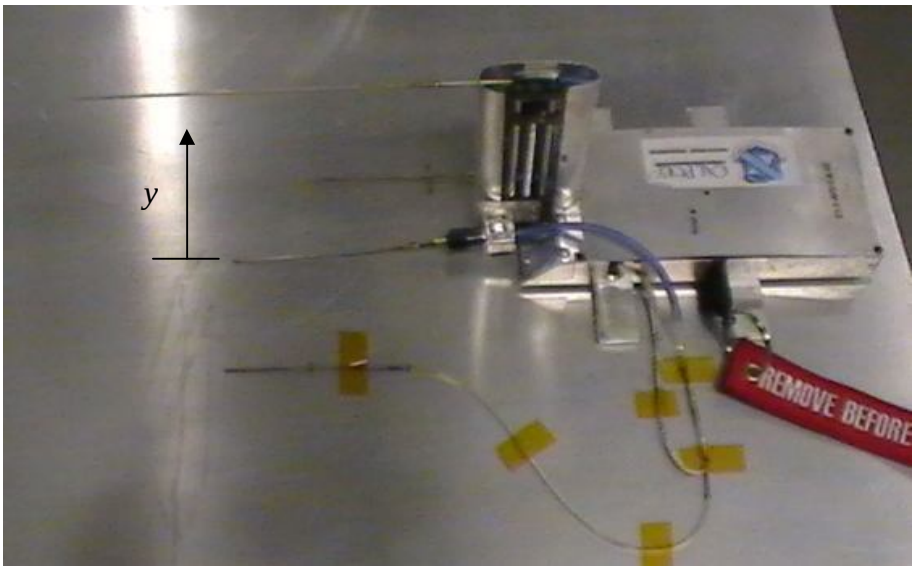

Figure 3.1 – Kulite sensor was configured with BLDS to take boundary layer measurement.

The average pressure measurement taken by the Kulite probe was first examined. From the velocity profile, the boundary layer thickness for the laminar flow was determined to be approximately 0.05 inches while the boundary layer thickness of the turbulent boundary layer was 0.42 inches at the nominal free-stream dynamic pressure of 30 psf.

The turbulent boundary layer velocity profile was then compared in figure 3.2 to the velocity profile previously obtained by using a total probe at the same location. The velocity profile of the Kulite probe is shifted by 10%, indicating that the dynamic pressure sensed by the Kulite probe was higher than what was measured by the total probe. Since the error is consistent throughout the boundary layer, it was speculated that the zero shift of the Kulite sensor mainly contributed to the error. It shows, however, that the Kulite can be used to take average pressure measurement if the error was corrected.

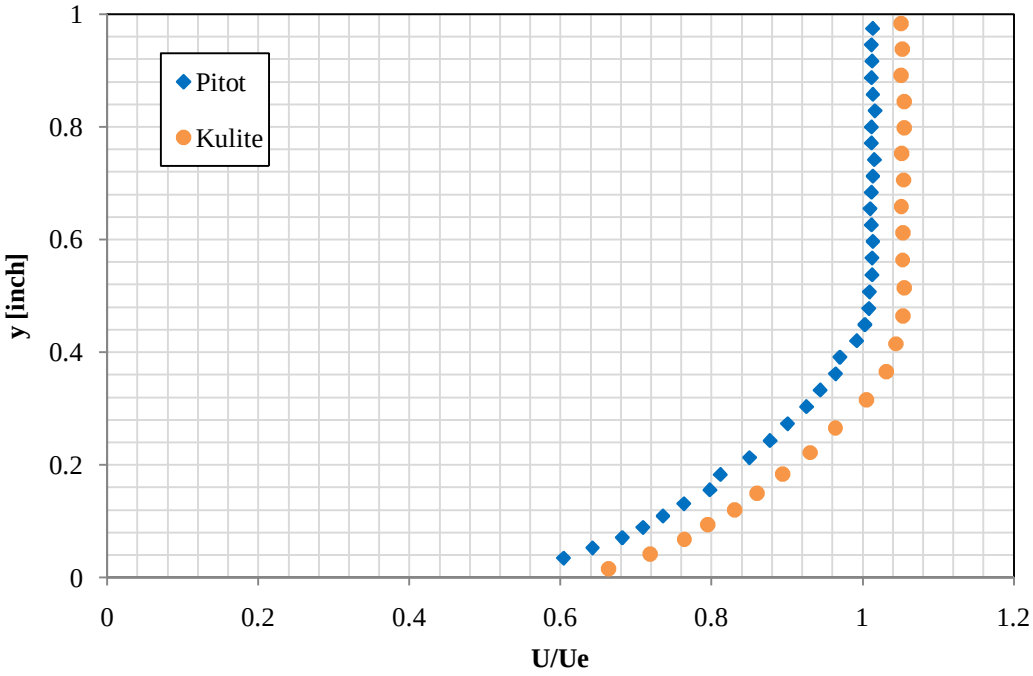

Figure 3.2 – *U/Ue* vs. *y* measured with total and Kulite probes in 2 ft x 2 ft wind tunnel at *x* = 35.5 in.

The distributions of the total pressure fluctuations are shown in figure 3.3 and 3.4, respectively. The vertical distance y was scaled with the boundary layer thickness δ of test locations to aid the comparison between the two. The local free-stream dynamic pressure measured by the total probe of the BLDS was used to normalize the root-mean-

square total pressure fluctuations. Noise calibration was done by subtracting the mean square of total pressure fluctuations at wind-zero condition from the mean square of the data collected to minimize the error on low Reynolds number flows as discussed earlier. The distributions of the total pressure fluctuations between the two states are noticeably different. The distinction can easily be made because the normalized root-mean-square total pressure fluctuations in laminar flow were confined in the range below 0.01, while the data points were scattered up to 7% of the local dynamic pressure in the turbulent boundary layer. The normalized root-mean-squared pressure fluctuations in the turbulent boundary layer close to the surface were approximately $0.012 \leq p'_{t_{rms}}/q_e \leq 0.020$ for the maximum 30 psf free-stream dynamic pressure, as it was expected. Interestingly, the magnitudes of the pressure fluctuation in turbulent boundary layer were somewhat constant up until 0.5δ of and then decreased further from the surface. This can work advantageously because it is now possible to elevate the sensor without altering the results. As discussed earlier, sensing holes located around the periphery of the Kulite sensor face caused errors in total pressure measurements. The possible application of the shroud flush to the sensor face should not affect the results as long as the sensor stays within 0.5δ, where the root-mean-square values of turbulent fluctuations do not vary much. Regardless, the profiles of the total pressure fluctuations successfully illustrated that the Kulite sensor can be used to distinguish the laminar or turbulent state of a boundary layer; turbulent flows provided $p'_{t_{rms}}/q_e > 0.015$ whereas $p'_{t_{rms}}/q_e > 0.01$ for laminar flow.

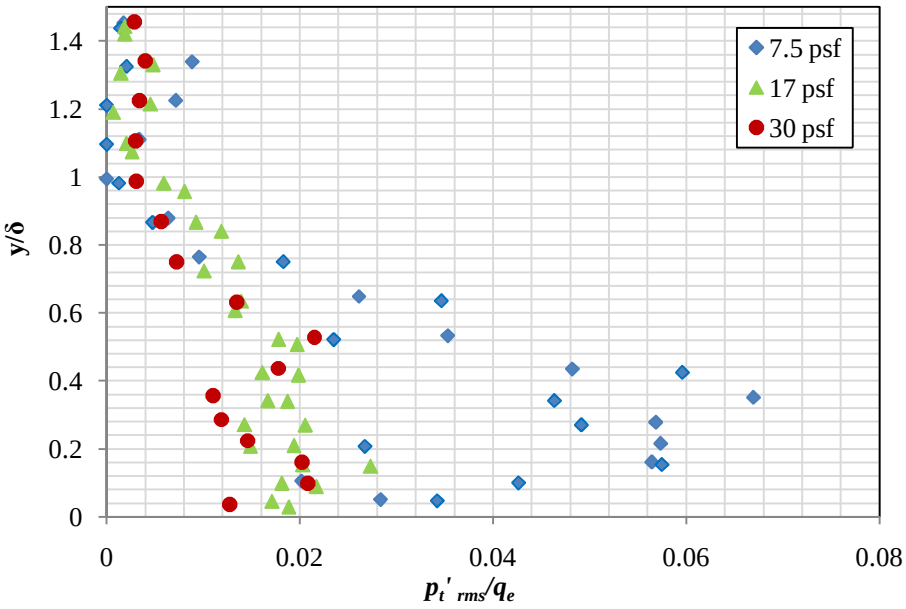

Figure 3.3 – The distribution of normalized total pressure fluctuation in a turbulent boundary layer at x = 35.5 in.

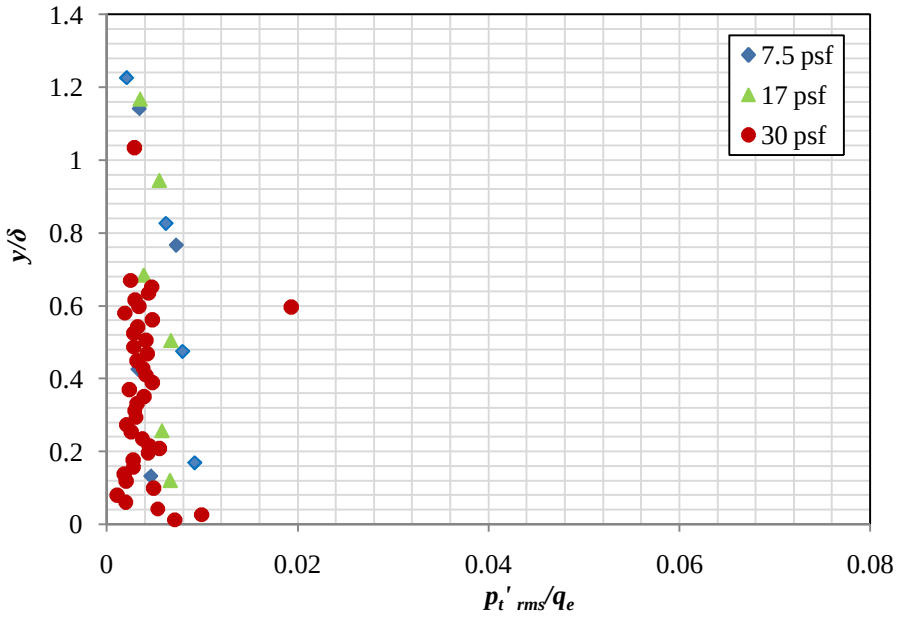

Figure 3.4 – The distribution of normalized total pressure fluctuation in a laminar boundary layer x = 6.25 in.

The previous results have proven that the unsteady total pressure distribution in the boundary layer measured by the Kulite sensor can be used to distinguish the laminar and the turbulent boundary layer flow. The Kulite sensor was then tested to diagnose the location of transition. The sensor-probe configuration utilized for this transition measurement is shown in figure 3.5. The sensor side of the Kulite pressure transducer was plumbed to the 0.032 in diameter probe via 2.5 in clear vinyl tubing with 1/16 in ID, and the backing pressure port was connected to a static probe. The Kulite was integrated with the PTDS and was attached on the elliptical nose flat plate in-line with the free-stream direction of the tunnel section as shown in figure 3.6. The local free-stream dynamic pressure was measured with a total pressure probe located 3 inches above the surface. The entire testing was conducted with the wind tunnel running at the maximum speed of 110 mph, which corresponds to 30 psf free-stream dynamic pressure.

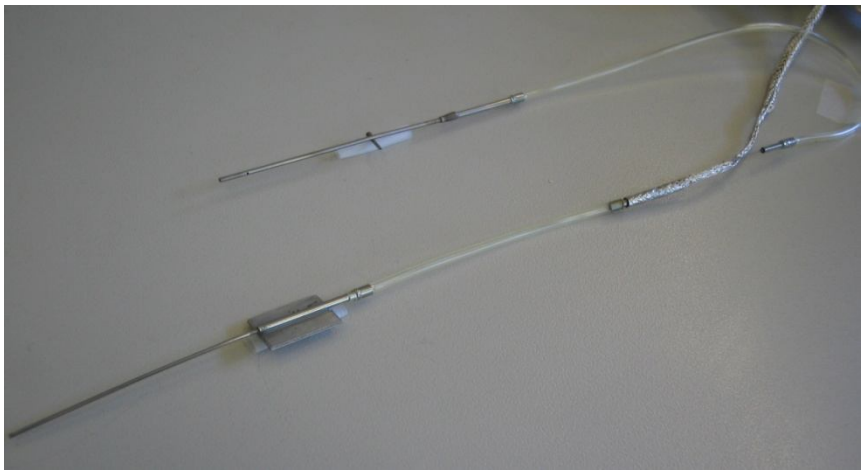

Figure 3.5 – The sensor-probe configuration of the Kulite pressure transducer used to measure root-mean-squared total pressure fluctuation in transition.

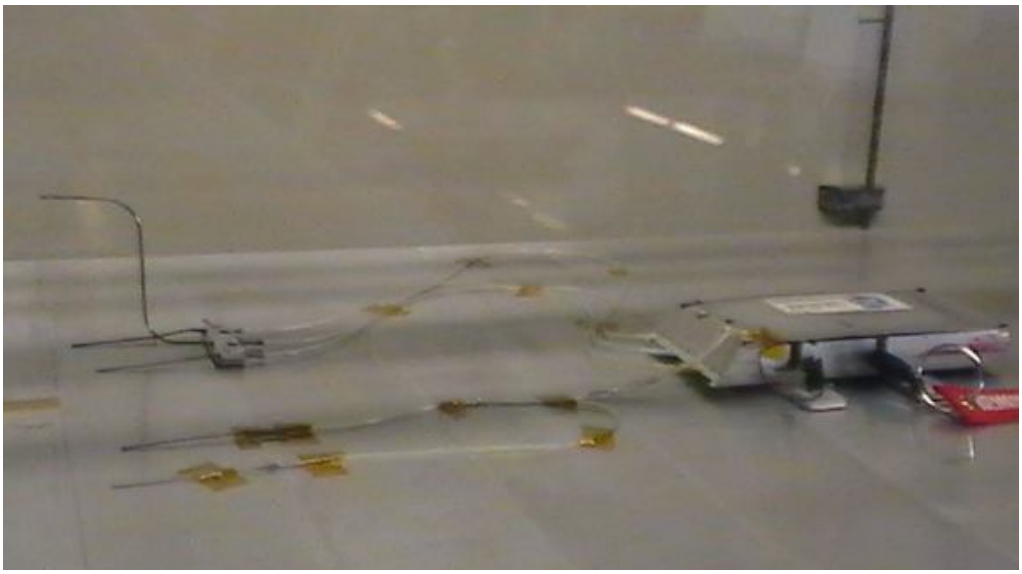

Figure 3.6 – PTDS and the Kulite installed on flat pate in the 2 ft x 2 ft wind tunnel test section.

The data was taken from 4 < x < 12 inches by incrementing forward by one inch per run. An extra data point at x = 24 in was also included to represent a fully developed turbulent flow. The starting location was chosen to ensure the laminar boundary layer condition as the previous velocity profile measurement x = 6.5 in revealed that the flow was laminar with approaching flow velocity at 110 mph. A stethoscope, as shown in figure 3.8, was also used to supplement the assessment of flow states. A laminar boundary layer can be distinguished from a turbulent boundary layer by listening to the flow because the pressure fluctuations generated by turbulence create audible noise. The stethoscope was moved along the centerline of the flat plate to locate the transition. By listening to the flow and recording the noise level, it was confirmed that transition was occurring somewhere between 8 < x <10 inches, or 0.16 < x/c <0.21.

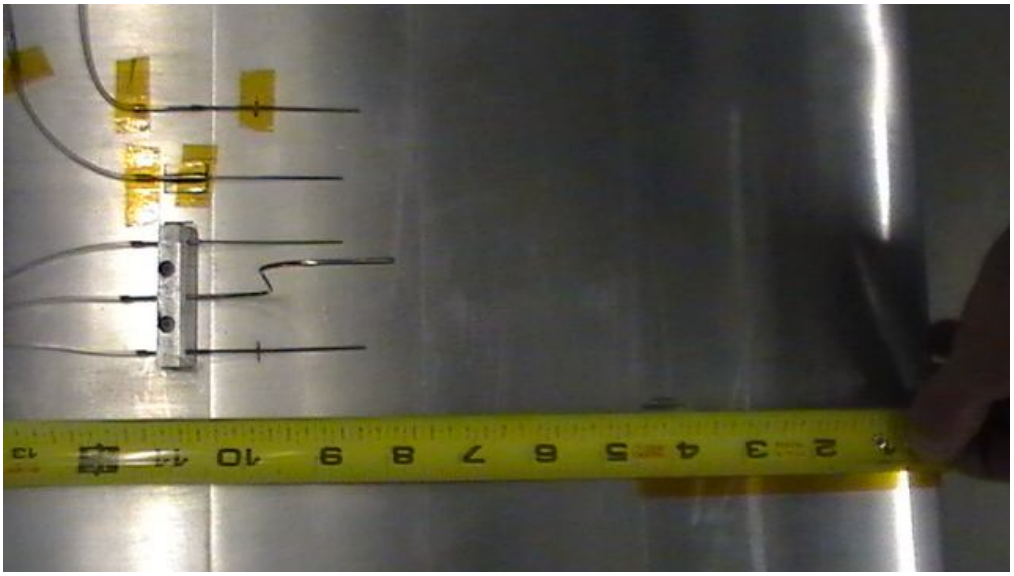

Figure 3.7 – The distance *x* was measured from the leading edge of the elliptical nose flat plate to the tip of the Kulite probe.

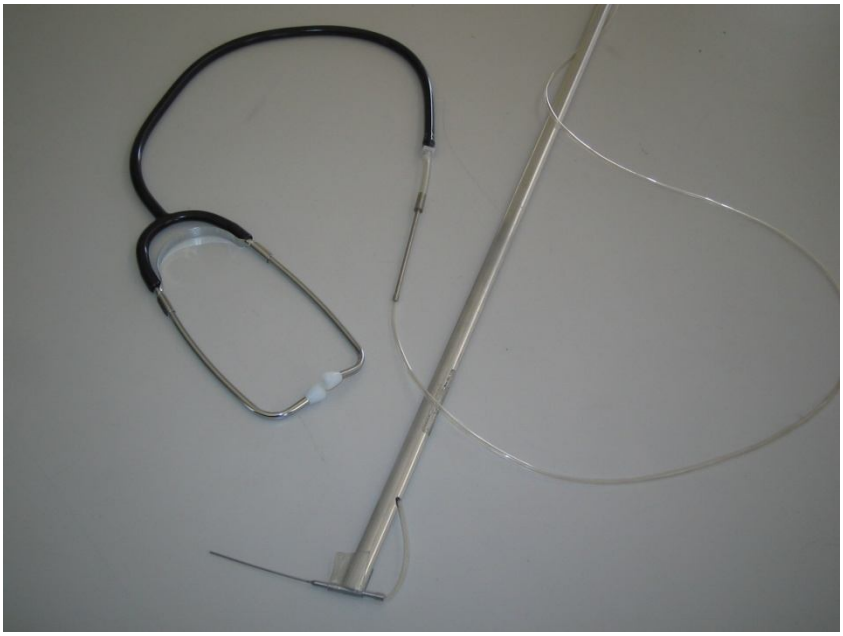

Figure 3.8 – A stethoscope used to evaluate the state of boundary layer.

The result in figure 3.9 shows the root-mean-square of total fluctuating pressures measured at eleven locations along the centerline of the flat plate, which were normalized by the local free-stream dynamic pressure. The root-mean-square pressures were below

1% of the local dynamic pressure in the laminar boundary layer where non-dimensional chord length $x/c < 0.18$. The dramatic increase in root-mean-square pressure to about 4% of local dynamic pressure was observed at a location 9 inches ($x/c = 0.19$) from the leading edge, where the stethoscope analysis indicated that laminar-to-turbulent transition was occurring. The root-mean-square pressures stayed relatively large for the next two data points, but subsided at $x/c > 0.25$. From there on, the Kulite recorded the root-mean-square of the total pressure fluctuations of about 2% of local dynamic pressure until $x/c = 0.5$ where the flow was fully turbulent. Two conclusions were drawn from the result. First, the magnitude of root-mean-square pressure fluctuations in the laminar boundary layer was adequately different from those in the fully developed turbulent flow so that it could be used to distinguish the flow states between the two. Next, the root-mean-square pressure fluctuations recorded in the laminar-to-turbulent transition region was significantly higher than those in either laminar or turbulent boundary layers. This is an exciting result because it brings out a possibility that the total pressure fluctuation measurement can not only discriminate a turbulent boundary layer from a laminar boundary layer, but can also differentiate the region where the flow is transitioning from laminar to turbulent.

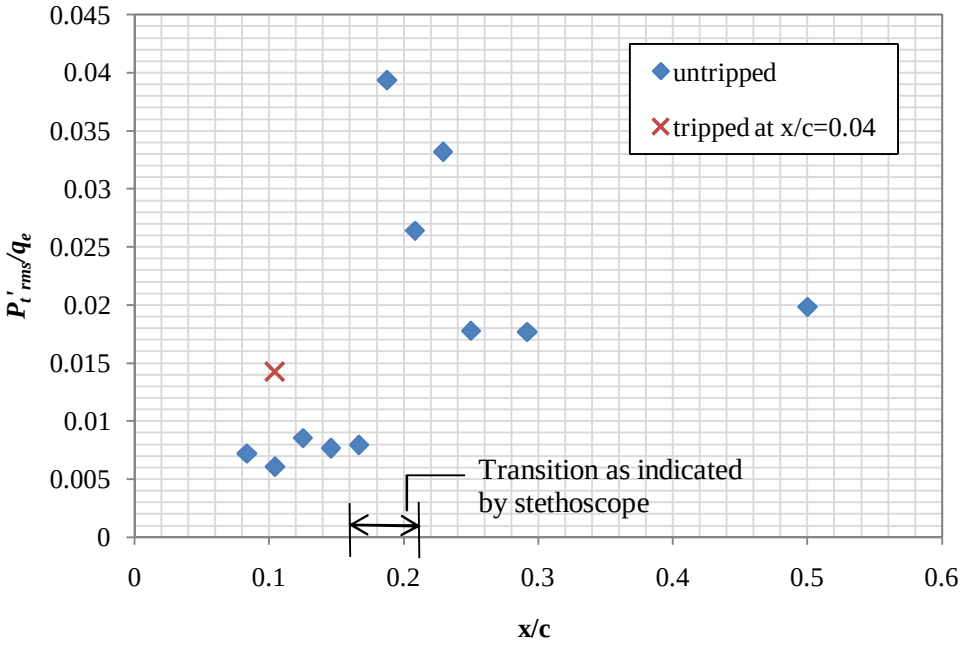

Figure 3.9 – The root-mean-square total pressure fluctuation normalized by local free-stream dynamic pressure during transition.

The effect of a trip was also examined in the 2 ft x 2 ft wind tunnel. A wire was attached on the surface of the flat plate, 2 inches from the leading edge to trip the flow as displayed in figure 3.10. The local Reynolds number at the wire location was greater than 10^5 to ensure the disturbance caused by the wire tripped the flow. Reynolds number calculated based on the wire diameter of 0.010 in and the free-stream velocity of 162 ft/s was about 800. The Kulite probe was placed 3 inches downstream of the trip. When the trip was introduced, the total pressure fluctuation more than doubled, exhibiting a clear difference from the data points taken in the laminar boundary layer.

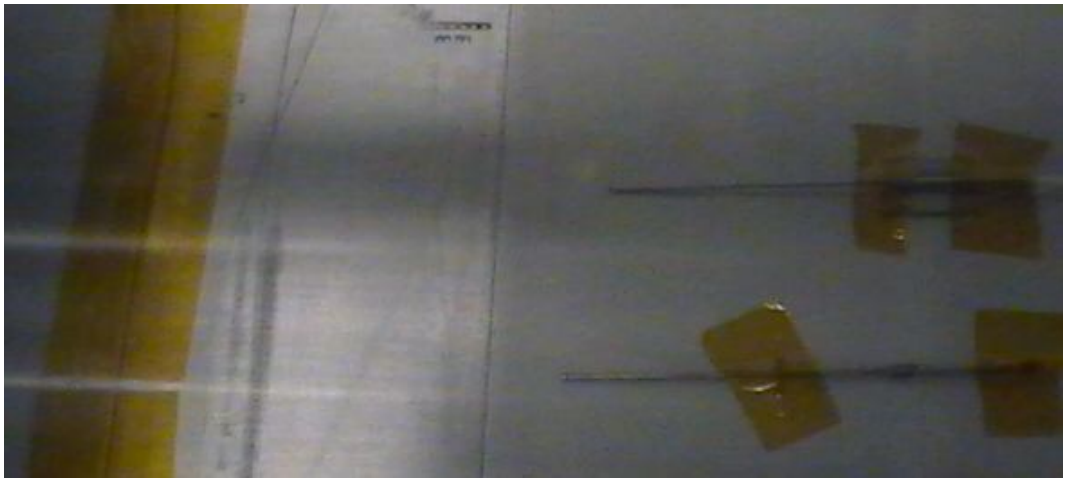

Figure 3.10 – A wire attached to trip the flow on the flat plate.

After the root-mean-square pressure distributions along the centerline of the flat plate was examined in 2 ft x 2 ft wind tunnel, the Kulite sensor was tested in the NGC owned 7 ft x 10 ft wind tunnel located in Hawthorne, CA. The Kulite testing was carried out as a part of NGC's testing to determine the influence of excrescences on transition on a wing model. The model could be fitted with various excrescences such as forward- or after-facing steps located at s = 19 inches. The distance s is a surface coordinate measured from the nose of the model wing. The schematic of the wind model is illustrated in figure 3.11. For this testing, the Kulite sensor was integrated with a stand-alone Kulite signal conditioner instead of using the BLDS. The device was equipped with a switch to provide three amplification levels, and a low pass filter knob with options to attenuate above 100, 1k, or 10 kHz. The specifications of the device and the calibration results are summarized in below table 3.2.

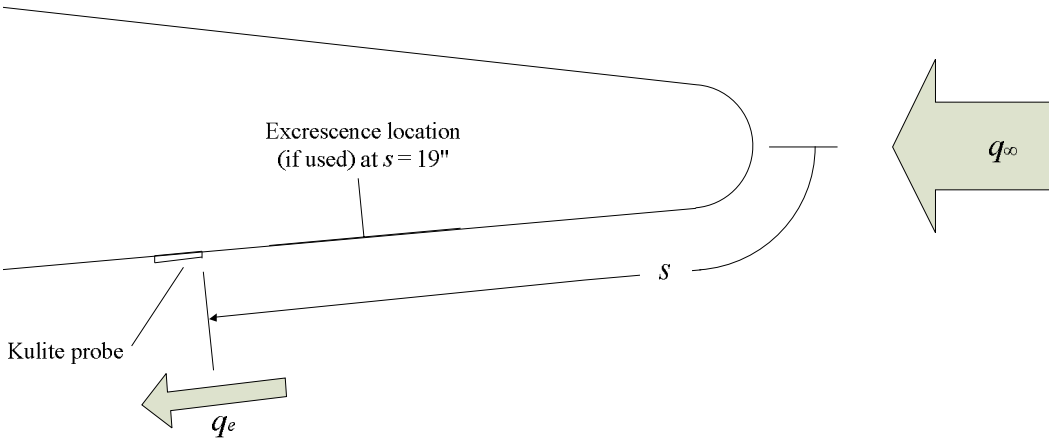

Figure 3.11 – Experimental configuration for 7 ft x 10 ft wind tunnel testing.

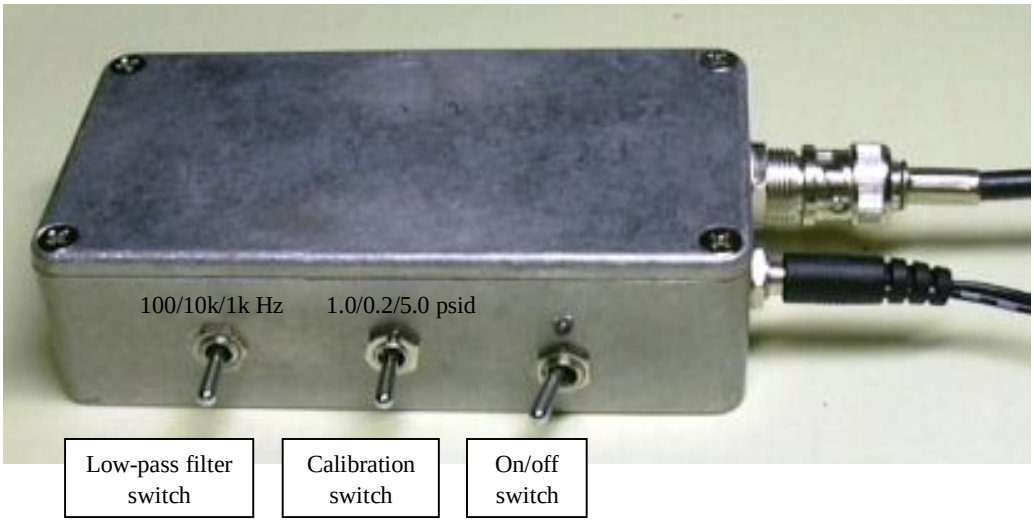

Figure 3.12 – Stand-alone Kulite signal conditioner.

Table 3.2 – Specifications of the stand-alone Kulite signal conditioner.

Input voltage	6-9 V
Output voltage range	0.1-4.9 V
Calibrations	Nominal 0.2, 1.0, or 5.0 psid at max output voltage
Sensitivity	23.05, 4.59, 0.93 V/psi (Actual)
Low-pass filter	100, 1k, or 10 kHz

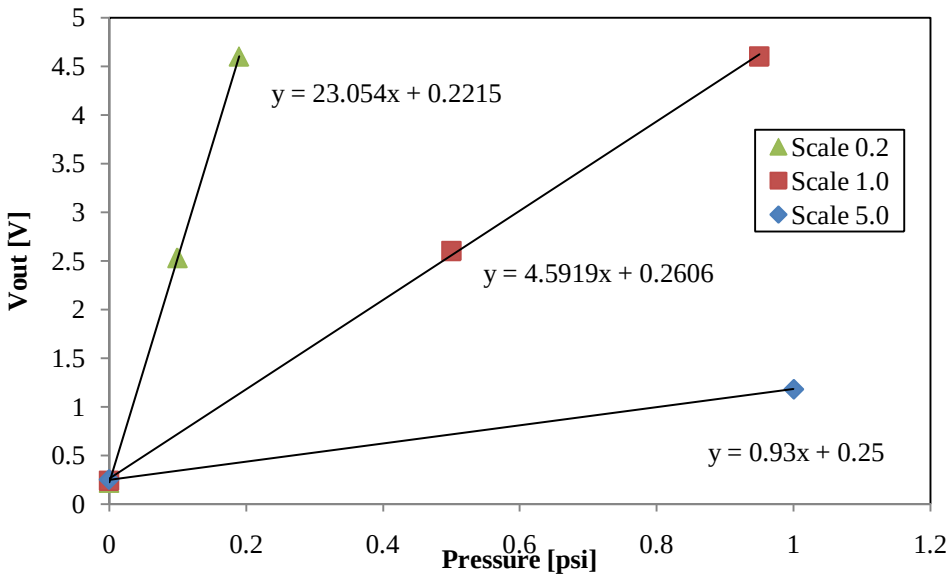

Figure 3.13 – The calibration of the Kulite sensor with the stand-alone Kulite signal conditioner.

The stand-alone Kulite-based setup was employed on the wing model to measure surface pressure fluctuations. The configuration consisted of a 0.032 in Preston tube plumbed with a short tubing of 1/16 in (nominal) to the Kulite whose reference port was connected to a surface static probe. The signal conditioning electronics were set for 10 kHz low-pass filter and nominal 0.2 psid at maximum voltage. The signal conditioner's output was averaged during the course of a steady free-stream velocity using a Fluke model 179 true root-mean-square digital multimeter. The pressure fluctuations on the wing model were measured in three different conditions with approaching free-stream velocities ranging from 15-50 m/s. The tip of the Preston tube and the static probe ports were initially positioned at s = 16.25 inches, upstream of excrescence at s = 19 inches, where the flow was known to be entirely laminar at all free-stream speeds. Subsequently, the probe assembly was moved to s = 50 inches, well downstream of the excrescence. At this location, the pressure fluctuations were documented with a 0.045 inch forward-facing

step as well as without it. The pressure fluctuation data were divided by local free-stream dynamic pressure, q_e, which was calculated using the pressure coefficient C_p, from the nearby pressure tap. The pressure coefficient C_p is defined with local static pressure $p_s(x)$, static pressure at free-stream$p_{s,\infty}$, and the free-stream dynamic pressure q_∞.

$$C_p = \frac{p_s(x) - p_{s,\infty}}{q_\infty} \tag{3.1}$$

By rearranging terms, the local free-stream dynamic pressure q_e can be attained.

$$q_e = q_\infty(1 - C_p) \tag{3.2}$$

Results for pressure fluctuations as a function of approach flow dynamic pressure are shown in figure 3.14.

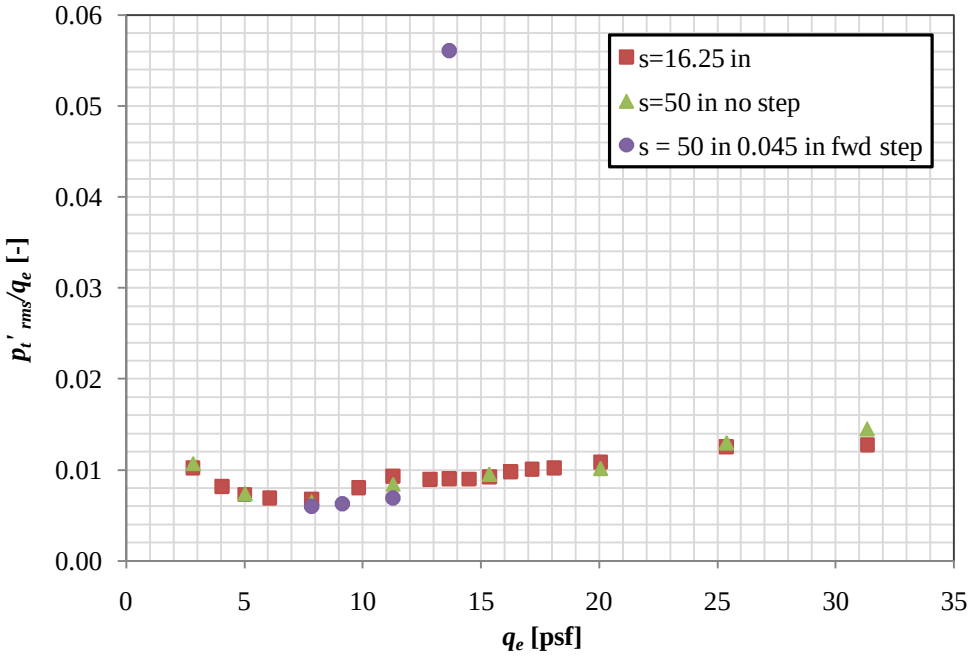

Figure 3.14 – Kulite results for root-mean-square pressure measured at the surface of a wing model in NGC owned 7 ft x 10 ft wind tunnel.

Based on the previous experiments and analysis, the flow was expected to be laminar for every case except for the highest dynamic pressure run for the 0.045 inch forward step, where transition to turbulence upstream of the Kulite location was documented with oil film interferometry [34]. The root-mean-square of total pressure fluctuations increased above 5% of local free-stream at this location. The high root-mean-square value is consistent with values observed for laminar-to-turbulent transition during the previous 2 ft x 2 ft wind tunnel testing. For all other runs, where the boundary layer was laminar, the root-mean-square pressure fluctuations never exceeded 1.5% of local free-stream even at high Reynolds number. The result from the 7 ft x 10 ft wind tunnel agrees quite well with the data obtained from the Cal Poly 2 ft x 2 ft wind tunnel at similar approach flow dynamic pressures. The results demonstrated that the root-mean-square total pressure fluctuation values measured by the Kulite sensor can set apart laminar and turbulent boundary layers, and can be used as a diagnostic tool for laminar-to-turbulent transition.

4. CONCLUSIONS

The root-mean-square of total pressure fluctuations in a turbulent boundary layer was derived from the Goldstein's [23] stagnation pressure equation for incompressible flows. Based on the previous surface static pressure measurements, it was estimated that the root-mean-square of total pressure fluctuations in a turbulent boundary layer was approximately three times that of static pressure fluctuations. As fluctuating parameters are the distinct traits of a turbulent boundary layer, the total pressure fluctuation was evaluated as a possible identifier of laminar-to-turbulent transition in a boundary layer. A Kulite dynamic pressure transducer model XCS-062-5D was used in conjunction with the Boundary Layer Data System to measure the total pressure fluctuations.

The Kulite sensor was first evaluated in the Northrop Grumman Research Wind Tunnel with free-stream dynamic pressure up to 70 psf. The root-mean-square of total pressure fluctuations was about 0.5-1.0 % of the average pressure measured by the Kulite sensor in free-stream, while it was 6-10% when the Kulite sensor was placed in a turbulent boundary layer. The testing confirmed that the total pressure fluctuations measured by the Kulite can be used to distinguish the flow in a free-stream and in a turbulent boundary layer. To examine the effect of different sensor-probe configurations of the Kulite pressure transducer, a series of tests were performed in a 2 ft x 2 ft wind tunnel. The Kulite sensor-probe setups configured with the BLDS were affixed on the surface of a 48 in elliptical nose flat plate in a wind tunnel with 2 ft square test section. The unit was placed 35.5 in from the leading edge of the flat plate to ensure a turbulent boundary layer condition. The results from the testing established the following: (i) The

connection between the Kulite sensor and the total pressure probe should use the shortest possible plumbing, if necessary. The normalized root-mean-square of total pressure fluctuations decreased as the plumbing length increased. (ii) The results indicated that the diameter of the connecting tube has an effect on the pressure readings, and should be kept small. (iii) The use of a shroud as a total pressure probe should be avoided because it was speculated that resonances were forming inside of the shroud. This effect was not observed, however, when a total pressure probe was attached in addition to the shroud. (iv) A static pressure probe should be connected to the reference pressure port as the location, from which the reference pressure reading is taken, affects the average total pressure measured by the Kulite sensor. (v) The total pressure fluctuations measured by the Kulite was approximately three times larger than static pressure fluctuations, and agreed with the result expected from the existing literatures.

Once the effects of the sensor-probe configurations on the total pressure fluctuations measured by the Kulite sensor were analyzed, the Kulite sensor's ability to differentiate the laminar and turbulent boundary layers was attested in the wind tunnel with 2 ft square test section at a nominal dynamic pressure of 30 psf. The Kulite sensor was plumbed to a total pressure probe using plastic tubing, which also connected the reference pressure probe and a surface static probe. The PTDS setup was used to measure local dynamic pressure in free-stream and to process data from the Kulite. The setup was placed between 4 to 24 in from the leading edge of the elliptical flat plate by 1 in increments to document the total pressure fluctuations during laminar-to-turbulent transition. The root-mean-square of total pressure fluctuations measured by the Kulite setup was less than 1% of the local dynamic pressure in the laminar boundary layer, but

was about 2% when the boundary layer was fully turbulent. Moreover, the root-mean-square of total pressure fluctuation increased up to 4% of the local dynamic pressure when the flow was transitioning from laminar to turbulent. Similar results were documented in the Northrop Grumman Corporation's wind tunnel with 7 ft by 10 ft test section, indicating that the total pressure fluctuations intensify in the region of transition. The amplification of total pressure fluctuation during the transition is convenient because it facilitates the detection of the laminar-to-turbulent transition location.

The successful measurements in both laminar and turbulent boundary layers demonstrated the expediency of the total pressure fluctuation as a means of diagnosing the laminar-to-turbulent transition. The Kulite sensor configured with the BLDS was able to effectively measure the total pressure fluctuations in a boundary layer, and is ready to be tested in flight.

BIBLIOGRAPHY

[1] Hinze, J.O. *Turbulence, 2nd ed.* . New York: McGraw-Hill, 1975.

[2] Westphal, R.V., Bleazard, M., Drake, A., Benger, A.M., Frame, and Jordan, S.R. "A compact, Self-Containing System for Boundary Layer Measurement in-Flight." *AIAA-2006-3828, AIAA Meeting Papers on Disc [CD-ROM].* Reston, VA: AIAA, 2006. No.10-13.

[3] Bender, A.M., Drake, A., Westphal, R.V., Jordan, S.R. "Development and Flight Demonstration of Self-Contained Boundary Layer Measurement Devices." *AIAA-2008-7333, AIAA Meeting Papers on Disc [CD-ROM].* Reston, VA: AIAA, 2008.

[4] Ulk, Rocky. *Implementation of Conrad probe on a boundary layer measurement system.* MS Thesis, California Polytechnic State University, San Luis Obispo, 2010.

[5] Fernholz, H. H., Finley, P. J. "The incompressible zero-pressure-gradient turbulent boundary layer: an assessment of the data." *Prog. Aerospace Sci.* 32, no. 245-311 (1996).

[6] Willmarth, W. "Wall pressure fluctuations in a turbulent boundary layer." *The Journal of the Acoustical Society of America* 28, no. 6 (1956): 1048-1055.

[7] Mull, H.R., Algranti, J.S. "Preliminary flight survey of aerodynamic noise on an airplane wing." (NACA) March 1956.

[8] Lofdahl, L., Gad-el-Hak, M. "MEMS-based pressure and shear stress sensors for turublent flows." (Meas. Sci. Technol.) 10 (1999): 665-686.

[9] Tsuji, Y., Fransson, J.H.M., Alfredsson, P.H., Johansson, A.V. "Pressure statics and their scaling in high-Reynolds-number turbulent boundary layers." *J. Fluid Mech* 585 (2007): 1-40.

[10] Lauchle, G.C., Daniels, M.A. "Wall-pressure fluctuations in turbulent pipe flow." *Phys. Fluids* 30, no. 10 (October 1987).

[11] Willmarth, W.W. "Pressure fluctuations beneath turbulent boundary layers." *Annual Review of Fluid Mechanics* 7, no. 1 (1975): 13-39.

[12] Corcos, G.M. "The resolution of turbulent pressure at the wall of a boundary layer." *Journal of Sound and Vibration* 6 (1963): 59-70.

[13] Blake, W. K. *Turbulent boundary layer wall pressure fluctuations on smooth and rough walls.* Vol. 30. 1970.

[14] Schewe, G. "On the structure and resolution of wall-pressure fluctuations associated with turbulent." *J. of Fluid Mech.* 134 (1983): 311–328.

[15] Bryzek, Janusz. "Handbook of Measuring System Design." John Wiley & Sons, Ltd., 2005.

[16] Berns, A., Obermeier, E. "AeroMEMS Sensor Arrays for Time Resolved Wall Pressure and Wall Shear Stress Measurements." *Imaging Measurement Methods for Flow Analysis NNFM* 106 (2009): 227-236.

[17] Huang, C., Naguib, A., Soupos, E. "A silicon micromachined microphone for fluid mechanics research." *J. Micromech. Microeng.* 12 (2002): 767-774.

[18] A. Naguib, E. Soupos, H. Nagib, C. Huang, and K. Naja. "Characterization of a MEMS acoustic/pressure sensor." *37th AIAA Aerospace Sciences Meeting.* Reno, NV: AIAA, 1999. AIAA Paper #99-0520.

[19] Brouckaert, J. F. "Fast response aerodynamic probes for measurements in turbomachines." *IMechE.* J. Power and Energy, 2007. 803-813.

[20] Ainsworth, RW, Willer, RJ, Moss, RW, Thorpe, SJ. "Unsteady pressure measurement." *Meas. Sci. Technol.* 11 (2000): 1055-1076.

[21] Kang, Jeong-Seek, Yang, Soo-Seok. "Fast-response total pressure probe for turbuomachinery application." *Journal of Mechanical Science and Technology* 24, no. 2 (2010): 569-574.

[22] Rizzi, S.A. et al. *Flight Test Measurements From The Tu-144LL Structure/Cabin Noise Follow-On Experiment.* Hampton: NASA, 2000.

[23] Goldstein, S. "A note on the measurement of total head and static pressure in a turbulent." *The Royal Society.* London: Mathematical and Physical Sciences, 1938. 570.

[24] White, Frank M. *Viscous fluid flow, third edition.* New York: McGraw-Hill, 2006.

[25] Lumle, J. L., Tennekes, H. *A first course in turbulence.* The MIT Press, 1972.

[26] Keith W, Hurdis D, Abraham B. "A comparison of turbulent boundary layer wall-pressure spectra." *J. Fluids Eng.* 114 (1992): 338-47.

[27] Lueptow, R M. "Transducer resolution and the turbulent wall pressure spectrum." *J. acousti. soc. Am.* 97 (1995): 370-378.

[28] Sproston, J.L., and Goksel, O.T. "The Calibration of a Surface Static Tube." *Aeronautical Journal* 76 (February 1972): 101-103.

[29] Farabee, Theodore M., Casrella, Mario J. "Spectral features of wall pressure fluctuations eneath turbulent boundary layers." *Physics of Fluids A* 3, no. 10 (October 1991): 2410-2420.

[30] Bull, M.K. "Wall-Pressure Fluctuations Beneath Turbulent Boundary Layers: Some Reflections on Forty Years of Research."

[31] Shaw, R. "The influence of hole dimensions on static pressure measurements." *J. of Fluid Mech.* 9 (1960): 550-556.

[32] Tropea, C., Yarin, A.L., Foss, J.F. *Handbook of Experimental Fluid Mechanics.* New York: Springer, 2007.

[33] Kinsler L.E., Frey A.R., Coppens A.B., Sanders J.V. *Fundamentals of Acoustics Third Edition.* New York: Wiley, 1982.

[34] White, Jonathan. *High-frame-rate oil film interferometry.* MS Thesis, San Luis Obispo: California Polytechnic State University, 2011.

Appendix A: Kulite sensor specification

kulite

HIGH SENSITIVITY ULTRAMINIATURE IS® PRESSURE TRANSDUCER

XCS-062 SERIES

- High Sensitivity
- Silicon on Silicon Integrated Sensor VIS®
- Superior Signal To Noise Ratio
- Static And Dynamic Capability
- Wide Dynamic Range

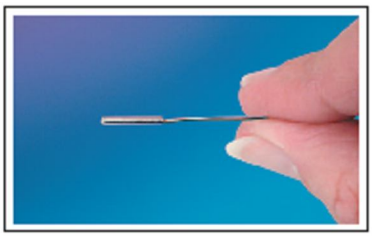

The XCS Series uses a diaphragm of advanced design which gives a substantially higher basic output allowing for high mV/psi sensitivities and improved signal to noise ratio.

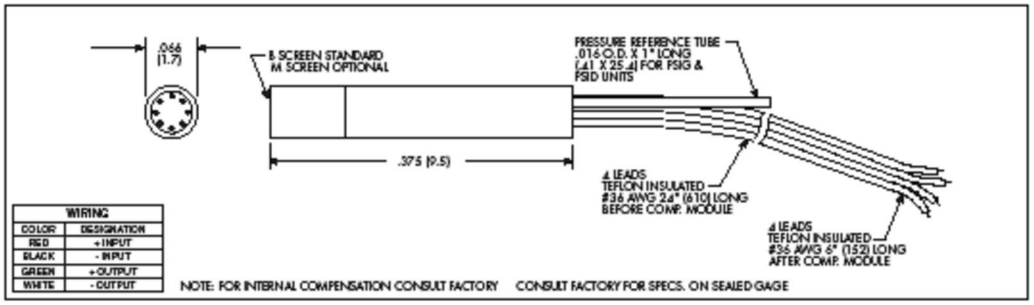

WIRING	
COLOR	DESIGNATION
RED	+ INPUT
BLACK	- INPUT
GREEN	+ OUTPUT
WHITE	- OUTPUT

NOTE: FOR INTERNAL COMPENSATION CONSULT FACTORY CONSULT FACTORY FOR SPECS. ON SEALED GAGE

INPUT Pressure Range	0.35 5	0.7 10	1.0 BAR 15 PSI
Operational Mode	Absolute, Gage, Sealed Gage, Differential		
Over Pressure	2 Times Rated Pressure With No Change in Calibration		
Burst Pressure	3 Times Rated Pressure		
Pressure Media	All Nonconductive, Noncorrosive Liquids or Gases		
Rated Electrical Excitation	10 VDC/AC		
Maximum Electrical Excitation	12 VDC/AC		
Input Impedance	1000 Ohms (Min.)		
OUTPUT Output Impedance	1000 Ohms (Nom.)		
Full Scale Output (FSO)	125 mV (Nom.) 50 mV (Nom.) for SG	125 mV (Nom.) 50 mV (Nom.) for SG	200 mV (Nom.) 100 mV (Nom.) for SG
Residual Unbalance	± 5 mV (Typ.)		
Combined Non-Linearity, Hysteresis and Repeatability	± 0.1% FSO BFSL (Typ.), ± 0.5% FSO (Max.)		
Resolution	Infinitesimal		
Natural Frequency (KHz) (Typ.)	150	175	200
Acceleration Sensitivity % FS/g Perpendicular Transverse	$1.5x10^{-3}$ $2.2x10^{-4}$	$1.0x10^{-3}$ $1.0x10^{-4}$	$7.0x10^{-4}$ $9.0x10^{-5}$
Insulation Resistance	100 Megohm Min. @ 50 VDC		
ENVIRONMENTAL Operating Temperature Range	-65°F to +250°F (-55°C to +120°C)		
Compensated Temperature Range	80°F to +180°F (25°C to +80°C) Any 100°F Range Within The Operating Range on Request		
Thermal Zero Shift	± 1% FS/100°F (Typ.)		
Thermal Sensitivity Shift	± 1% /100°F (Typ.)		
Steady Acceleration	10,000g. (Max.)		
Linear Vibration	10-20,000 Hz Sine, 100g. (Max.)		
PHYSICAL Electrical Connection	4 Leads 36 AWG 30" Long		
Weight	.2 Gram (Nom.) Excluding Module and Leads		
Pressure Sensing Principle	Fully Active Four Arm Wheatstone Bridge Dielectrically Isolated Silicon on Silicon		

Note: Custom pressure ranges, accuracies and mechanical configurations available. Dimensions are in inches. Dimensions in parenthesis are in millimeters. Continuous development and refinement of our products may result in specification changes without notice - all dimensions nominal. (K)

KULITE SEMICONDUCTOR PRODUCTS, INC. • One Willow Tree Road • Leonia, New Jersey 07605 • Tel: 201 461-0900 • Fax 201 461-0990 • http://www.kulite.com

Appendix B: Total Pressure Fluctuation Derivation

For incompressible flow, the total pressure is the sum of the static pressure and the dynamic pressure [23].

$$p_t = p_s + \frac{1}{2}\rho|\vec{V}|^2 \tag{1.1}$$

$$\vec{V} = u\hat{\imath} + v\hat{\jmath} + w\hat{z} \tag{1.2}$$

Squaring both side of the equation (1.1) and applying Reynolds decomposition to the total and static pressures and the velocity will lead to the equation (1.3). Note that $\bar{v} = \bar{w} = 0$ assuming that the Pitot tube is aligned with the flow in $\hat{\imath}$ direction.

$$p_t = \bar{p_t} + p_t' \tag{1.3}$$

$$p_s = \bar{p_s} + p_s' \tag{1.4}$$

$$u = \bar{u} + u' \tag{1.5}$$

$$v = \bar{v} + v' \tag{1.6}$$

$$w = \bar{w} + w' \tag{1.7}$$

$$(\bar{p_t} + p_t')^2 = \left(\bar{p_s} + p_s' + \frac{1}{2}\rho\left(\sqrt{(\bar{u} + u')^2 + (v')^2 + (w')^2}\right)^2\right)^2 \tag{1.8}$$

Next, the averaging the entire equation and applying bar rules will yield the following form.

$$\begin{aligned}\overline{p_t}^2 + \overline{p_t'^2} = {} & \overline{p_s}^2 + \overline{p_s'^2} + \rho\left(\overline{p_s}\,\overline{\bar{u}^2} + \overline{p_s}\,\overline{u'^2} + \overline{p_s}\,\overline{v'^2} + \overline{p_s}\,\overline{w'^2}\right) \\ & + \rho\left(\overline{p_s'\bar{u}^2} + 2\overline{p_s'\bar{u}u'} + \overline{p_s'u'^2} + \overline{p_s'v'^2} + \overline{p_s'w'^2}\right) \\ & + \frac{1}{4}\rho^2\left(\bar{u}^4 + 6\overline{\bar{u}^2u'^2} + 4\overline{\bar{u}u'^3} + 2\overline{\bar{u}^2v'^2} + 2\overline{\bar{u}^2w'^2}\right. \\ & + 4\overline{\bar{u}u'v'^2} + 4\overline{\bar{u}u'w'^2} + 2\overline{u'^2v'^2} + 2\overline{u'^2w'^2} \\ & \left. + 2\overline{v'^2w'^2} + \overline{u'^4} + \overline{v'^4} + \overline{w'^4}\right)\end{aligned} \tag{1.9}$$

Applying the Reynolds decomposition to the total pressure equation (1.1), we get

$$\overline{p_t} + p_t' = \overline{p_s} + p_s' + \frac{1}{2}\rho((\bar{u} + u')^2 + (v')^2 + (w')^2) \tag{1.10}$$

Baring the entire equation will give us equation (1.11). Note that $\overline{p_t}' = \overline{p_s}' = \overline{\bar{u}u}' = 0$.

$$\overline{p_t} = \overline{p_s} + \frac{1}{2}\rho(\bar{u}^2 + 2k) \tag{1.11}$$

where

$$k = \frac{1}{2}\left(\overline{u'^2} + \overline{v'^2} + \overline{w'^2}\right) \tag{1.12}$$

Squaring both sides of the equation (1.11) will yield the equation for the averaged total pressure.

$$\begin{aligned}\overline{p_t}^2 = {} & \overline{p_s}^2 + \rho\left(\overline{p_s}\,\bar{u}^2 + \overline{p_s}\,\overline{u'^2} + \overline{p_s}\,\overline{v'^2} + \overline{p_s}\,\overline{w'^2}\right) \\ & + \frac{1}{4}\rho^2\left(\bar{u}^4 + 2\bar{u}^2\overline{u'^2} + 2\bar{u}^2\overline{v'^2} + 2\bar{u}^2\overline{w'^2}\right. \\ & + 2\overline{u'^2v'^2} + 2\overline{u'^2w'^2} + 2\overline{v'^2w'^2} + \overline{u'^2}^2 + \overline{v'^2}^2 \\ & \left. + \overline{w'^2}^2\right)\end{aligned} \tag{1.13}$$

Subtracting the above from equation (1.9),

$$\overline{p_t'^2} = \overline{p_s'^2} + \rho\left(2\bar{u}\overline{p_s'u'} + \overline{p_s'u'^2} + \overline{p_s'v'^2} + \overline{p_s'w'^2}\right) + \frac{1}{4}\rho^2\left(4\bar{u}^2\overline{u'^2} + 2\bar{u}\overline{u'^3} + 4\bar{u}\overline{u'v'^2} + 4\bar{u}\overline{u'w'^2} + \overline{u'^4} + \overline{v'^4} + \overline{w'^4} - \overline{u'^2}^2 - \overline{v'^2}^2 - \overline{w'^2}^2\right) \quad (1.14)$$

Since $\bar{u} \gg u', v', w'$, the magnitude of the multiples of the fluctuating velocities are negligible. The average of the total fluctuating pressure can be expressed as follows.

$$\overline{p_t'^2} = \overline{p_s'^2} + 2\rho\bar{u}\overline{p_s'u'} + \rho^2\bar{u}^2\overline{u'^2} \quad (1.15)$$

Finally, rearranging the above equation and dividing it by the square of the mean dynamic pressure will yield the following.

$$\frac{\overline{p_t'^2} - \overline{p_s'^2}}{\frac{1}{4}\rho^2\bar{u}^4} = 4\frac{\overline{u'^2}}{\bar{u}^2} + \frac{8\overline{p_s'u'}}{\rho\bar{u}^3} \quad (1.16)$$

Or the root mean square of the total pressure fluctuation normalized by the dynamic pressure is expressed as below.

$$\frac{\sqrt{\overline{p_t'^2}}}{\frac{1}{2}\rho\bar{u}^2} = \sqrt{\frac{\overline{p_s'^2}}{\frac{1}{4}\rho^2\bar{u}^4} + 4\frac{\overline{u'^2}}{\bar{u}^2} + \frac{8\overline{p_s'u'}}{\rho\bar{u}^3}} \quad (1.17)$$

Appendix C: Testing at Northrop Grumman Research Wind Tunnel

Testing of a Kulite sensor was conducted at the Northrop Grumman Research Wind Tunnel (RWT) on June 16, 2010. The test objective was to measure mean and root-mean-square (RMS) of total pressure fluctuations with the Kulite sensor up to free-stream dynamic pressures of 70 psf, which is over twice what was possible in the Cal Poly 2x2 tunnel, to evaluate its possible application as a turbulence detector for the Boundary Layer Data System (BLDS). The pressure measurements were made using a Kulite model XSC-062-5D sensor interfaced with the BLDS through a custom-made amplifier and operated through a satellite input. A schematic of the Kulite sensor is shown in figure C.1.

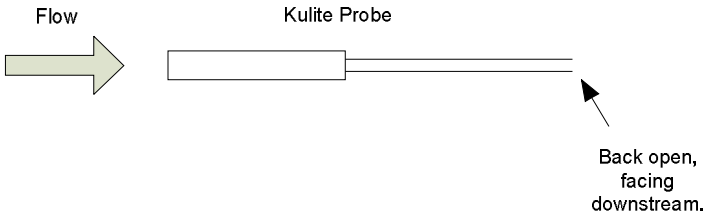

Figure C.1 – Kulite sensor configuration.

The Kulite sensor was positioned in the free-stream to document its readings in a non-turbulent flow. At this location, the sensor was "bare", or it was not plumbed to a probe. The Kulite sensor was also placed flush on the surface both "bare" and with a standard Preston tube to measure the average total pressures and the root-mean-square of total pressure fluctuations at the surface. In all cases, the reference pressure connection for the Kulite was left open, facing downstream, and was not connected to a static pressure probe. Based on previous works in the RWT, it was assumed that the boundary layer at

the test section floor was turbulent and about an inch thick at the measurement station; this was confirmed with profile measurements taken using the BLDS configured with its standard total pressure probe. At the measurement location, the BLDS free-stream probe measured somewhat lower dynamic pressures than the nominal values from the RWT operator's display as shown in table C.1. In all the figures that follow, abscissa scales with "free-stream dynamic pressure" are the values that were actually measured by the BLDS at the location shown in figure C.2.

Table C.1 – Nominal and measured local free-stream dynamic pressures.

Nominal [psf]	Measured [psf]
30	28.62
50	46.36
70	64.98

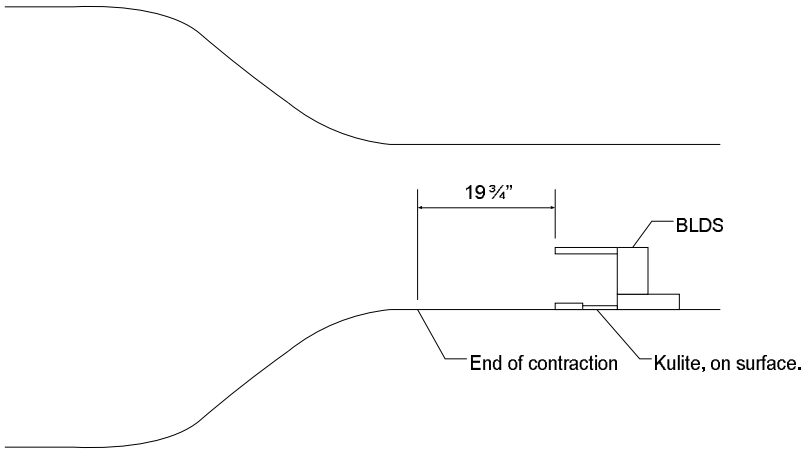

Figure C.2– Kulite testing configuration at RWT.

Figures C.3 and C.4 show the turbulent boundary layer profiles on the test section floor, 19.75 inches downstream of the contraction exit, for the nominal free-stream dynamic

pressures of 30, 50, 70 psf. These results confirmed the turbulent boundary layer for 30 to 70 psf as had been expected.

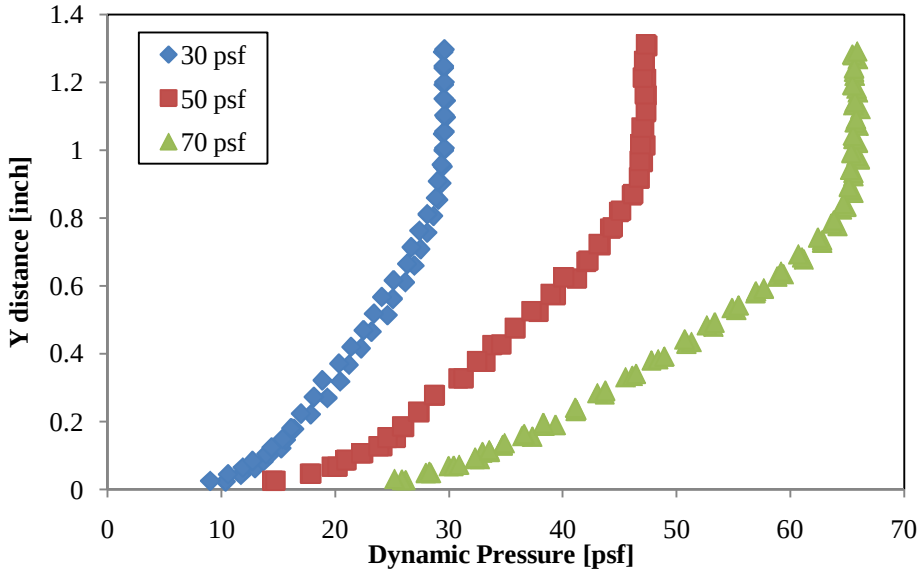

Figure C.3 – Dynamic pressure profiles at RWT test section (BLDS).

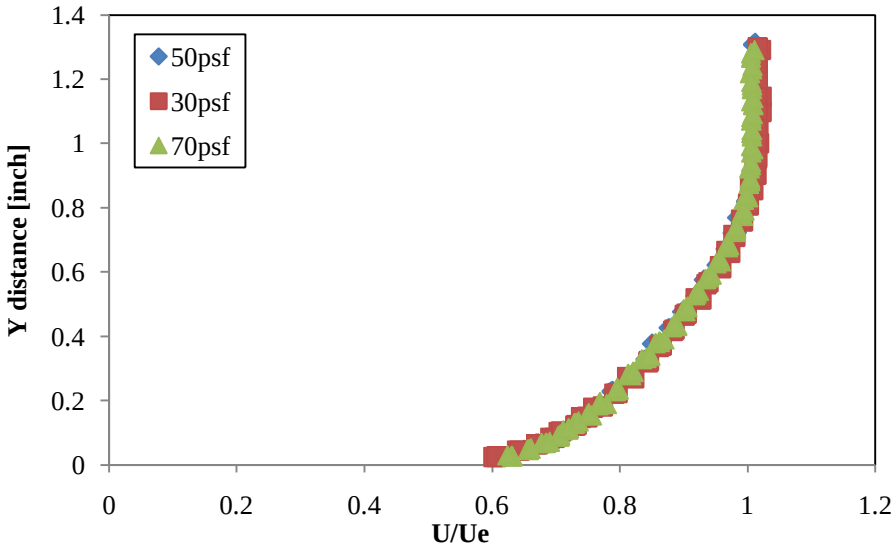

Figure C.4 – Boundary layer total pressure probe profiles at RWT test section (BLDS).

The Kulite average pressures in the free-stream were compared to the free-stream dynamic pressures measured with the BLDS total probe in order to assess the effect of

the reference pressure and the Kulite's sensor geometry. Figure 3.2 showed that the Kulite average pressure measurements were slightly lower than dynamic pressures measured with BLDS (the dotted line representing 1:1 ratio). The nearly constant ratio of the measured Kulite and dynamic pressure strongly suggests that the pressure field of the sensor itself is the reason for the difference. Two explanations are suggested; either the reference pressure of the Kulite is slightly higher than the static pressure, or, the bare sensor's active face experiences a pressure slightly lower than total pressure. Of course, a combination of both effects is also possible. By connecting the reference pressure port to the static pressure probe, the former explanation can be tested, while the use of a shroud can be used to test the latter.

The Kulite sensor measurements in the RWT free-stream provided an opportunity to evaluate total pressure fluctuations in the non-turbulent free-stream flow outside the turbulent boundary layer. The results in figure C.5 shows approximately constant values of the root-mean-square total pressure fluctuations in the range of 0.25-0.35 psf as the tunnel dynamic pressure varied from 10 to 70 psf. Since the fluctuation values were nearly constant with increasing dynamic pressure, the ratio of root-mean-square to average total pressure fluctuations, or %RMS, dropped as the average pressures measured by the Kulite increased. At 70 psf, the %RMS decreased to about 0.5% in the RWT free-stream as displayed in figure C.6. This was a very encouraging result because the root-mean-square of the total pressure fluctuations in a flat plate turbulent boundary layer were expected to be less than 10%, thus, discriminating between turbulent and non-turbulent areas would require that the sensor noise be well below a few percent.

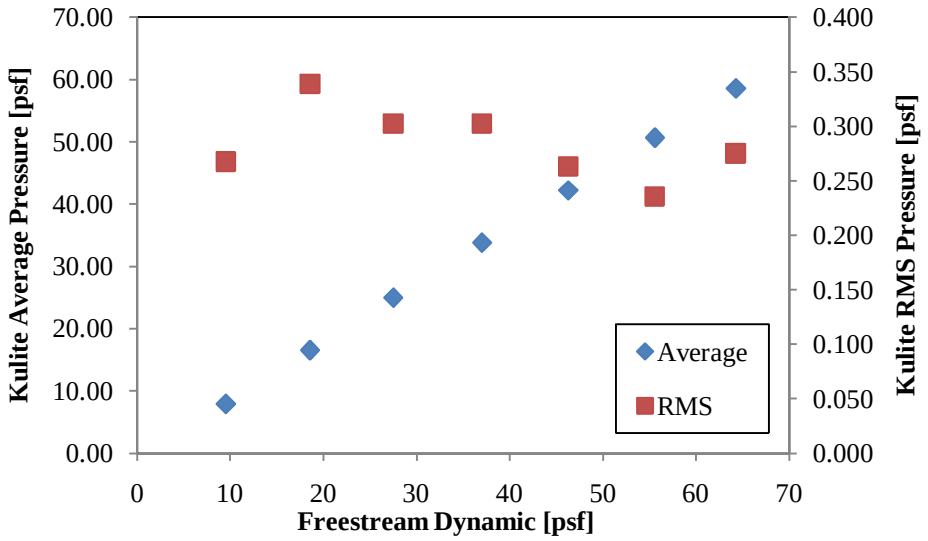

Figure C.5 – Kulite bare sensor average and RMS perssure measurements in free-stream of RWT.

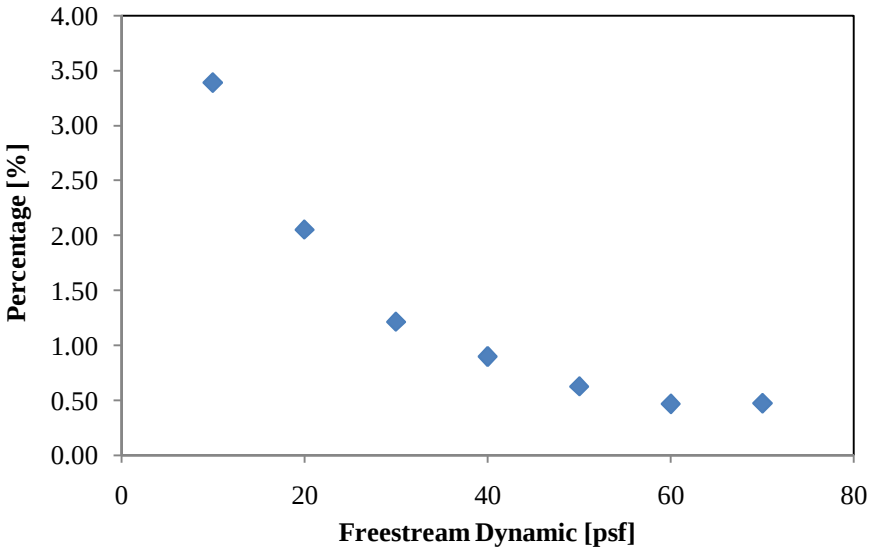

Figure C.6 – Kulite bare sensor %RMS measured in free-stream of RWT.

Next, two different sets of test were run while the Kulite sensor was placed on the RWT floor. The bare Kulite sensor was positioned facing upstream for the first setup and the Kulite was connected to a standard Preston probe of 0.032 in diameter for the second setup. The results for the average and the root-mean-square of total pressure fluctuations,

and the ratio of the two, given as %RMS, are shown in figures C.7, C.8, and C.9, respectively. The average pressures measured by the Kulite sensor were oddly lower for the bare sensor case than the probe-connected case at all dynamic pressures; this may have been caused by the location of the reference pressure being different between the two cases. The total pressure fluctuation measurements should not be affected by the location of reference pressure, however. When the Kulite sensor was either bare or connected to a Preston probe, the data showed an increase in total pressure fluctuations as the tunnel dynamic pressure increased. The bare Kulite measured a linear increase in total pressure fluctuations while they leveled off at high free-stream dynamic pressures when the Kulite sensor was connected to a Preston probe. The latter result may be the evidence for the attenuation of the fluctuations caused by the probe and its interconnecting plumbing. Thus, the effect of a probe connected to the Kulite requires further investigation. The %RMS showed a similar trend for both the bare Kulite sensor and the Kulite connected to the Preston probe. For both cases, %RMS decreased when the free-stream dynamic pressure was increased. At 70 psf, the %RMS for the bare Kulite was about 10% and that of the Kulite connected to the Preston tube was about 6%. At low dynamic pressures, the level of noise may have overwhelmed the pressure fluctuations caused by the turbulence, resulting in large %RMS values. Once the effect of noise subsided at higher dynamic pressures, however, the %RMS values showed a trend of reaching a constant value.

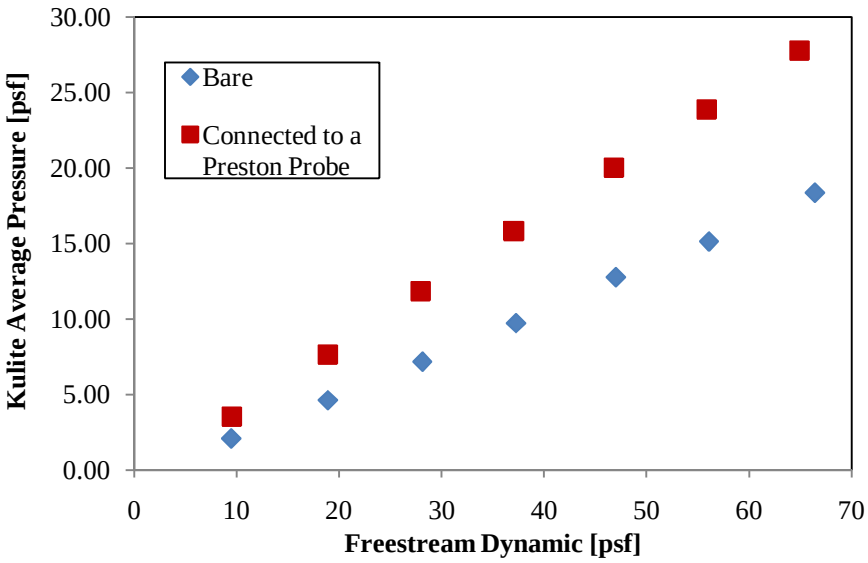

Figure C.7 – Average total pressures measured by the Kulite on the surface of RWT. The Kulite probe was bare for the first test, and it was connected to a Preston probe (0.032 in dia) for the second test.

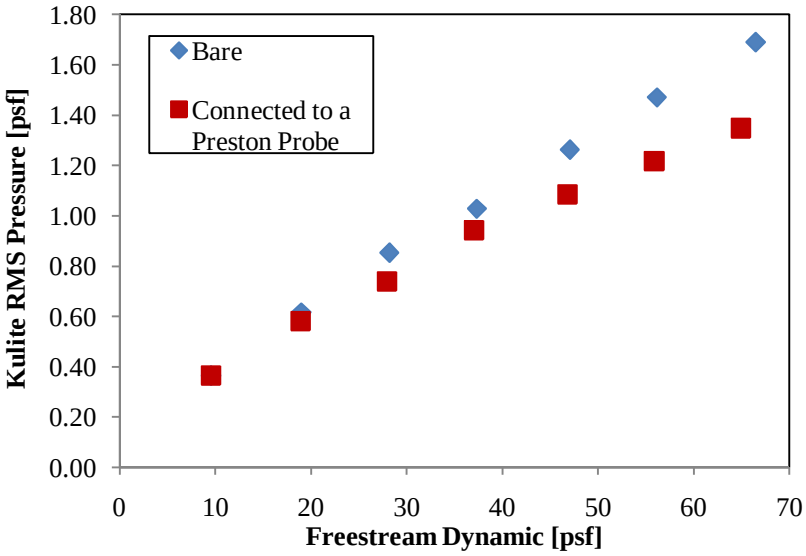

Figure C.8 – The root-mean-square of total pressure fluctuations measured by the Kulite on the surface of RWT. The Kulite probe was bare for the first test, and it was connected to a Preston probe (0.032 in dia) for the second test.

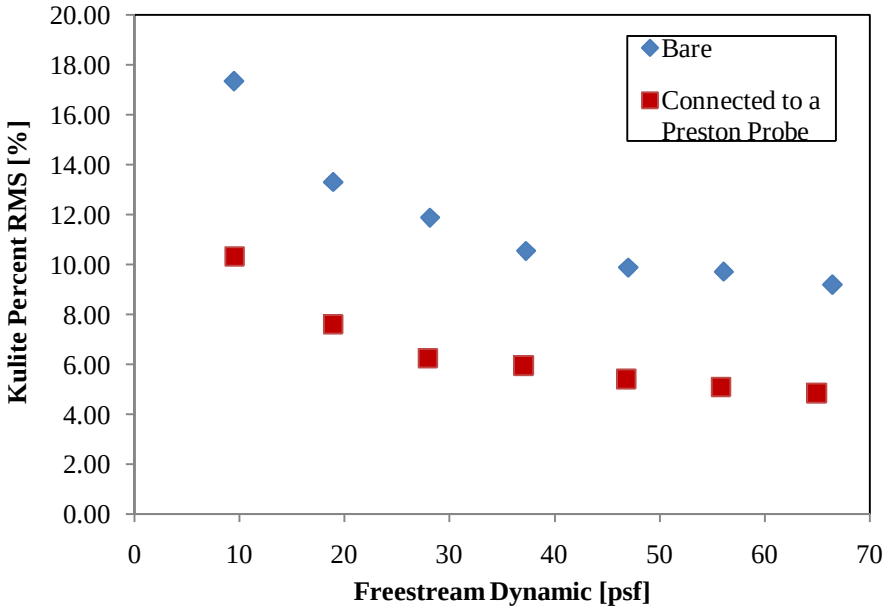

Figure C.9 – Percent RMS on the surface of RWT. The percent RMS was calculated from the ratio of the root-mean-square of total pressure fluctuations and average total pressures measured by the Kulite at a free-stream dynamic pressure.

The results from the RWT were then compared to the earlier measurements made in the Cal Poly 2x2 wind tunnel at lower dynamic pressures. In the 2x2 tunnel, the Kulite sensor was placed on a flat plate model ("MEATLOAF TASK 0" model), 31 inches from the leading edge. From previous measurements made on this model in the 2x2 tunnel, the boundary layer at this point was known to be turbulent. The results showed that the root-mean-square of total pressure fluctuation values obtained at the Cal Poly 2x2 tunnel were similar to those at the RWT (figure C.11), but the bare Kulite's average total pressure data (figure C.10) were quite different. The average total pressures measured with the bare Kulite sensor were higher in the Cal Poly 2x2 wind tunnel than those measured in the RWT, which resulted in lower %RMS values as shown in figure C.12. The results from the total pressure fluctuation measurements in the turbulent boundary layers at the 2x2 and RWT demonstrated that Kulite sensor should be useful as a laminar-to-turbulent

transition indicator, so long as the Kulite sensor noise does not exceed the turbulent total pressure fluctuations. The noise should not be a problem since the %RMS results exhibited that the effect of noise was negligible for the free-stream dynamic pressures exceeding about 40 psf, which is well below the most typical applications for the BLDS.

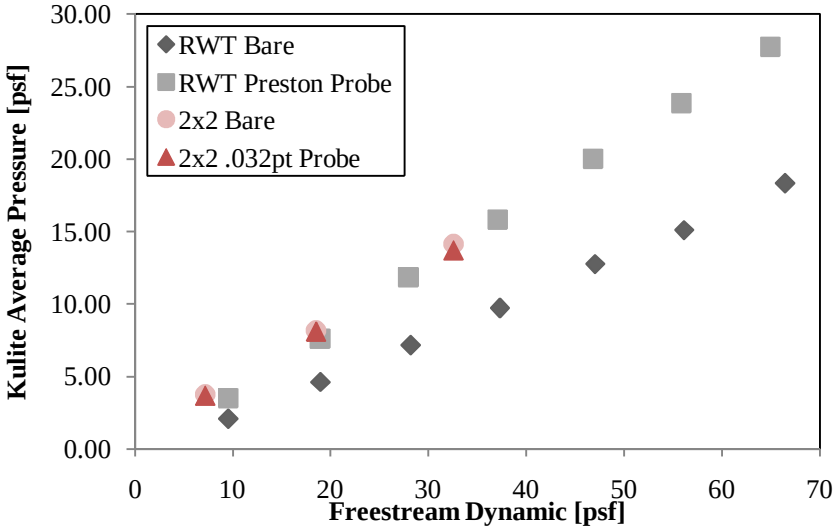

Figure C.10 – The comparison of the average pressures measured by the Kulite in the Cal Poly 2x2 wind tunnel and in the RWT.

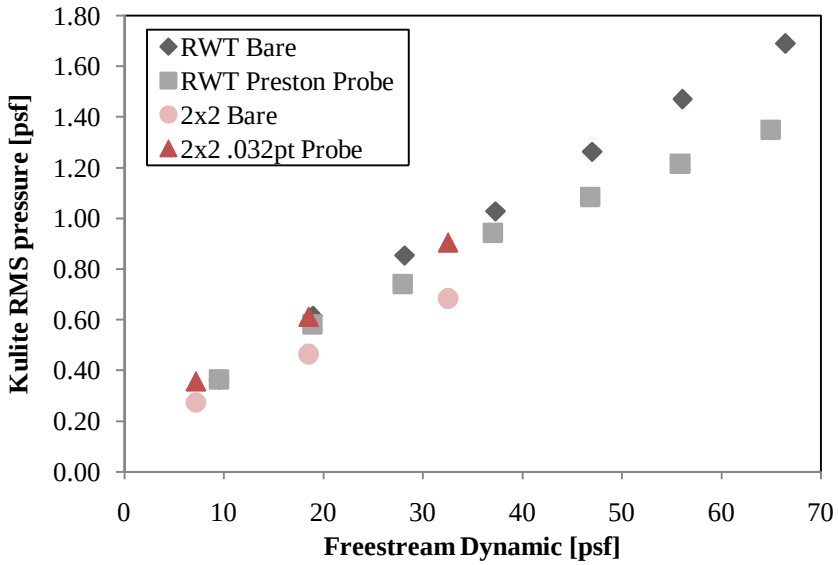

Figure C.11 – The comparison of the root-mean-square of total pressure fluctuations measured by the Kulite in the Cal Poly 2x2 wind tunnel and in the RWT.

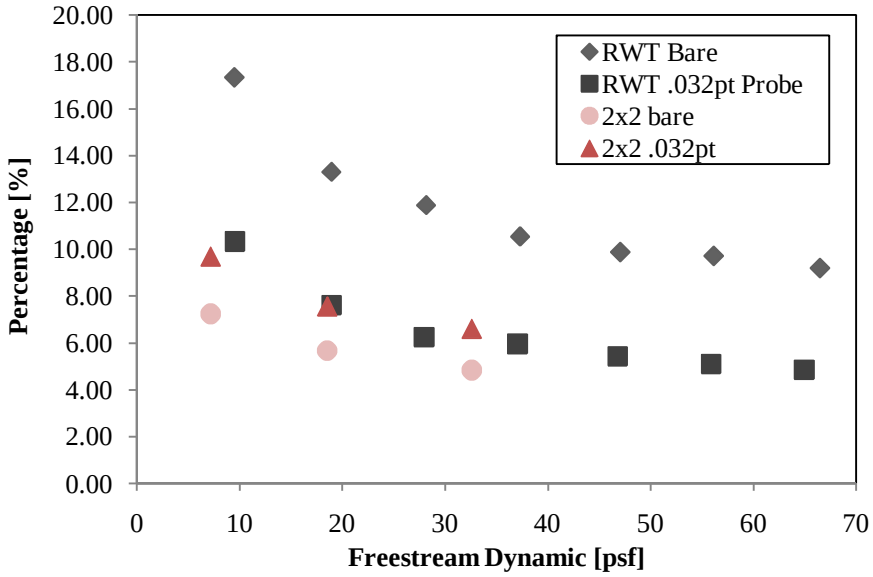

Figure C.12 – Kulite %RMS measured in the Cal Poly 2x2 wind tunnel compared to the RWT results.

Appendix D: Experimental results from 2 ft × 2 ft wind tunnel

The effects of probe length, *l*, on the average and the root-mean-square of total pressure fluctuations measured by the Kulite were first examined. The Kulite sensor was connected to a 0.025 inch OD probe via plastic tubes. A step connector was used to accommodate the difference in diameters. The schematic below shows the configuration of the Kulite sensor and the probe.

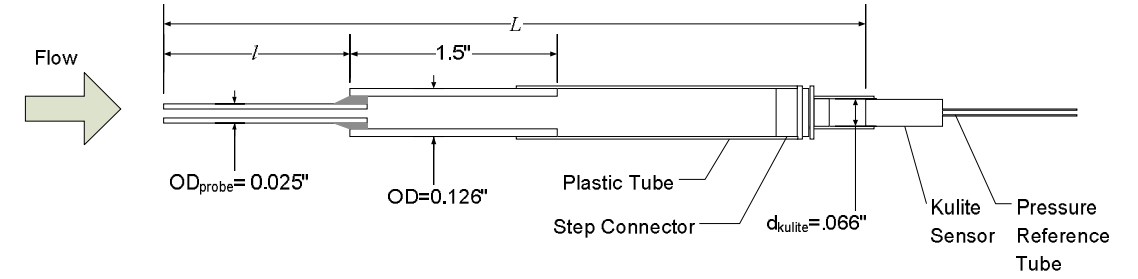

Figure D.1 – The Kulite probe configuration. The probe length, *l*, was changed to examine its effect on the Kulite pressures.

As figure D.2 through D.4 display, the Kulite average pressure remained relatively constant, but the root-mean-square of total pressure fluctuations and the % RMS slightly decreased as the probe length, *l*, increased. It should be noted that the root-mean-square of total pressure fluctuation values were quite different when they were compared to the data obtained with 0.032 inch OD probe. It indicates that the probe diameter may have an effect on the pressure readings, and was later investigated. The difference in the root-

mean-square of total pressure fluctuations readings between 0.025 in and 0.032 in probes may also be due to the difference in plumbing configurations. The plastic tubing used for this experiment was 3.5 in blue silicon fuel tubing with 3/32 in ID, while 0.4 in clear vinyl tubing with 1/16 in ID was used for the 0.032 in probe measurements. The longer and more elastic silicon tube could have caused damping, resulting in lower pressure readings.

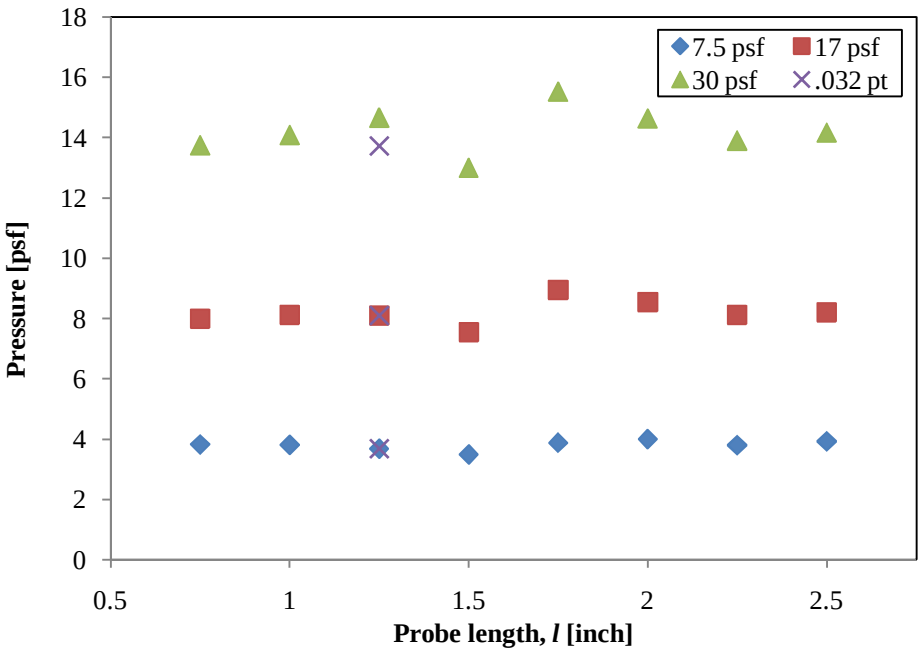

Figure D.2 – Average pressure measurements of the Kulite with .016 in probe connected by plastic tubing. The probe length, *l*, was varied between 0.75 in to 2.5 in. A measurement made with .032 in probe is also shown in the figure.

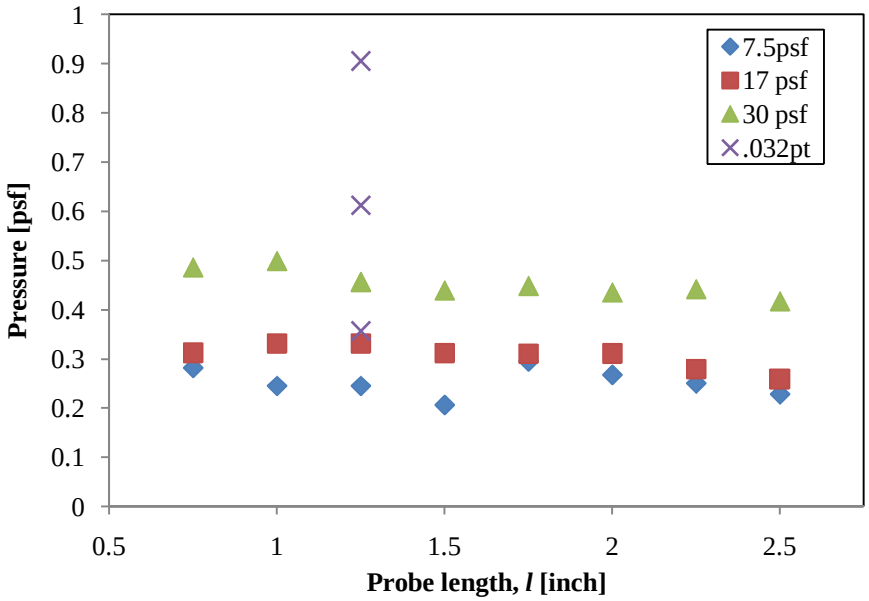

Figure D.3 – The root-mean-square of total pressure fluctuations measured with the Kulite with .016 in probe connected by plastic tubing. The probe length, *l*, was varied between 0.75 in to 2.5 in. A measurement made with .032 in probe is also shown in the figure.

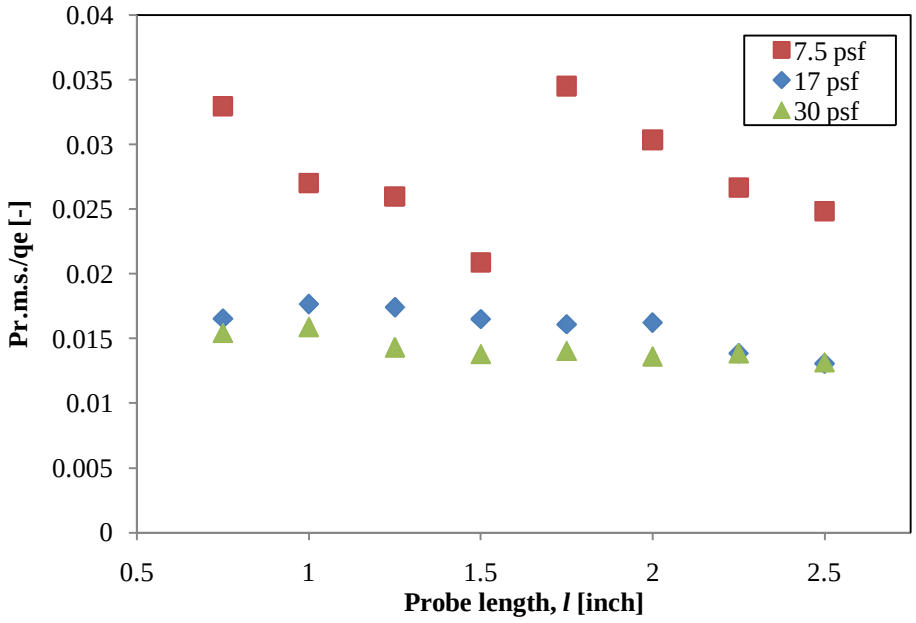

Figure D.4 –% RMS. The data show a trend of slightly decreasing % RMS with increasing probe length, *l*, at higher free-stream dynamic pressures. The discrepancy between 0.016 in and 0.032 in in % RMS values is due to their difference in RMS measurements.

In order to eliminate the possibility of connecting tube damping out the Kulite RMS readings, stainless steel tube, or shroud, was introduced to connect the probe and the Kulite sensor instead. The Kulite sensor was attached to a shroud, and was placed flush on the surface of the wind tunnel in the direction of flow. The shroud used in this experiment was stainless steel tubing with 0.067 in ID and 0.083 in OD. The gap between the shroud and the Kulite sensor was sealed with vacuum grease. The schematic of the testing configuration is shown in figure D.5.

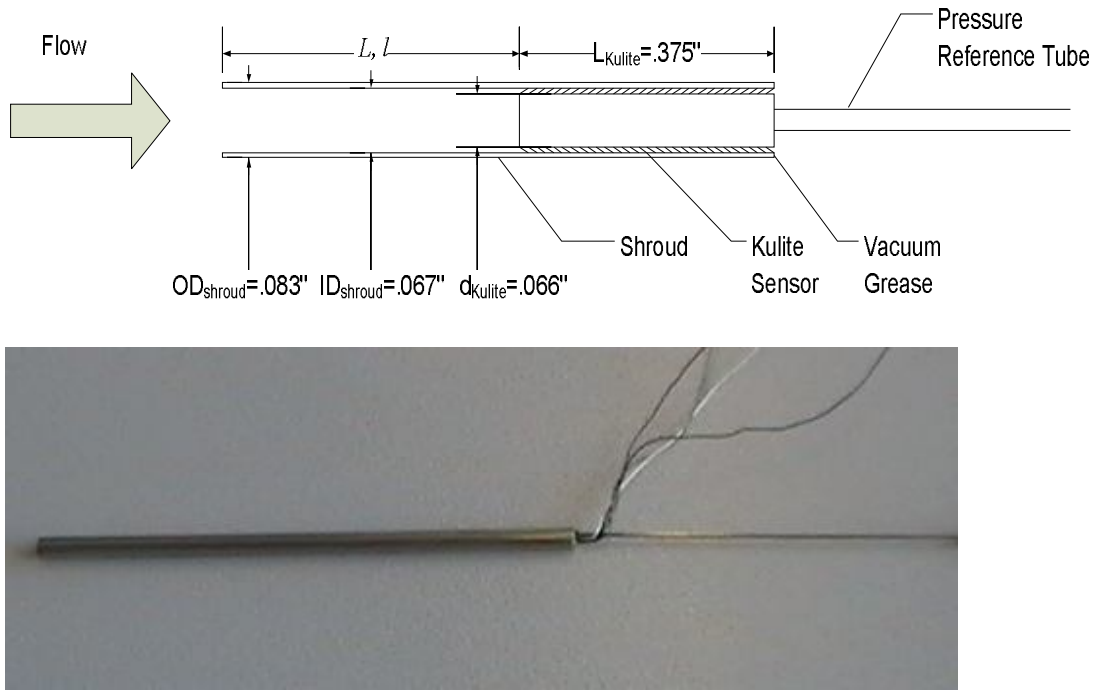

Figure D.5 – Shrouded Kulite sensor configuration.

First, the effect of shroud thickness on the Kulite probe was tested and was compared to the bare Kulite measurement. This was done by applying a shroud on the Kulite probe with no extension (L = 0). The results of the Kulite average and RMS pressures as well as calculated %RMS are shown in figures D.6, D.7, and D.8. Both average and RMS pressure readings for the Kulite with shroud were higher than those of the bare Kulite. At

the maximum dynamic pressure of 60 psf, the average pressure for the Kulite with shroud was approximately 15% higher than that of the bare Kulite, and the RMS pressure was about 8.7% higher than the bare Kulite. The steep decrease in %RMS at lower dynamic pressures was again observed due to sensor and amplifier noises.

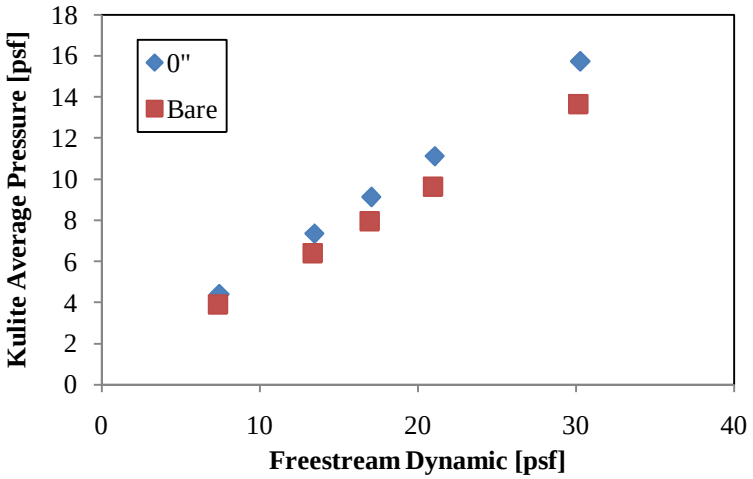

Figure D.6 – Average pressure measurements for the bare and the shrouded Kulite with no extension (*L*=0). The shrouded Kulite recorded slightly higher pressures than the bare Kulite.

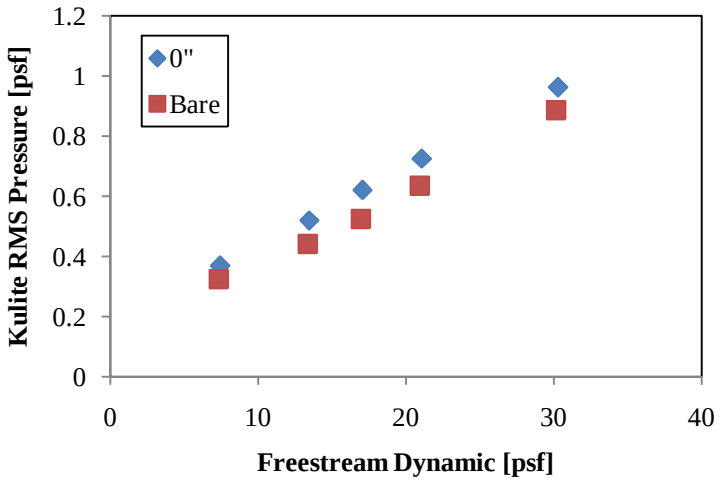

Figure D.7 – RMS pressure measurements for the bare and the shrouded Kulite with no extension (*L*=0). The shrouded Kulite recorded slightly higher pressures than the bare Kulite.

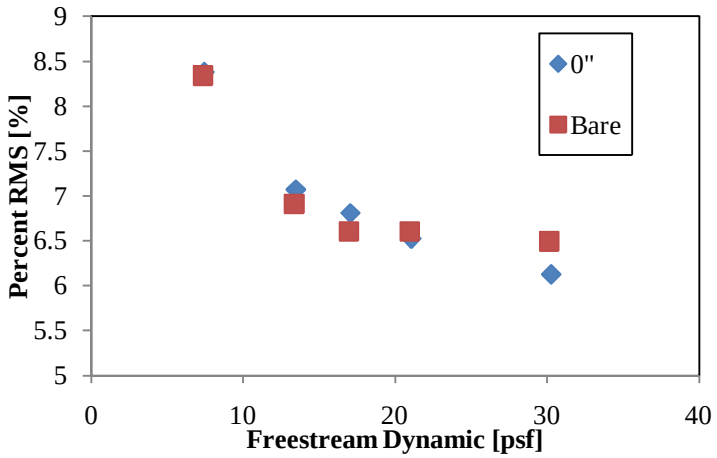

Figure D.8 – Calculated % RMS for the bare and the shrouded Kulite with no extension (*L*=0). Despite the difference in average and RMS readings, the % RMS resulted in similar values.

The higher pressure readings can be explained by the position of the shrouded Kulite sensor in the boundary layer as it was elevated due to shroud thickness. However, the effect of Kulite sensor geometry should also be considered. The ratio of inner to outer diameter for a cylindrical square-ended pitot probe is typically designed to be 0.6 to avoid blocking. As shown in below figures, the Kulite sensor has pressure holes on the perimeter of the sensor head. The ratio of inner to outer diameter of the bare Kulite is greater than 0.6. By attaching a shroud to the Kulite sensor, the ratio of inner to outer diameter was decreased. As a result, the blocking effect was reduced and the pressure readings were improved.

Next, the effect of shroud length was examined by varying the shroud length, *l*. The average Kulite pressure increased linearly as expected for all configurations. When compared to the average pressure with the bare Kulite, the Kulite sensor recorded higher average pressures when it was shrouded. In addition, the average pressure readings were

nearly constant when the shroud was less than 1.5 inches, but increased when the shroud length exceeded 1.5 inches.

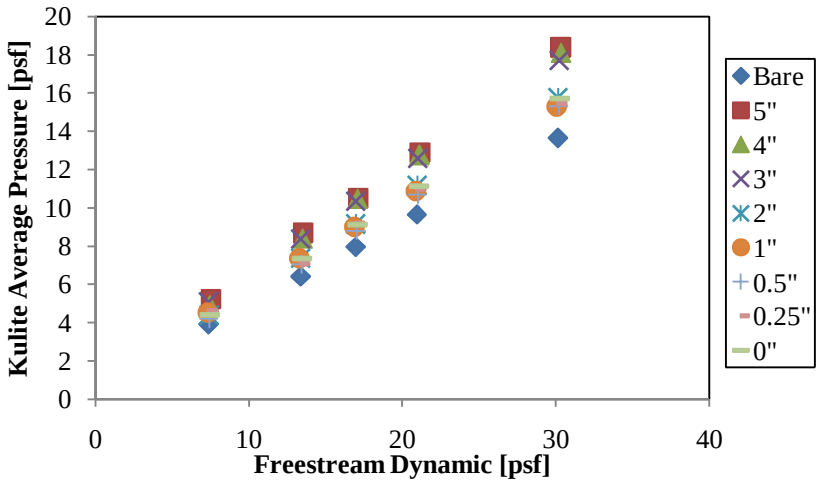

Figure D.9 – Kulite average pressure measurements with different shroud lengths as function of free-stream dynamic pressures.

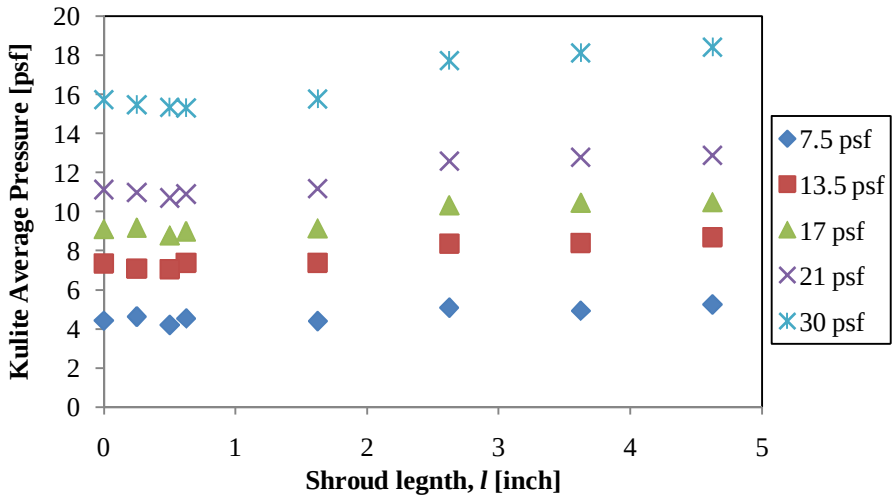

Figure D.10 – Kulite average pressure measurements with different shroud lengths as a function of shroud length. The average pressures were relatively constant when shroud lengths were less than 1.675 in. When the shroud length was increased, however, the average pressure discontinuously increased.

The Kulite RMS pressures increased as expected as the free-stream dynamic pressure increased. However, the increase in Kulite RMS pressure with shroud length is not explained as the edge of the shroud was fixed at the same position. However, the position of the reference pressure was advancing as the shroud length became shorter. If the reference pressure changed as it advanced its position, this could have affected readings. Regardless of this effect, the %RMS remained relatively constant throughout the experiment at about 6-7%.

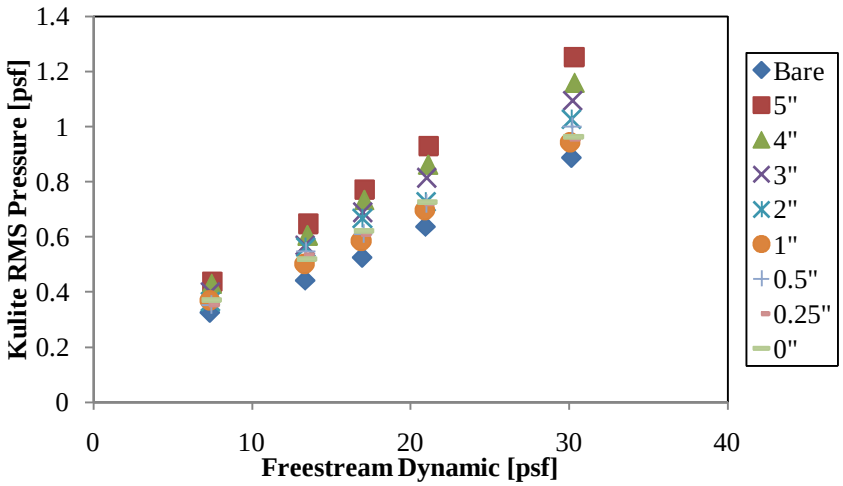

Figure D.11 – Kulite RMS pressure measurements with different shroud lengths as function of free-stream dynamic pressures.

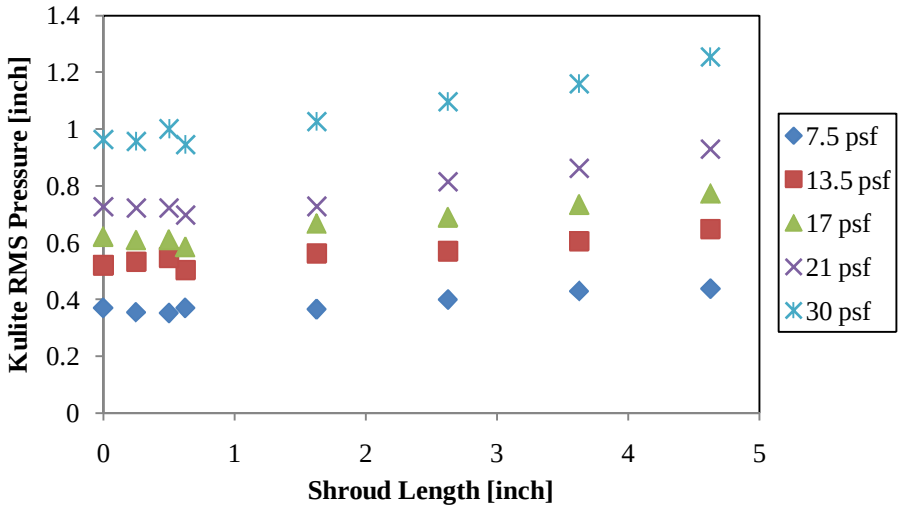

Figure D.12 – Kulite RMS pressure measurements with different shroud lengths as function of shroud length. While the RMS pressures were relatively constant when shroud lengths were less than 1.675 in, the RMS pressure increased when shroud length was increased beyond 1.675 in.

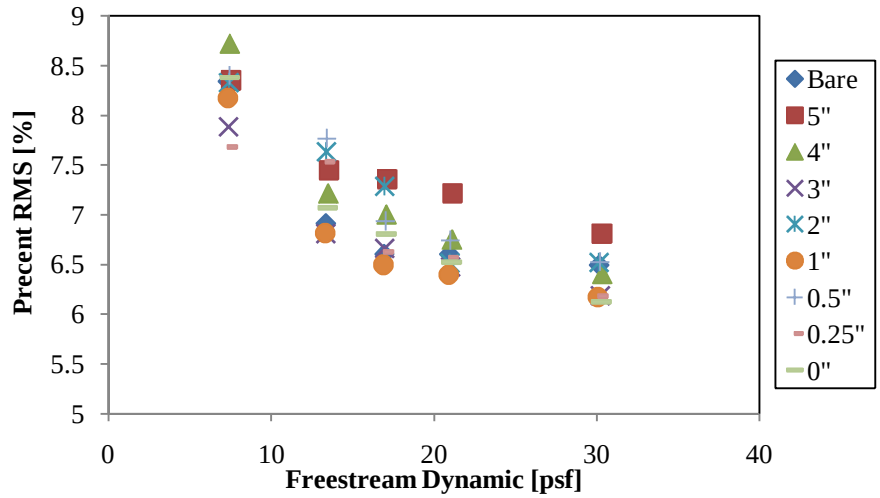

Figure D.13 – Calculated % RMS with different shroud lengths as function of free-stream dynamic pressure.

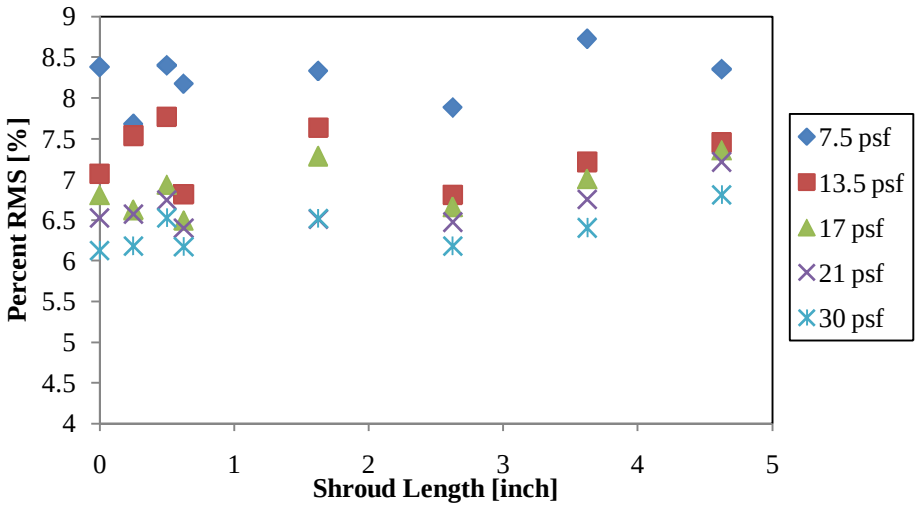

Figure D.14 – Calculated %RMS with different shroud lengths as function of shroud length. The data is somewhat sporadic, the calculated % RMS were relatively constant at higher free-stream dynamic pressures.

In order to eliminate the effect of varying reference pressure from our experimental results, a Kulite configuration to keep the reference pressure constant was necessary. In order to achieve a constant reference pressure, the end of the Kulite probe was modified and was attach to a static probe. The static probe was placed at a fixed position (35.5 inches AFT leading edge of the flat plate, facing the flow) to ensure the constant static pressure measurements throughout the experiment. The configuration of the modified Kulite probe is shown below. The end of the Kulite probe was attached to a connector tube by epoxy, which allowed to be plumbed to a plastic tube that connected to a static probe.

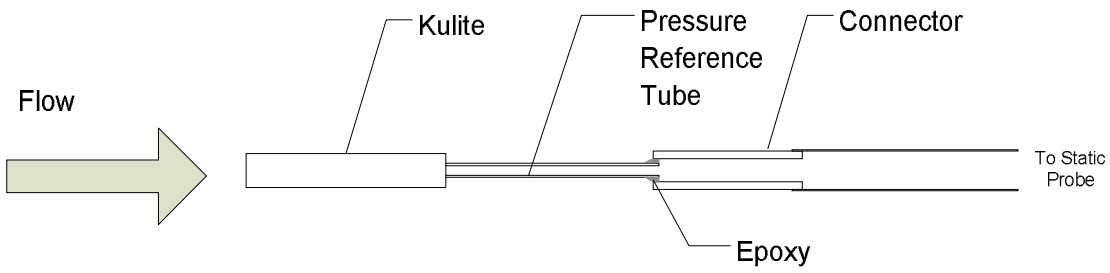

Figure D.15 – Kulite sensor configuration with a fixed static probe.

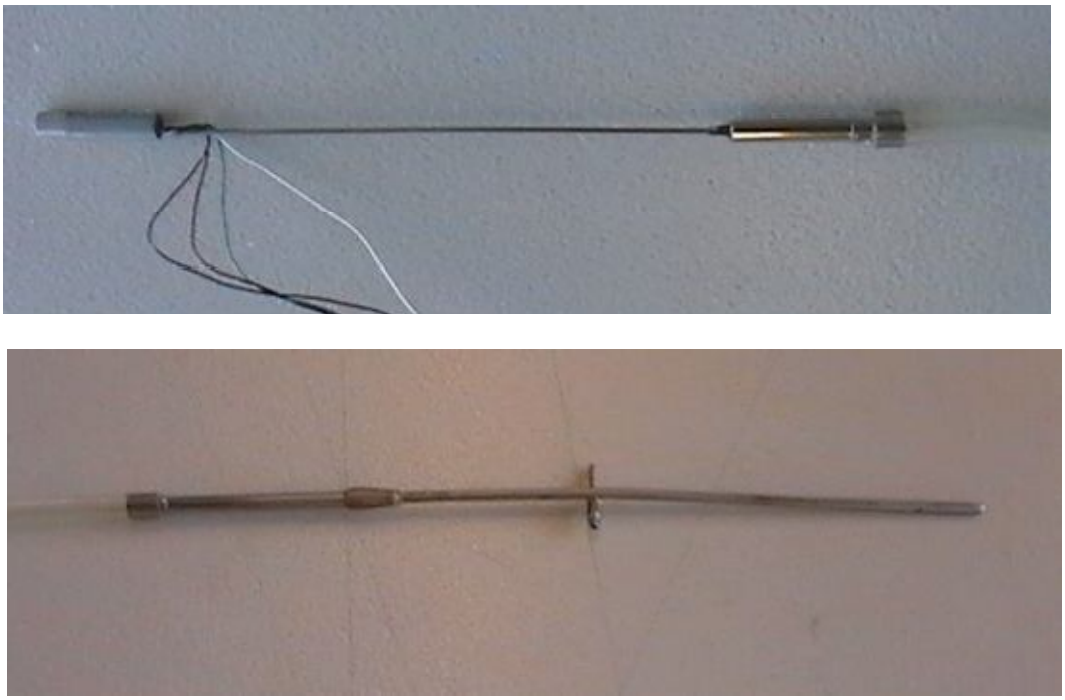

Figure D.16 – The Kulite sensor's reference tube is connected to a static probe via plastic tubing.

With the reference pressure fixed, the effect of shroud length on the Kulite probe was again examined. In order to see the difference, the shroud lengths l = 1.625 in and l = 4.625 in were used. As the results show, the fixed reference pressure had no impact on either the average or RMS readings for the short shroud, while the average pressure readings of the long shroud decreased. Therefore, we can conclude that the increase in average pressure with shroud length that we have seen in the previous experiment was

due to change in the reference pressure. The RMS reading, however, remained the same even with the fixed reference pressure. The mechanism that causes the RMS to linearly increase with increasing shroud length has not been resolved.

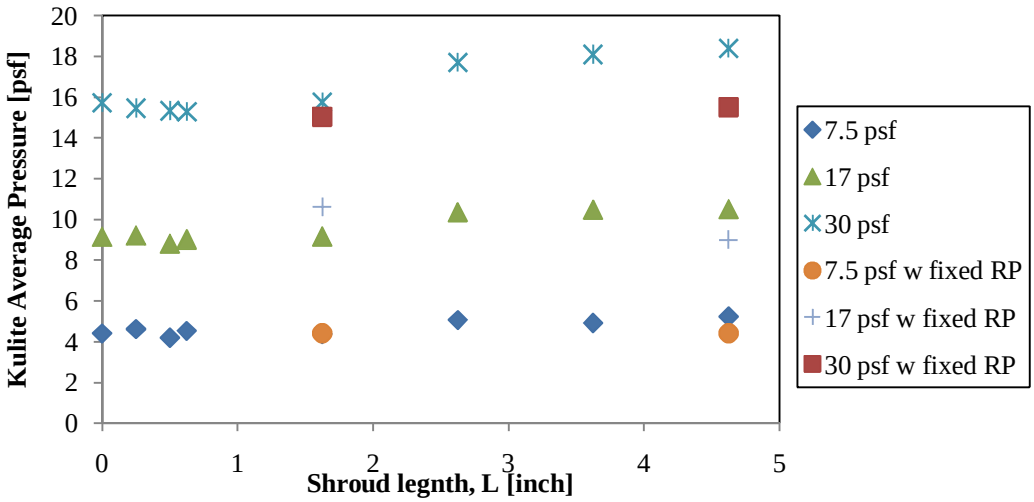

Figure D.17 – The Kulite average pressure readings with a fixed reference pressure were compared to the data that were taken previously with moving reference pressures. When the reference pressure was fixed, the Kulite average pressure readings became constant for both short and long shrouds.

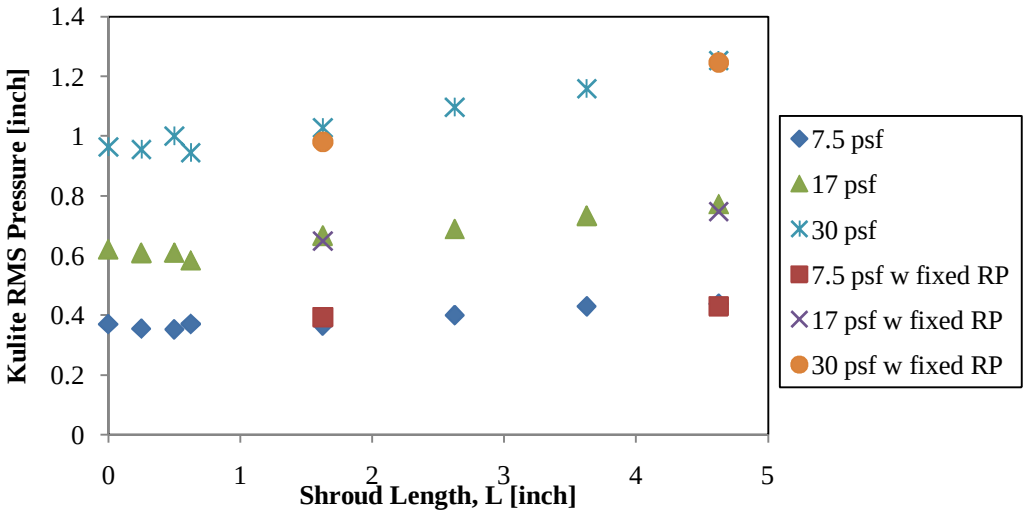

Figure D.18 – The Kulite RMS pressure readings with a fixed reference pressure were compared to the data that were taken previously with moving reference pressures. Even when the reference pressure was fixed, the RMS reading increased for the longer shroud.

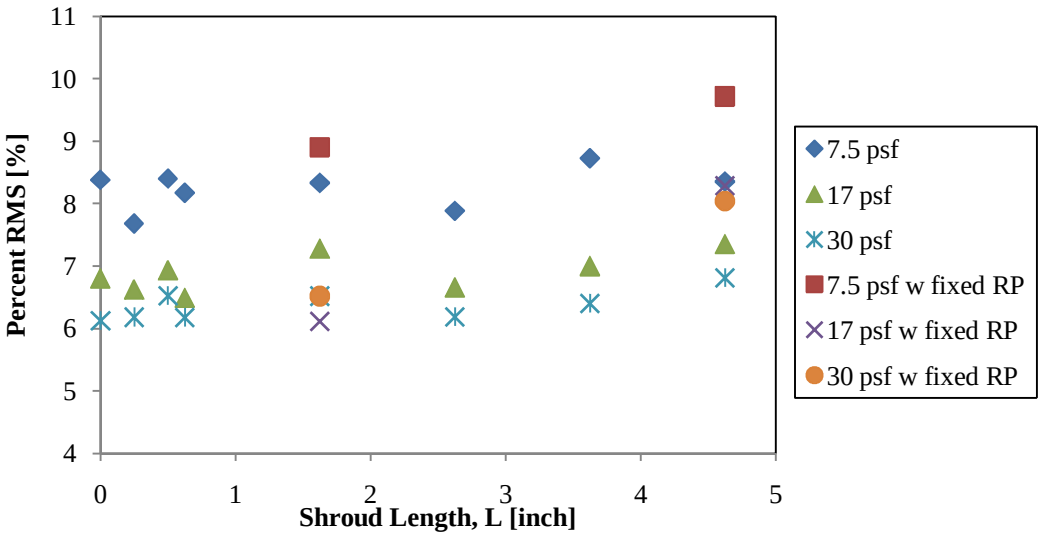

Figure D.19 – Calculated % RMS with a fixed reference pressure were compared to the data that were taken previously with moving reference pressures. Since the Kulite average pressure for the long shroud was corrected with a fixed reference pressure, higher % RMS values were calculated for the long shroud.

While shrouded Kulite read slightly higher average and RMS pressures when compared to bare Kulite readings, which might have to do with the elevated position of Kulite sensor in the boundary layer, the previous results demonstrated that the shroud length don't affect Kulite average pressure readings. In addition, the Kulite RMS remained relatively constant at a given dynamic pressure when the shroud length was less than 1.675 inches. Therefore, 1.375 inch long shroud was chosen to test the effect of probe length on the Kulite measurements. A probe with different length, *l*, was attached to the shroud with epoxy. In this experiment, a probe with 0.020 inch ID was used to measure the Kulite average and RMS pressures. The length of probe was varied between 1.25 in and 3 in by 0.5 in increments. Both the probe being tested and the static probe that is connected to the Kulite pressure reference tube was placed flush on the surface of the flat plate, x = 35.5 in in the 2x2 Cal Poly wind tunnel. The pressure measurements were

amplified and recorded by BLDS at nominal free-stream dynamic pressures at 7.5, 13.5, 21, and 30 psf. The configuration of the Kulite sensor used for this testing is shown in below figure D.20.

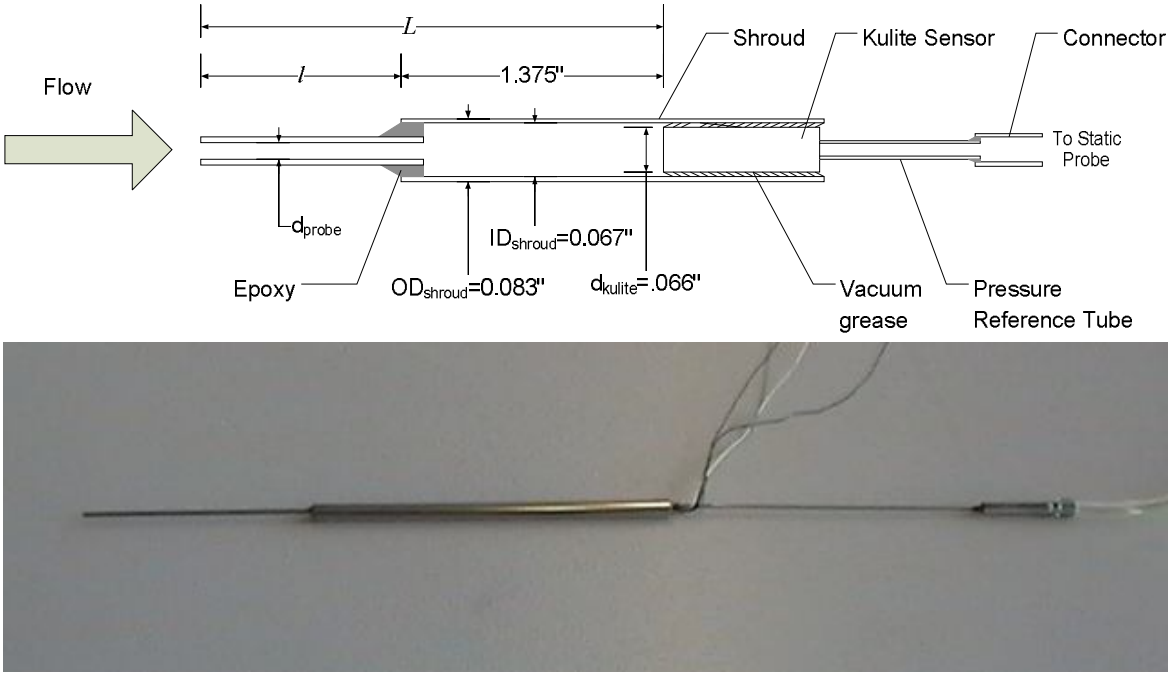

Figure D.20 – Kulite sensor configuration used to test the effect of probe length on Kulite measurements.

The results exhibited that the probe length had no effect on the Kulite readings when shroud was used as a connecting medium. The Kulite average, RMS, and % RMS all remained relatively constant throughout the experiment.

When the Kulite sensor was connected to a probe via plastic tubing, the results indicated that the Kulite average and RMS pressure both varied with probe diameters. In order to confirm this account, two more sets of experiments will be conducted using probes with different ID's while the Kulite configuration stays the same. The test results will be compared to unveil the effect of probe diameter on the Kulite pressure measurements.

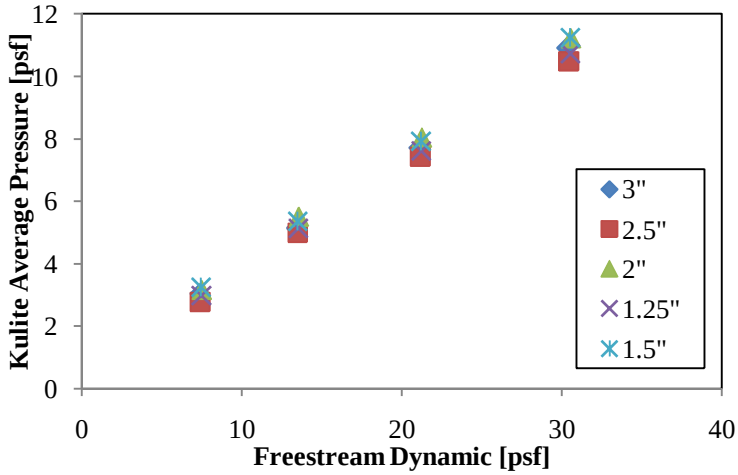

Figure D.21 – Kulite average pressure measurements with different probe lengths as function of free-stream dynamic pressures.

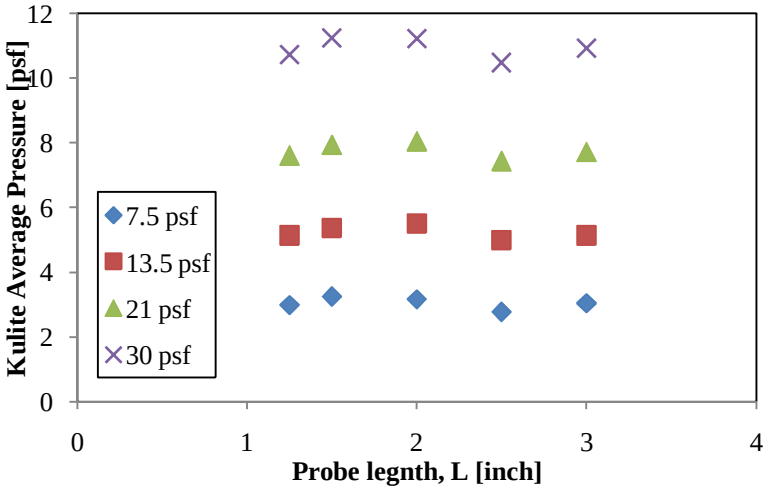

Figure D.22 – Kulite average pressure measurements with different shroud lengths as a function of probe length. The average pressures remained relatively constant as probe length increased.

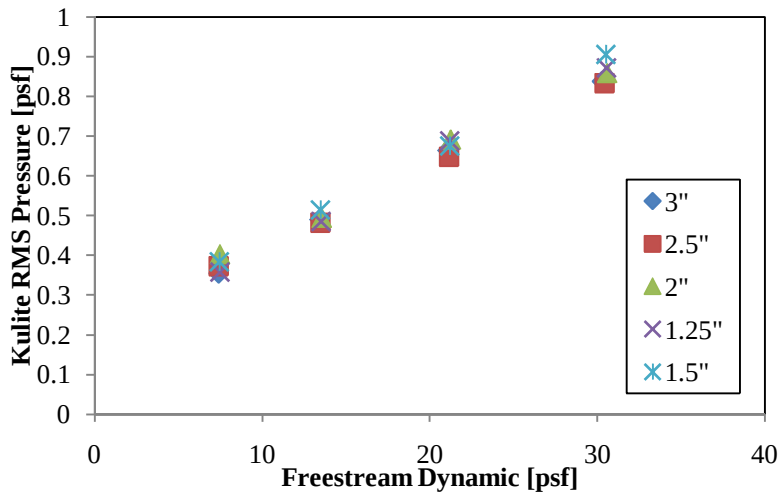

Figure D.23 – Kulite RMS pressure measurements with different probe lengths as function of free-stream dynamic pressures.

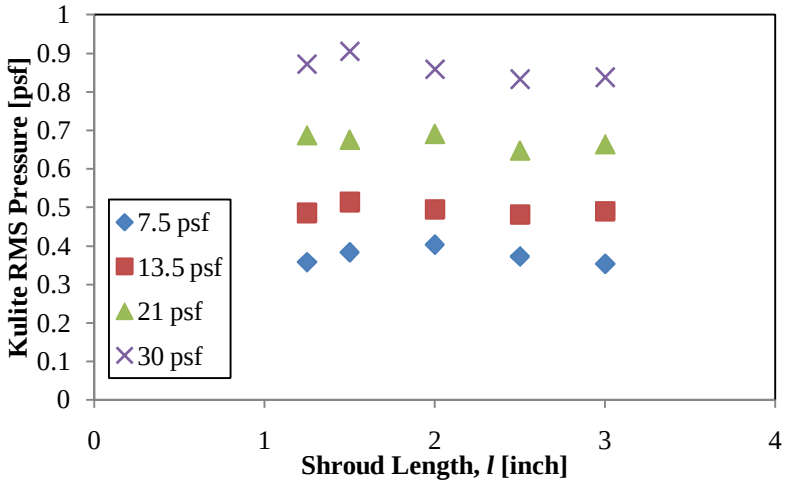

Figure D.24 – Kulite RMS pressure measurements with different shroud length, *l*.

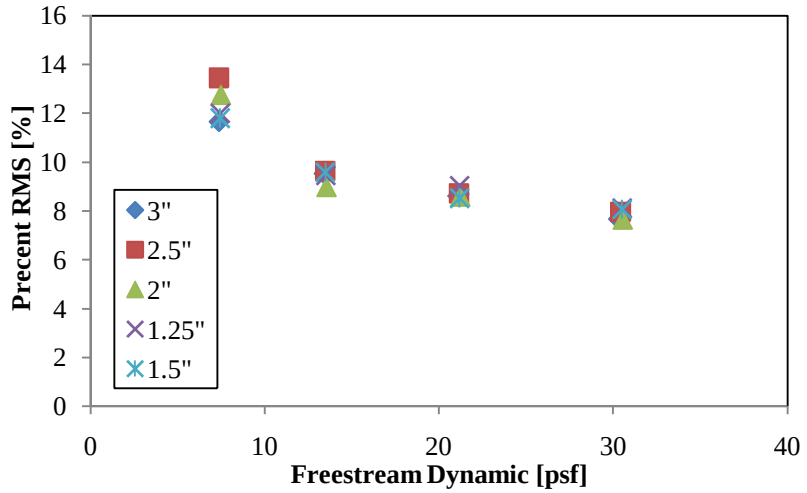

Figure D.25 – Calculated % RMS values as function of free-stream dynamic pressures.

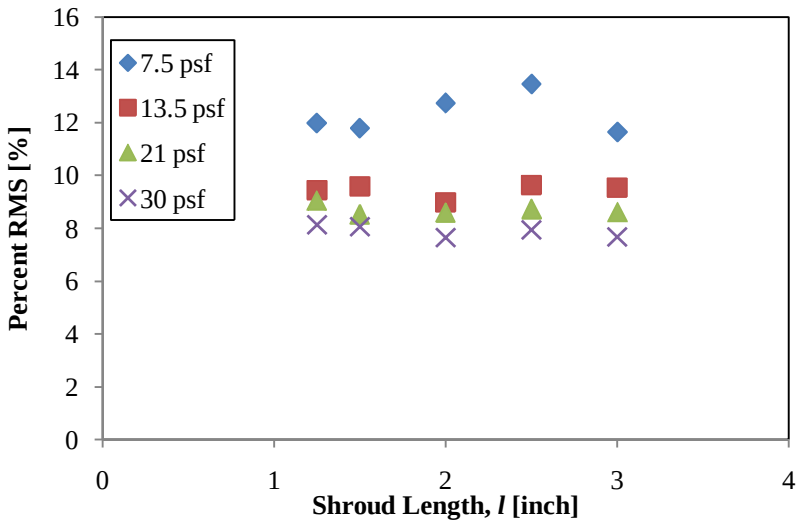

Figure D.26 – Calculated % RMS with different shroud lengths, *l*.